## San Jose State University
# SJSU ScholarWorks

1991

# The Miocene dike swarm of the Mohave Mountains, Arizona : petrography, geochemistry, geochronology, and paleomagnetism

Victoria L. Pease
*San Jose State University*

Follow this and additional works at: https://scholarworks.sjsu.edu/etd_theses

# INFORMATION TO USERS

This manuscript has been reproduced from the microfilm master. UMI films the text directly from the original or copy submitted. Thus, some thesis and dissertation copies are in typewriter face, while others may be from any type of computer printer.

**The quality of this reproduction is dependent upon the quality of the copy submitted.** Broken or indistinct print, colored or poor quality illustrations and photographs, print bleedthrough, substandard margins, and improper alignment can adversely affect reproduction.

In the unlikely event that the author did not send UMI a complete manuscript and there are missing pages, these will be noted. Also, if unauthorized copyright material had to be removed, a note will indicate the deletion.

Oversize materials (e.g., maps, drawings, charts) are reproduced by sectioning the original, beginning at the upper left-hand corner and continuing from left to right in equal sections with small overlaps. Each original is also photographed in one exposure and is included in reduced form at the back of the book.

Photographs included in the original manuscript have been reproduced xerographically in this copy. Higher quality 6" x 9" black and white photographic prints are available for any photographs or illustrations appearing in this copy for an additional charge. Contact UMI directly to order.

## U·M·I

Order Number 1344302

The Miocene dike swarm of the Mohave Mountains, Arizona:
Petrography, geochemistry, geochronology, and paleomagnetism

Pease, Victoria L., M.S.

San Jose State University, 1991

# U·M·I

THE MIOCENE DIKE SWARM OF THE MOHAVE MOUNTAINS, ARIZONA:

PETROGRAPHY, GEOCHEMISTRY, GEOCHRONOLOGY, AND PALEOMAGNETISM

A Thesis

Presented to

The Faculty of the Department of Geology

San Jose State University

In Partial Fulfillment

of the Requirements for the Degree

Master of Science

By

Victoria L. Pease

May, 1991

APPROVED FOR THE DEPARTMENT OF GEOLOGY

_Edward E. Geary_
Dr. Edward Geary

_John W. Hillhouse_
Dr. John Hillhouse

_Robert B Miller_
Dr. Robert Miller


APPROVED FOR THE UNIVERSITY

_Serena H. Stanford_

# ACKNOWLEDGEMENTS

# TABLE OF CONTENTS

# LIST OF ILLUSTRATIONS

# LIST OF TABLES

# ABSTRACT

Combined paleomagnetic and geochronologic studies of
Tertiary dikes in the Mohave Mountains of Arizona have been
used to characterize the style and timing of detachment
faulting associated with the Crossman block. Geochemical
and petrographic techniques applied to the dike samples
place constraints on their compositions, their petrogenesis,
and allow for petrogenetic comparison with the Chamber's
Well dike swarm of the Whipple Mountains.

Petrographic data indicate that dikes in the eastern
Mohave Mountains were emplaced at greater depths and altered
at higher temperatures than those in the west. The
association of sericite, chlorite, calcite, and epidote
suggests that this alteration resulted from hydrothermal
circulation which lasted <5000 years. Textures associated
with severe potassic metasomatism are absent in contrast to
other parts of the Basin and Range.

The dike swarm ranges in composition from basalt to
rhyolite and a calcalkaline trend is defined. This trend is
probably a magmatic differentiation trend and not the result
of potassic metasomatism. Significant oxide variation
within the basalts suggests that variable degrees of crustal
contamination or partial melting may have occurred. The

dike swarm of the Mohave Mountains may be correlative with
the Chamber's Well dike swarm, but a cogenetic relationship
cannot be established without trace-element and isotopic
analyses.

$^{40}Ar/^{39}Ar$ isotopic data on biotite and hornblende
mineral separates suggest that the dike swarm of the Mohave
Mountains was intruded over a short period of time about 20
m.y. ago and that it cooled quickly. Hydrothermal
circulation has not reached temperatures >300°C since that
time.

The dike swarm records two polarities of magnetization:
1) CNH, the Crossman block normal polarity, high-temperature
or high coercivity magnetic component, and 2) CRH, the
Crossman block reversed polarity, high-temperature or
high-coercivity magnetic component. These two components of
magnetization are not antipodal. In as much as the isotopic
data suggest that the dikes cooled quickly and the
baked-contact test suggests a stable magnetization, these
magnetic directions are likely to be Miocene in age. The
deviation of CRH from CNH and the expected direction of the
axial dipole in the Miocene is best explained as a result of
differential rotation about a horizontal axis trending 144°,
the same as the observed tilt axis recorded by the local
geology.

These data further suggest that CRH dikes were emplaced and acquired their magnetic direction after the Crossman block had been tilted 65° to the SW. Subsequent deformation along the Crossman Peak detachment fault tilted the Crossman block 80 to 100° to the SW. The earth's magnetic field then reversed and CNH dikes were intruded. The mean magnetic direction of CNH is not coincident with the expected axial dipole field, therefore a small amount of tilt ($\approx$10°) may have occurred after CNH dikes were intruded.

During this time a change in the stress field associated with the Crossman block occurred. The paleomagnetic data suggest that CRH dikes were intruded vertically, whereas CNH dikes were intruded in non-vertical ($\approx$60°) orientations. This implies that the orientation of the stress field associated with the Crossman block detachment fault was initially orthogonal (with $\sigma_1$ vertical) and that it either rotated or became non-orthogonal as faulting progressed.

INTRODUCTION

## Location and Regional Setting

The Mohave Mountains of west-central Arizona occur within a belt of highly extended and tilted fault blocks defined by Howard and John (1987) as the Colorado River extensional corridor (fig. 1A). This corridor lies within the Basin and Range Province, where Tertiary rocks tilt uniformly to the west-southwest (Stewart, 1980). The corridor is 50-100 km wide, is bounded to the east by the block-faulted margin of the Colorado Plateau, and extends west into southeastern California. Low-angle normal (detachment) faults extend the upper 10-15 km of crystalline crust within the extensional corridor. These detachment faults are best exposed around domal metamorphic core complexes, where brittlely deformed upper-crustal rocks are juxtaposed against ductilely deformed lower-crustal rocks (Coney, 1979; Crittenden et al., 1980). Metamorphic core complexes in the central part of the extensional corridor include the Whipple and Rawhide Mountains (Davis et al., 1980; Frost and Martin, 1982), the Chemehuevi Mountains (John, 1982), the Sacramento Mountains (McClelland, 1982; Spencer and Turner, 1982; Spencer, 1985), and the Dead and Newberry Mountains (Mathis, 1982; Spencer, 1985).

A



B
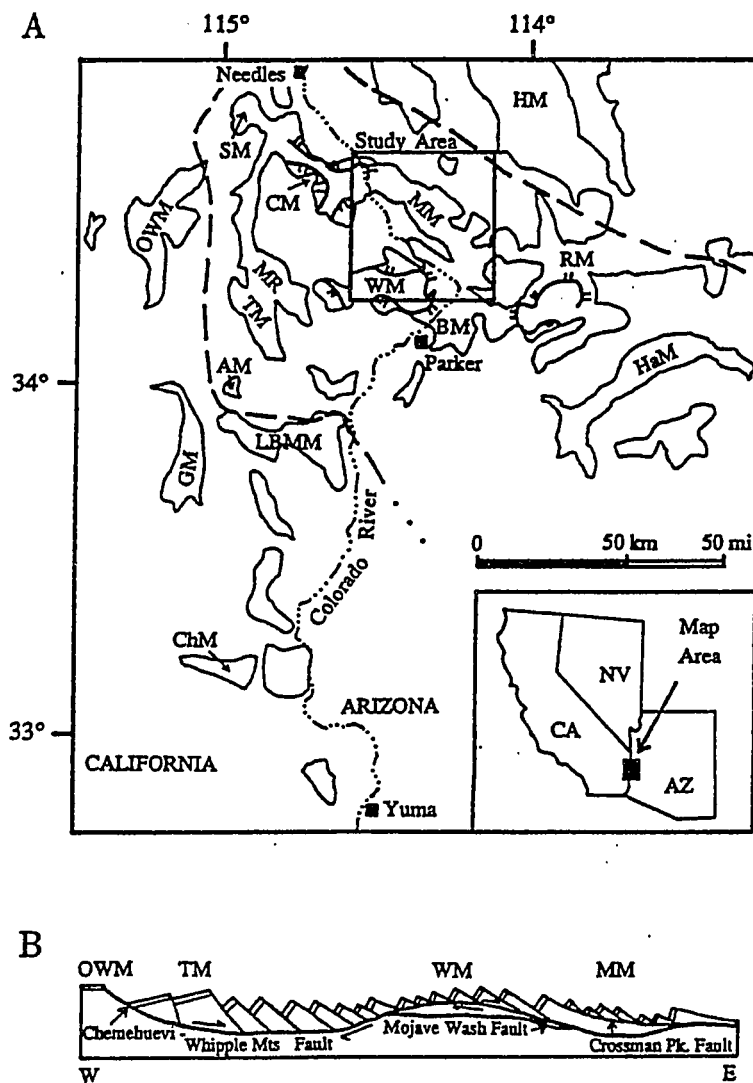


Figure 1. A) Location map of the study area.
Extensional corridor (within the dashed lines); AM, Arica
Mountains; BM, Buckskin Mountains; CM, Chemehuevi Mountains;
ChM, Chocolate Mountains; GM, Granite Mountains; HM,
Hualapai Mountains; HaM, Harcuvar Mountains; LBMM, Little
and Big Maria Mountains; MM, Mohave Mountains; MR, Mopah
Range; OWM, Old Woman Mountains; RM, Rawhide Mountains; SM,
Stepladder Mountains, TM, Turtle Mountains; WM, Whipple
Mountains. Major detachment faults shown (teeth on upper-
plate). B) Schematic cross-section of Chemehuevi-Whipple
Mountains detachment fault (headwall breakaway in OWM).
Modified from Howard and John (1987).

In the Colorado River extensional corridor, almost all of the fault blocks developed during mid-Tertiary extension tilt to the southwest. A fan of steep to gentle dips in latest Oligocene(?) and Miocene volcanic and sedimentary rocks records syntectonic deposition accompanying extension and tilt (Nielson and Beratan, 1990). Most of the faulted syntectonic rocks are Early Miocene (17 and 22 Ma). Fanglomerates and basalts of 10-15 Ma overlie the highly faulted rocks of the extensional corridor (Davis et al., 1980; Dickey et al., 1980; Spencer, 1985) and place a Late Miocene limit on the timing of regional extension.

Howard and John (1987) have proposed that successively higher and more distal fault blocks (allochthons) are displaced farther from a main headwall breakaway located in the Old Woman Mountains (fig. 1B). Slip indicators (e.g.-stratal tilts, slickensides, offset plutonic contacts, marker unit offsets) along faults exposed in all levels of the crust are unidirectional, indicating transport to the northeast. Detachment faults in the extensional corridor cut down-section to the northeast, the direction of tectonic transport. Eastward from the headwall, block tilts generally steepen as the allochthons are rotated east-side up. Approximately 50 km of extension has occurred across the corridor. Extension is accommodated along multiple normal faults which coalesce at depth into the basal Chemehuevi-Whipple Mountains detachment fault(s). This

shoaling fault system initially cut upper-crustal rocks to paleodepths of at least 10-15 km, transporting these rocks as fault blocks to the east-northeast and tilting them by progressively greater amounts as distance from the main headwall increased.

This geometry is illustrated in the Mohave Mountains where a 10-15 km vertical section of upper-crust is now uplifted and tilted to the southwest (Howard et al., 1982). Sub-vertical and overturned volcanic and sedimentary strata in the Mohave Mountains indicate large amounts of upper-crustal extension (Wernicke and Burchfiel, 1982; Gans and Miller, 1983). The Chemehuevi-Whipple Mountains detachment fault(s) is inferred to underlie the Mohave Mountains (Howard and John, 1987). In this interpretation, a reconstruction for the Mohave Mountains prior to detachment faulting would place this range near the Whipple Mountains; rocks from the Whipple Mountains would then be the lower-crust equivalents of rocks from the Mohave Mountains.

## Geology of the Mohave Mountains

Nielson (1986) divided the Mohave Mountains into three structural domains separated by northeast-trending faults. In subsequent work, Nielson and Beratan (1990) were able to correlate the Tertiary stratigraphy of these domains with the Tertiary stratigraphy in areas of the Aubrey Hills and Whipple Mountains. The three structural domains within the

Mohave Mountains are: 1) the Aubrey Hills-Standard Wash domain, 2) the Crossman Peak domain, and 3) the Yucca Mine domain (fig. 2). In this study these fault-bounded structural domains are referred to as "blocks." The Crossman block is bound by the Castle Rock fault to the north and by the Crossman Peak fault to the south (fig. 2). The Standard Wash block lies south of the Crossman Peak fault and the Yucca Mine block lies north of the Castle Rock fault. These faults cut the upper-crustal rocks of the Mohave Mountains and coalesce at depth with the Chemehueve-Whipple Mountains detachment fault(s) (Howard et al., 1982; Howard and John, 1987). The Mohave Mountains consist primarily of Proterozoic metamorphic rocks and Proterozoic to Mesozoic igneous rocks (Howard et al., 1982). In the Standard Wash block, Pre-Tertiary rocks consist entirely of Mid-Proterozoic granite, quartz monzonite, and diorite. This block is cut by Tertiary dikes. Pre-Tertiary rocks in the Crossman block are predominantly Early Proterozoic gneisses (granitic and granodioritic gneiss, granitic orthogneiss, biotite gneiss), amphibolite, and subordinate metasedimentary rocks. These rocks are cut by diabase dikes of probable Late Proterozoic age, small Cretaceous(?) plutons, and a swarm of Tertiary dikes. In the Yucca Mine area, pre-Tertiary rocks include Cretaceous intrusions, a variety of gneisses similar to those of the Crossman block, as well as Mid-Proterozoic granitic rocks.
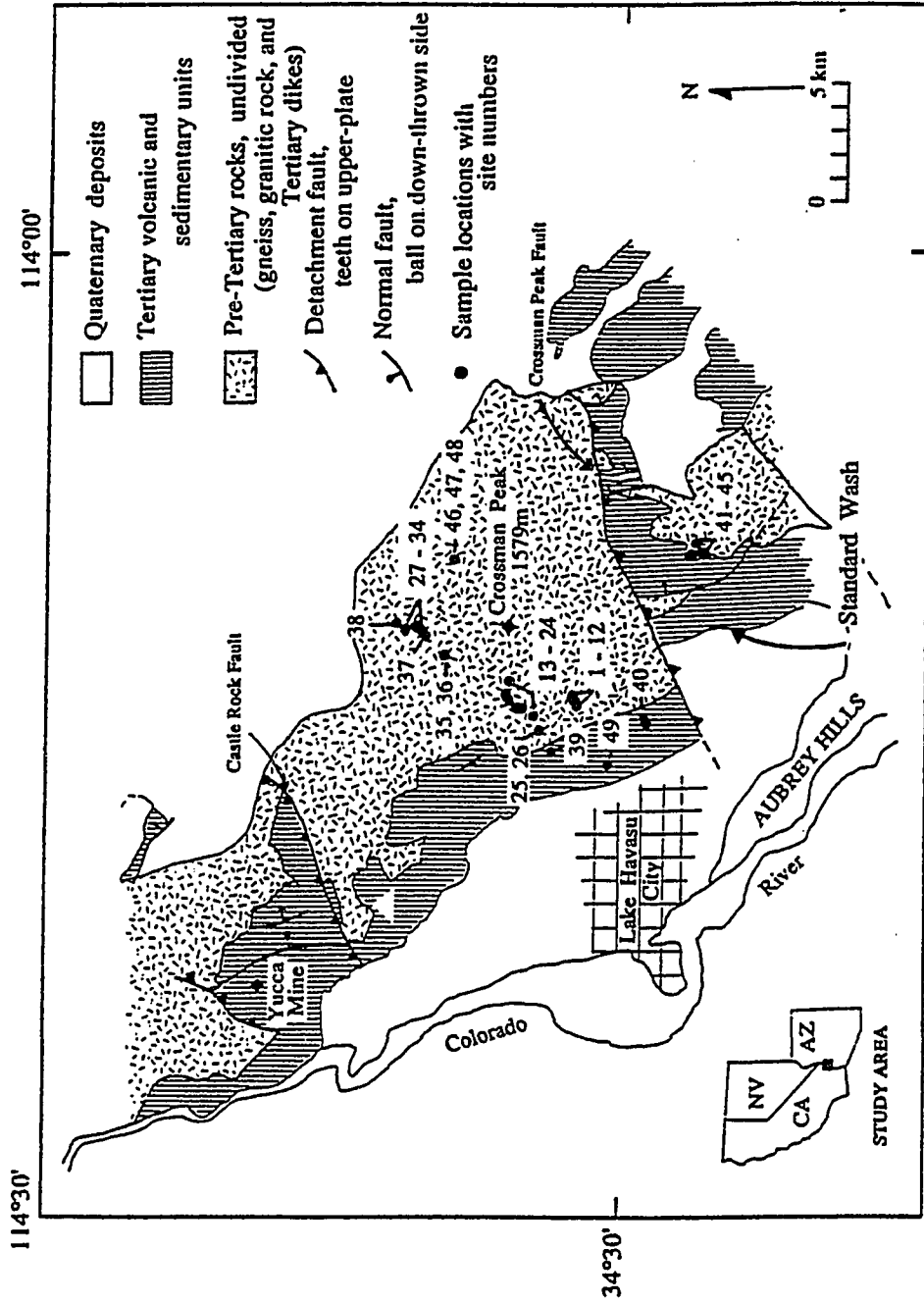
Figure 2. Simplified geologic map of the Mohave Mountains.
Triangle marks location of Tertiary magmatic center. Modified from
Nielson and Beratan (1990).

The Tertiary dike swarm in the Mohave Mountains is the subject of this investigation. These dikes were originally mapped by Nakata (1982) and he determined that they record extension of 16.5% in the Crossman block. Howard et al. (1982), however, suggested that distension could be as great as 20-30%. These dikes range from basalt to rhyolite and represent the Miocene "leucocratic suite," "young mafic," "trachytic-textured," and "young gabbroic and andesitic" dikes of Nakata (1982). The older granitic and ophitic diabase dikes of Nakata (1982) were only briefly studied. These older rocks can be distinguished from the younger dikes in the field on the basis of cross-cutting relationships and the greater weathering of the older dikes. The age of the dike swarm is poorly constrained and is discussed in the following chapter on geochronology.

On the basis of structural and stratigraphic relations, Nielson (1986) was able to subdivide the Tertiary strata in the Mohave Mountains into four sequences. Subsequent work by Nielson and Beratan (1990) further refined these sequences. These sequences are schematically illustrated in figure 3. They are numbered I-IV from oldest to youngest, tilt progressively steeper with age, and have a total thickness of about 2000 m. The thickness of each sequence varies between structural domains due to abrupt facies changes and coeval faulting. In sequence I, sedimentary rocks of mixed volcanic and arkosic derivation, tuff and
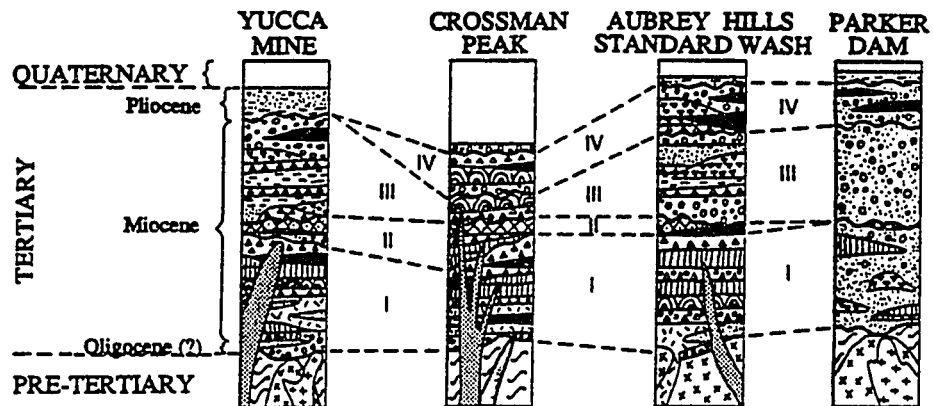
EXPLANATION
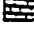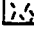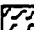
**TERTIARY ROCKS:**

☐ Quaternary surficial deposits

▨ Dikes

◾ Basalt flows and sills

▨ Megabreccia

▨ Ash flow tuff

▨ Peach Springs Tuff of
Young and Brennan (1974)

▨ Rhyolite flows

▨ Tuff and tuff breccia

▨ Shale and claystone

▨ Sandstone

▨ Conglomerate

▨ Limestone

▨ Andesite (?) and altered
lava flows and sills

▨ Jackstraw porphyry

**PRE-TERTIARY ROCKS:**

▨ Granite (Cretaceous ?)

▨ Proterozoic sills

▨ Proterozoic igneous rocks

▨ Proterozoic gneiss

Figure 3. Simplified stratigraphic column of Tertiary
units in the Mohave Mountains and correlated areas.
Modified from Beratan et al. (1990).

tuff breccia, and variable volumes of lava flows are interbedded. Sequence I is capped by a unit of white silicic airfall tuff that is locally interbedded with, or intruded by, basalt. At the base of the section sequence I rocks are steeply tilted (near-vertical to overturned). The uppermost units of sequence I dip moderately ($\approx$50°). There are no angular unconformities within the section. Sequence I has yielded an age of 23 ± 2.4 Ma (a single fission-track zircon date near the base of the section; Beratan, 1990). A minimum age for this sequence is provided by the age of the overlying Peach Springs Tuff, 18.5 ± 0.2 Ma ($^{40}Ar/^{39}Ar$ on sanidine; Nielson et al., 1990).

Sequence II consists mostly of intermediate to silicic flows and welded tuff, including the Peach Springs Tuff. Sequence II rocks range in age from 19.9 ± 0.6 to 17.9 ± 0.5 Ma (K-Ar on biotite and plagioclase separates, respectively; written communication from J. Nakata in Nielson and Beratan, 1990). The ages of sequence II rocks vary between structural domains of the Mohave Mountains. Large variations in dip are typical of units in this sequence, with dips of 25-35° to the southwest characteristic of the uppermost units.

Sedimentary rocks which are locally interbedded with sparse fragmental volcanic rocks or basalt flows comprise sequence III. Also ubiquitous within sequence III are interbedded glideblocks and masses of megabreccia which have

been interpreted as landslide deposits. Sequence III rocks show fanning of dips from moderate to gentle (50-15°) going upsection. The maximum age of sequence III strata is constrained by the age of the underlying Peach Springs Tuff. A date of 14.1 ± 0.3 Ma was obtained from a basalt flow in the upper part of sequence III in the Aubrey Hills (K-Ar on whole rock; written communication from J. Nakata in Nielson and Beratan, 1990).

Sequence IV rocks are similar to those of sequence III, but include a thick stack of rhyolite and basalt flows in the Aubrey Hills-Standard Wash domain. These units are horizontal to slightly tilted with dips of 5° or less. The age of sequence IV ranges from 12.2 Ma (K-Ar on sanidine; written communication from J. Nakata in Nielson and Beratan, 1990) to 8.6 Ma (K-Ar on whole rock; Suneson and Lucchitta, 1983).

## Objectives

In order to characterize the style and timing of detachment faulting in the Mohave Mountains, samples were collected from Tertiary dikes and their extrusive equivalents for paleomagnetic and geochronologic investigations. These dikes intrude the Precambrian crystalline core of the Mohave Mountains, thus providing some structural control for determining the degree to which the crystalline core has participated in the deformation

recorded by the Tertiary strata. Additional structural control was provided by sampling the overlying Tertiary volcanic rocks (sequences I and IV). These samples were distributed between the Crossman and Standard Wash blocks in order to compare the style and amount of deformation which occurred within upper crustal rocks across the Crossman Peak fault. In addition, they were collected in an east-west traverse to evaluate what may represent about 12 km of continuous vertical crustal section now tilted approximately 90°. By determining the age of the dikes, the timing of detachment faulting of the Crossman block may be constrained. Petrographic and geochemical techniques were also applied to the dike samples to determine their compositions, their petrogenetic relationships, and to determine whether they are cogenetic with the Chamber's Well dike swarm of the Whipple Mountains. A summary of sampling and sample locations is presented in table 1 and shown on fig. 2.

Table 1.  Sampling Summary – Crossman Block

| Site # | U.S.G.S. I.D. | N.Lat. | W.Long. | Mineral separate | Thin-section | Major elements |
|---|---|---|---|---|---|---|
| 1 | 5H001 | 34.522 | 114.229 | | 1 n | |
| 2 | 5H005 | 34.522 | 114.230 | | 1 n | |
| 3 | 5H008 | 34.522 | 114.230 | | 1 n | |
| 4 | 5H011 | 34.522 | 114.230 | | 1 n | |
| 5 | 5H014 | 34.521 | 114.230 | | 1 n | 2 n,c |
| 6 | 5H017 | 34.521 | 114.231 | | 1 n | |
| 7 | 5H020 | 34.521 | 114.231 | | 1 n | |
| 8 | 5H023 | 34.521 | 114.231 | | 1 n | |
| 9 | 5H026 | 34.521 | 114.233 | | 1 n | 1 n |
| 10 | 5H029 | 34.521 | 114.233 | | 1 n | |
| 11 | 5H032 | 34.519 | 114.234 | | 1 n | |
| 12 | 5H035 | 34.519 | 114.234 | | 1 n | |
| 13 | 5H038 | 34.549 | 114.222 | | 1 n | |
| 14 | 5H041 | 34.549 | 114.221 | | 1 n | |
| 15 | 5H044 | 34.550 | 114.224 | | 1 n | |
| 16 | 5H047 | 34.551 | 114.229 | hb, n | 1 n | 1 n |
| 17 | 5H050 | 34.551 | 114.229 | | 1 n | 1 n |
| 18 | 5H053 | 34.550 | 114.231 | | 1 n | |
| 19 | 5H056 | 34.550 | 114.231 | | 1 n | 1 n |
| 20 | 5H059 | 34.550 | 114.232 | | 1 n | |
| 21 | 5H062 | 34.549 | 114.232 | | 1 n | |
| 22 | 5H065 | 34.546 | 114.236 | | 1 n | |
| 23 | 5H068 | 34.544 | 114.236 | | 1 n | |
| 24 | 5H071 | 34.539 | 114.239 | | 1 n | |
| 25 | 5H074 | 34.537 | 114.247 | | 1 n | |
| 26 | 5H077 | 34.537 | 114.246 | bi, n | 1 n | |
| 27 | 5H080 | 34.602 | 114.185 | | 1 n | 1 n |
| 28 | 5H083 | 34.601 | 114.186 | | 1 n | |
| 29 | 5H086 | 34.597 | 114.184 | | 1 n | |
| 30 | 5H089 | 34.597 | 114.184 | | | |
| 31 | 5H090 | 34.597 | 114.184 | | 1 n | |
| 32 | 5H093 | 34.597 | 114.184 | | 1 n | |
| 33 | 5H096 | 34.597 | 114.185 | | | |
| 34 | 5H099 8P010 | 34.596 | 114.185 | | 1 n | |
| 35 | 5H102 | 34.583 | 114.202 | bi, n | 1 n | 1 n |
| 36 | 5H105 | 34.581 | 114.205 | | 1 n | 1 n |
| 37 | 5H108 | 34.591 | 114.191 | hb, n | 1 n | 1 n |
| 38 | 5H111 | 34.606 | 114.182 | | 1 n | |
| 39 | 7J081 | 34.532 | 114.258 | | 2 c | 1 n |
| 40* | 7J091-130 8P026-037 | 34.490 | 114.243 | | | |

Table 1 con't. - Crossman Block

| Site # | U.S.G.S. I.D. | North Lat. | West Long. | Mineral separate | Thin-section | Major elements |
|---|---|---|---|---|---|---|
| 46 | 7J162 | 34.576 | 114.145 | | 1 n | 1 n |
| 47 | 7J168 | 34.576 | 114.145 | hb/bio, c | 2 n,c | 1 n |
| 48 | 7J172 | 34.576 | 114.145 | | 1 n | |
| 49 | 8P016 | 34.506 | 114.264 | | | |

Standard Wash Block

| Site # | U.S.G.S. I.D. | North Lat. | West Long. | Mineral separate | Thin-section | Major elements |
|---|---|---|---|---|---|---|
| 41 | 7J131 | 34.468 | 114.151 | | 1 n | 1 n |
| 42 | 7J138 | 34.468 | 114.151 | | 2 c | 1 c |
| 43 | 7J144 | 34.470 | 114.156 | | 1 n | 1 n |
| 44 | 7J150 | 34.470 | 114.157 | | 1 n | 1 n |
| 45 | 7J156 | 34.467 | 114.155 | | 2 c | 1 c |

c= chilled-margin, n= interior; hb= hornblende, bi= biotite;
U.S.G.S. I.D. = United States Geological Survey
identification; *= latitude and longitude of geographic
midpoint of linear sampling traverse reported.

PETROGRAPHY

## Sampling and Analytical Techniques

Petrographic analyses of dikes from the Mohave
Mountains were conducted using standard thin-section
techniques. Forty-nine petrographic descriptions from
forty-five dikes are given in Appendix A (four dikes have
thin-sections from both the chilled margin and the dike
interior). Forty-two of these thin-sections are from the
Crossman block, an approximately 12 km thick crustal section
(fig. 2; Howard et al., 1982). Sites 1 through 26 and site
39 are from the southwest side of the Mohave Mountains.
These samples are from upper-crustal levels in the Crossman
block (2-5 km). Sites 27 through 38 and 46 through 48 are
from the northeast side of the Mohave Mountains. These
samples represent crustal depths in the Crossman block of
approximately 7-12 km. Sites 41 through 45 are from the
southern Mohave Mountains in the Standard Wash block (fig.
2). Samples from the Standard Wash block are from
upper-crustal levels as well (a maximum of 5 km of crustal
thickness beneath the Tertiary strata). A summary of
sampling and sampling locations is provided in table 1.

## Analytical Results

Crossman Block

Group A. Of the sites on the west-southwestern side of
the Crossman block, only the shallowest exhibit textures
typically associated with volcanic rocks, e.g.- phenocryst
phases in a felty groundmass of feldspar laths with or
without interstitial quartz. These samples (sites 1-13,
16-26, and 39; hereafter refered to as Group A) are
holocrystalline, allotriomorphic, porphyritic, and generally
fine-grained. They exhibit spherulitic textures which
indicate intrusion at shallow depths or intrusion into cool
country rock and suggest some glass was originally present.
The spherules are too fine-grained to optically determine
their mineralogy. Spherules, however, are commonly composed
of radial aggregates of acicular feldspar and quartz
(MacKenzie et al., 1982). A sample from site 8 displays an
excellent example of this texture with euhedral crystals of
quartz forming the nuclei for subsequent spherulitic crystal
growth (fig. 4).

Textures more representative of intrusive igneous
rocks, e.g.- granophryic or concertal textures, were seen in
only 10% of these thin-sections. These occurrences were
from the interiors of some of the thickest ($\approx$10 m) dikes
sampled and their development is attributed to the slower
cooling rates associated with dike interiors. Group A
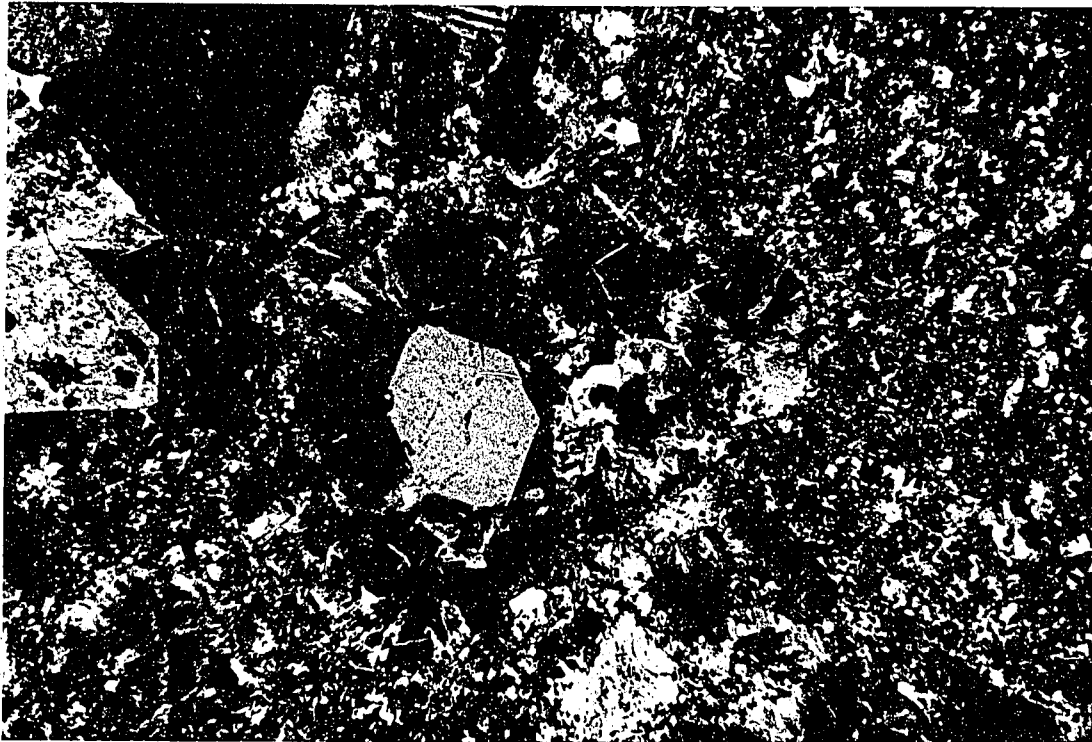
Figure 4. Spherulitic texture of acicular feldspar and quartz (?) in radial growth around a single quartz crystal (from site 8). Field-of-view width ≈6 mm.

samples are dominated by hypabyssal igneous textures.

Phenocryst phases of samples from Group A include augite, hornblende, plagioclase, and/or potassium feldspar (fig. 5). Augite phenocrysts are often twinned, zoned, include opaque minerals, and lack exsolution lamellae. Hornblende phenocrysts are usually zoned, include opaque minerals, and are variably altered to chlorite. Feldspar phenocrysts are also strongly zoned and typically include opaque minerals. The strong zoning in these primary phases indicates that disequilibrium-fractional crystallization was an important process in the evolution of these dikes.

Feldspar phenocrysts from Group A are saussuritized. Definitive mineralogical identification of the alteration phases is not optically possible due to their very fine grain size, but it is characterized by a colorless, highly birefringent (0.035), and secondary (replacement) occurrence associated with the calcic cores of plagioclase phenocrysts. Saussuritization is characterized by the replacement of plagioclase in basalts and gabbros by a fine-grained aggregate of zoisite, epidote, albite, calcite, sericite, and zeolites and is regarded as a metamorphic or deuteric process (Deer et al., 1966).

The pervasive saussuritization of feldspar phenocrysts inhibits compositional identification because it obscures the twinning. Consequently, plagioclase is often identified on the basis of crystal habit and the presence of "relict"
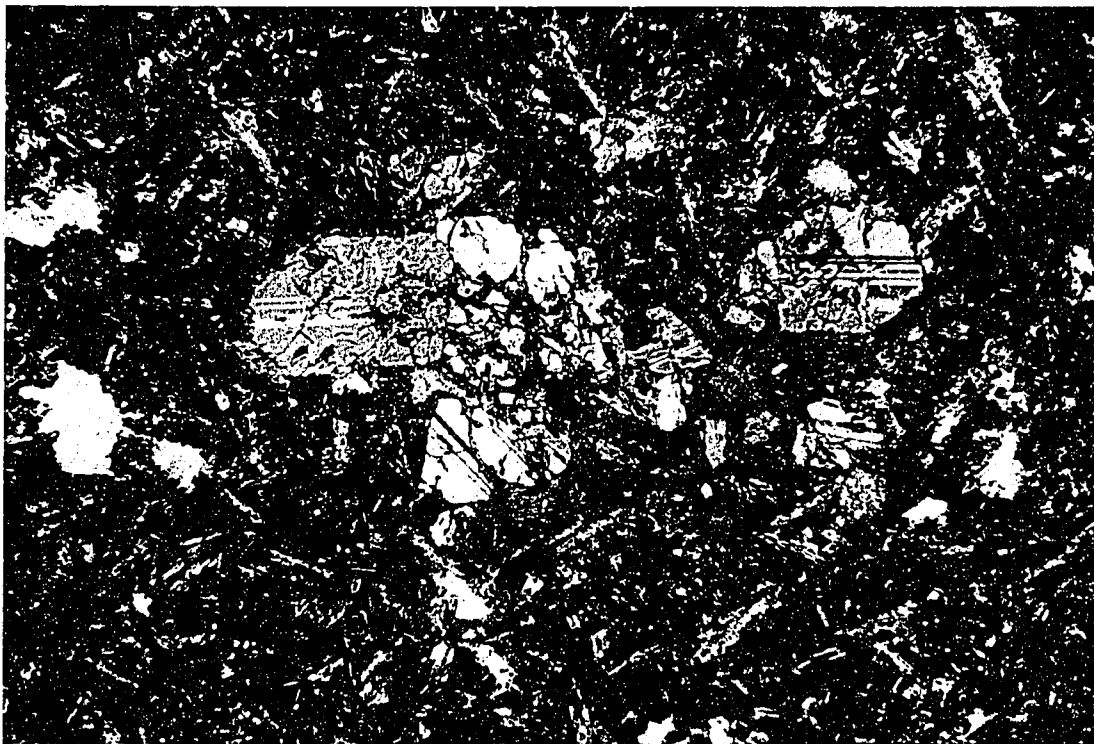
Figure 5.  Glomeroporphyritic augite phenocrysts in a groundmass of feldspar laths (from site 9).  Note twinning and slightly resorbed crystal edges.  Field-of-view width ≈6 mm.

or "ghost" twins, not by the optical properties of the twinning; in these circumstances, specific anorthite compositions could not be determined. Plagioclase compositions could be determined using the Michel-Levy method for 60% of the samples in Group A; these compositions range from $An_{32-42}$ where phenocryst and groundmass plagioclase coexist, and is $An_{52}$ in samples without a feldspar phenocryst phase. Because of saussuritization, the An compositions presented here may be less than the An content of plagioclase in the crystallizing magma.

When positive identification of potassic feldspar can be made it is based on the absence of lamellar twinning, an accompanying negative optic sign, and a smaller optic axial angle (as determined from the curvature of isogyres or Mallard's method). Sodic plagioclase ($<An_{20}$) and potassic feldspar can have similar optical properties. Relative refractive indices can be used if the thin-section is made using Canada balsam. These thin-sections, however, were made using a synthetic epoxy and relative relief could not be used to identify the feldspar present. In cases such as these, the presence of non-lamellar twinning (Manebach or Braveno) or textural association (micrographic, granophyric or myrmekitic) is used to identify the presence of potassic feldspar. This method is very inexact and rock staining or electron microprobe analyses should be performed to positively identify the composition(s) of the feldspar(s).

The potassic feldspar most likely to be found in these rocks is 1) orthoclase and/or 2) sanidine as rims around plagioclase phenocrysts in quenched samples. Phyric potassic feldspar is present only in samples with silica contents greater than 72 weight-percent. Plagioclase phenocrysts are usually mantled by a thin rim of untwinned feldspar which could be plagioclase, sanidine or perhaps adularia. Adularia is a common potassic metasomatic alteration product found as mantles around plagioclase phenocrysts (Glazner, 1988).

The opaque oxide minerals of Group A are mostly from the magnetite series of the spinel group, but also include haematite and possibly ilmenite. These oxides are present in <3% of the Group A samples and only magnetite can be conclusively deemed primary: It is included in feldspar, augite, and hornblende phenocrysts. It is also probable that some magnetite is secondary, i.e.- when it is clearly associated with such alteration minerals as chlorite or calcite and occurs in veins or along crystal boundaries. Red mantles (haematite, maghemite, goethite?) around magnetite indicate that oxidation has occurred. The variations in opaque oxide mineralogy and the relative timing of different phases is discussed in the following chapter on paleomagnetism.

Chlorite makes up ≈4 modal percent. It is often an alteration product of hornblende, but also psuedomorphs or

is intergrown with biotite. Chlorite is usually associated with calcite and opaque minerals and occurs interstitially. It can be either optically positive or negative, indicating variable degrees of oxidation.

Accessory phases in Group A samples include epidote, calcite, smectite (?), sphene, and apatite. These phases are present in abundances of less than 1%. They typically occur interstitially or as mantles around phenocryst phases.

The assembladge of chlorite, calcite, minor epidote, sericite and opaque minerals in Group A dikes is typical of hydrothermal alteration of calcic plagioclase, pyroxene, amphibole, and biotite (Deer et al., 1966). It is difficult to determine the extent to which this alteration is primary (deuteric) or secondary (later hydrothermal circulation of meteoric fluids). That these minerals sometimes occur as vein-fillings suggests that some of the alteration could be late syn-emplacement or post-emplacement.

Group B. Group B samples from the Crossman block (sites 27-38 and 46-48) are texturally and compositionally distinct from Group A. Group B samples, though also holocrystalline, allotriomorphic, porphyritic, and generally fine-grained, entirely lack quenching textures. Phenocrysts in granophyric, concertal, or micrographic groundmass are the norm (fig. 6). These textures are typical of intrusive igneous rocks. The dikes in Group B are not consistently
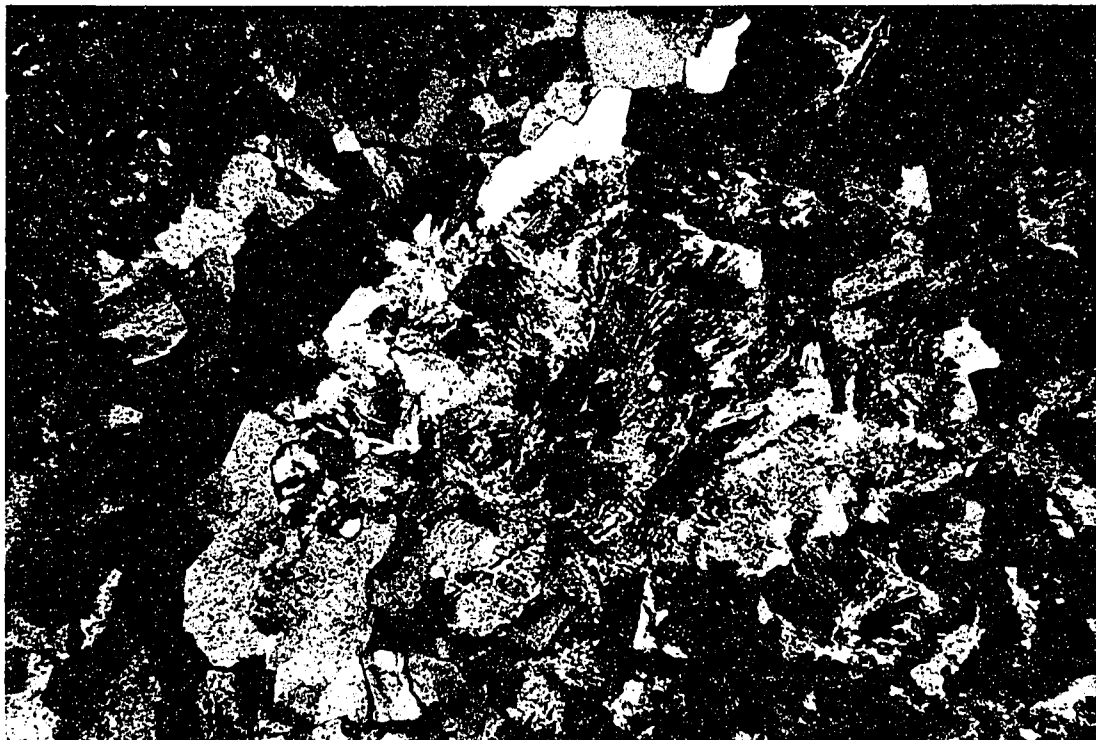
Figure 6. Granophyric texture from site 36:
intergrowths of alkali feldspar(?) and quartz around
phenocrysts of plagioclase. Field-of-view width ≈2.0 mm.

thicker than those of Group A, so slower rates of cooling related to thickness can not be called upon to explain this difference. It is possible that Group B dikes were intruded into relatively hotter country rock than Group A samples, i.e.-intrusion at greater depth or in an area with an elevated geothermal gradient. Foster et al. (1990) have presented $^{40}Ar/^{39}Ar$ isotopic data which suggest that a geothermal variation of 200-300°C existed in the Mohave Mountains. They propose that the western part of the Mohave Mountains was at temperatures of <100°C in the Early Miocene, while temperatures in the eastern Mohave Mountains were at 200-300°C. In this scenario, Group B dikes may have experienced a slower rate of cooling than Group A.

Plagioclase compositions range from $An_{32-62}$ where phenocrysts and groundmass coexist; this is somewhat higher than in Group A, but Group B samples are less saussuritized and perhaps provide a better record of the more calcic plagioclase compositions. When plagioclase is not present as phenocrysts, compositions range from $An_{32-52}$. Again, this is a wider range of compositions than in Group A and may be due to a protracted cooling history (as compared to the quenching experienced by Group A dikes).

Hornblende forms phenocrysts in 65% of the Group B samples and also occurs in the groundmass. The average total abundance of hornblende in Group B samples is 17% (as

compared to 10% hornblende in only 16% of Group A samples).
It is also more chloritized in Group B than in Group A.

Epidote increases from an accessory phase in Group A to
a principal phase in Group B. It occurs in variable
abundances and makes up as much as 46% of the thin-section.
Where abundant, it occurs as large, round crystals or
crystal aggregates. It is mantled by a blue-green amphibole
(actinolite?) which grades into a brown amphibole (fig. 7).
No replacement relationships are visible but it is likely
that epidote has thoroughly replaced another mineral phase
(calcic plagioclase?), which provided the nucleation site
for subsequent epidote crystal growth.

Chlorite is as widespread in Group B as in Group A, but
its abundance is more variable (1-10%). The opaque oxide
minerals have similar compositions, crystal habits, and
abundances in the two groups. Calcite, apatite, sericite,
and sphene occur as accessory phases. Augite is not present
in Group B samples; if it were originally present, it has
been thoroughly replaced by amphibole (actinolite ?) and
chlorite.

The iron-, magnesium-, and calcium- bearing phase(s)
have been the most affected by alteration in Group B
samples, as evidenced by the abundance of epidote and
chlorite. The high percentage of epidote in Group B samples
suggests extensive alteration, possibly under greenschist
facies conditions. This could be consistent with dike
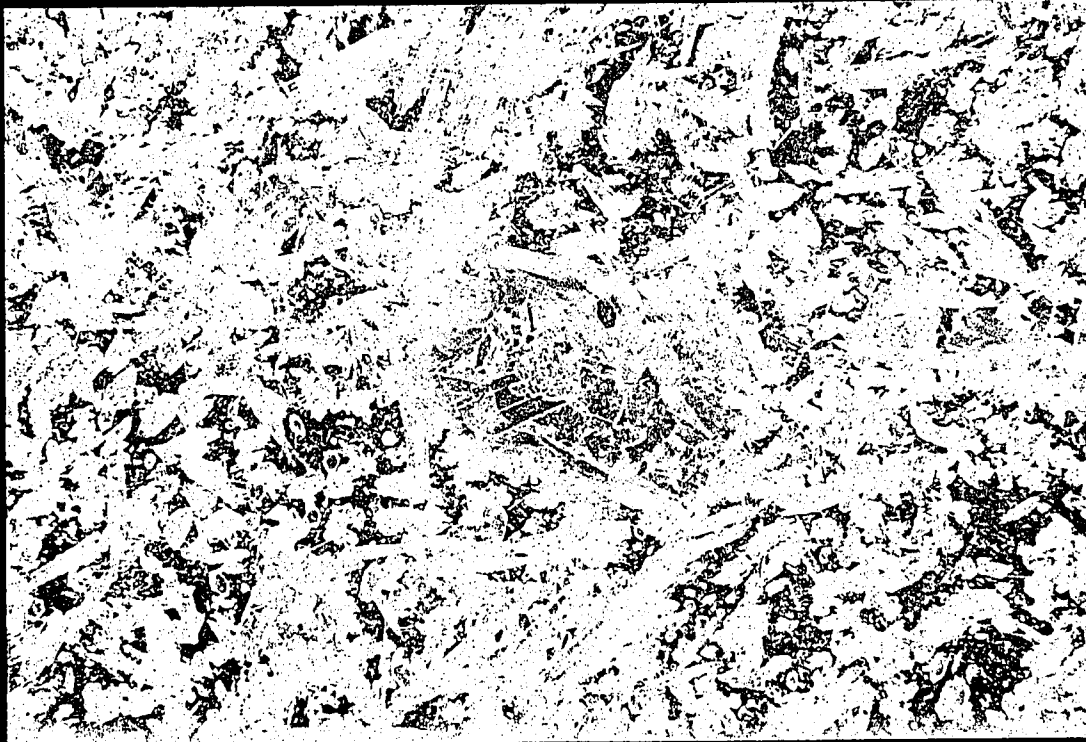
Figure 7. Alteration relationships typical in Group B samples (from site 32). Note high-relief epidote in center of crystal, surrounded by blue-green amphibole (actinolite?), which is in turn mantled by brown hornblende. Fine-grained, brown hornblende common in groundmass. Field-of-view ≈3.0 mm.

emplacement at depths of 10-12 km, as suggested by Howard et al. (1982). There is a greater abundance of groundmass hornblende in Group B samples than in Group A samples, even though overall phenocryst abundances are about the same. If Group B samples represent dike emplacement at depths of 10-12 km, it is possible that the ambient crustal temperatures at those depths resulted in a protracted cooling history, allowing for in-situ nucleation and growth of igneous hornblende in the groundmass.

Standard Wash Block

Standard Wash block samples are typically porphyritic to microporphyritic, fine-grained, holocrystalline, and allotriomorphic. Samples from this block are characterized by phenocryst phases in 1) a felty groundmass of plagioclase laths with or without interstitial quartz, or 2) a concertal groundmass of feldspar and quartz. Dikes from the Standard Wash block also exhibit spherulitic textures and chilled margins are common. These textures suggest hypabyssal intrusion and are similar to the textures associated with Group A from the Crossman block.

Phenocryst or microphenocryst phases are plagioclase and/or augite. Both phases are strongly zoned. Plagioclase phenocryst concentrations vary from 5-20% and plagioclase has an average composition of $An_{50}$. The determination of feldspar compositions in this block is subject to the same

limitations identified in the Crossman block. Augite is present in concentrations of about 3%.

Chlorite, opaque oxide minerals, calcite, and sericite are minor phases (<10%). Chlorite exibits variable degrees of oxidation, ranges in concentration from 1-10%, and commonly forms pseudomorphs after biotite. The opaque oxide minerals are also oxidized, as exemplified by haematite mantles. Opaque oxide concentrations are typically about 2%. Calcite is present in abundances of 1-2%. Sericite is present as an alteration product of feldspar in concentrations of about 3%. Accessory phases include hornblende, biotite, epidote, sphene, zircon, and smectite.

The presence of chlorite, calcite, and sericite again suggests hydrothermal alteration. The narrow range of plagioclase phenocryst and groundmass compositions in samples from the Standard Wash block suggests that these dikes cooled relatively quickly. The spherulitic textures also suggest quick cooling, as well as shallow depths of emplacement.

## Discussion

### Hydrothermal Alteration

It is difficult to determine whether primary (deuteric) or secondary (meteoric) hydrothermal circulation was the driving mechanism for the alteration which is present in all of the dike samples from the Mohave Mountains. Hydrothermal

circulation may have been driven by the latent heat associated with Tertiary volcanism. The main volcanic center in the Mohave Mountains is located a short distance south of the Castle Rock fault (fig. 2). Magmatic activity, however, is not restricted to this area, as evidenced by the dike swarm which cross-cuts the whole of the Crossman block, basement and lava flows alike. Work by Jaeger (1959) suggests that gabbroic dikes which are ≈10 m thick and intruded into cool, wet country rock near the surface will solidify within one year. Furthermore, the country rock 5 m from the dike contact will not be reheated to temperatures above ≈300°C. In this case, a long-lived hydrothermal event is not expected.

Multiple intrusions, such as those associated with a dike swarm, may increase the ambient temperature of the country rock. Dikes intruded into warmer country rock will take longer to solidify and the distance from the intrusive contact at which country rock is heated to ≈300°C will also increase. It seems likely that any associated hydrothermal circulation will also have a longer life-span. Cathles (1977) and Norton and Knight (1977) have modelled secondary hydrothermal circulation associated with cooling plutons and reached similar conclusions. Hydrothermal circulation of 200-300°C will result from the intrusion of a pluton that is 3.75 km wide and 4.5 km high, if emplaced 2 km beneath the surface at a temperature of 870°C (Norton and Knight, 1977).

Norton and Knight assumed an initial geothermal gradient of 20°C/km and that the pluton was intruded into stratified country rocks in which some water was present (model P4 of Norton and Knight, 1977). Hydrothermal circulation begins to wane about 5000 years after the pluton is emplaced. Hydrothermal circulation ceases sooner (in a non-linear fashion) for smaller plutons (Cathles, 1981). The life-span of secondary hydrothermal circulation associated with the dike swarm of the Mohave Mountains is likely to be greater than that of Jaeger's (1959) single dike intrusion and less than that of the model pluton: that is, tens of years to several thousands of years.

Group B samples are more extensively altered than Group A samples and the presence of epidote and actinolite (?) suggests higher temperatures for this alteration (greenschist facies). Alternatively, hydrothermal circulation may have simply lasted longer deeper in the crust; thus Group B samples are more altered than samples of either Group A or the Standard Wash block. In either case, the secondary (non-deuteric) hydrothermal alteration of the Crossman block and Standard Wash block probably occurred within several thousand years after dike emplacement. Later alteration resulting from hydrothermal circulation associated with the last stages of basaltic volcanism in the region can not be discounted, but this would have occurred on a much more localized scale.

Potassic Metasomatism

Glazner (1988) characterized severe potassic metasomatism associated with crustal extension using field, petrographic, isotopic, and geochemical data from lower Miocene volcanic rocks in the Sleeping Beauty area of the Mojave Desert, California. This type of alteration is widespread in the southwestern United States (Chapin and Glazner, 1983). The replacement of plagioclase by adularia and the oxidation of mafic minerals to clots of haematite and unidentified opaque alteration products which form pseudomorphs after hornblende and iddingsite are characteristic of potassic metasomatism. In the Mohave Mountains, plagioclase phenocrysts are saussuritized. Very thin, low-birefringent rims around plagioclase phenocrysts are common and they may be adularia. However, primary hornblende and augite in samples from the Mohave Mountains are generally pristine, even in the presence of abundant epidote. If the dike swarm of the Mohave Mountains has experienced potassic metasomatism, it was to a much lesser extent than that of the Sleeping Beauty area. The lack of obvious potassic metasomatism may be consistent with relatively short-lived hydrothermal circulation in the Mohave Mountains.

Summary

1.  Group A samples from the Crossman block were cooled quickly (quenched) upon dike emplacement, thus indicating very shallow intrusion.  Quenching may account for the disequilibrium-fractional crystallization textures present in these samples.  Group A samples were also subject to hydrothermal alteration which probably occurred within a few thousand years after dike emplacement.

2.  Dike emplacement in the Standard Wash block also occurred at shallow depths, accompanied by quick cooling.  These samples also experienced hydrothermal alteration which likely occurred soon after dike emplacement.

3.  Dikes of Group B in the Crossman block record emplacement at depth, accompanied by a slower rate of cooling.  This is evidenced by granophyric and concertal igneous textures and a greater range of compositions in groundmass plagioclase.  Group B samples were extensively deuterically/hydrothermally altered, probably shortly after dike emplacement.  The greater degree of alteration of these samples may reflect alteration at higher temperatures or may reflect a longer or more vigorous period of active hydrothermal alteration.  Longer-lived hydrothermal circulation for Group B samples would be consistent with a slower rate of cooling which resulted from dike emplacement at depth.

4.  Textures associated with severe potassic metasomatism are absent, although minor potassic metasomatism may have affected these rocks.  A lesser degree of metasomatism is consistent with the relatively short-lived hydrothermal circulation postulated for the dike swarm of the Mohave Mountains.

GEOCHEMISTRY

## Sampling and Analytical Techniques

Eighteen samples representative of the Tertiary dike swarm in the Mohave Mountains were analysed for major-element chemistry. Five analyses are from the Standard Wash block and the remainder are from the Crossman block (table 1, fig. 2). These samples, taken from paleomagnetic drill cores, are from the interiors and chilled margins of the dikes. To eliminate possible iron contamination from the drill-bit, the samples were sanded on all perimeters using a corundum lap-wheel. Geochemical analyses were performed by the U.S. Geological Survey, Branch of Analytical Chemistry using X-ray fluoresence spectrometry. These analyses are accurate to within measured precision, with an absolute standard deviation of 0.3 wt.% for $SiO_2$, 0.2 wt.% for $Al_2O_3$, and $\leq 0.1$ wt.% for all other oxides (Bacon and Druitt, 1988). An additional six analyses from the Crossman block (J. Nakata, unpublished data, also generated at the U.S.G.S. via the same technique) have been included in the data set. Analyses of Nakata are not accompanied by petrographic descriptions. FeO and $Fe_2O_3$ were calculated assuming 20% of $Fe_TO_3$ is $Fe_2O_3$. All of the analyses are presented as weight percent oxides in table 2, recalculated to 100% (volatile-free).

Table 2. Major element and calculated normative chemistry. Samples recalculated to 100% (volatile-free); Fe reported as FeO and Fe2O3; JN are samples from J. Nakata (unpublished); (c) = sample from chilled margin.

| Site # | 9 | 45(c) | JN | 46 | JN | 37 | 47 | 16 | JN |
|---|---|---|---|---|---|---|---|---|---|
| USGS ID | 5H026 | 7J159 | JN090 | 7J162 | JN163A | 5H108 | 7J168 | 5H047 | JN163 |
| SiO2 | 50.05 | 50.19 | 50.73 | 51.63 | 51.71 | 53.00 | 53.21 | 55.38 | 56.46 |
| Al2O3 | 16.96 | 15.35 | 17.99 | 18.60 | 14.95 | 14.66 | 16.18 | 16.36 | 16.65 |
| Fe2O3 | 2.03 | 1.91 | 1.72 | 1.73 | 2.05 | 1.69 | 1.82 | 1.87 | 1.68 |
| FeO | 7.31 | 6.89 | 6.20 | 6.23 | 7.39 | 6.09 | 6.55 | 6.72 | 6.05 |
| MgO | 6.21 | 5.12 | 6.98 | 3.68 | 7.03 | 7.88 | 6.00 | 5.07 | 4.85 |
| CaO | 7.44 | 9.15 | 10.40 | 7.61 | 8.62 | 8.29 | 8.02 | 6.39 | 7.01 |
| Na2O | 4.10 | 3.69 | 2.86 | 4.28 | 2.87 | 3.20 | 3.79 | 3.70 | 3.63 |
| K2O | 3.04 | 4.73 | 1.30 | 3.18 | 2.47 | 2.91 | 1.93 | 2.65 | 1.76 |
| TiO2 | 1.91 | 2.01 | 1.33 | 2.01 | 1.96 | 1.44 | 1.83 | 1.39 | 1.41 |
| P2O5 | .81 | .74 | .37 | .95 | .80 | .72 | .54 | .34 | .37 |
| MnO | .14 | .22 | .12 | .11 | .15 | .11 | .13 | .13 | .13 |
| LOI | 4.07 | 7.45 | 2.37 | .52 | 1.62 | 1.24 | 3.14 | 2.75 | 2.80 |
| TOTAL | 100.00 | 100.00 | 100.00 | 100.00 | 100.00 | 100.00 | 100.00 | 100.00 | 100.00 |

CIPW Norms

| | 9 | 45(c) | JN | 46 | JN | 37 | 47 | 16 | JN |
|---|---|---|---|---|---|---|---|---|---|
| q | --- | --- | --- | --- | --- | --- | --- | 1.45 | 5.74 |
| or | 17.97 | 27.95 | 7.68 | 18.79 | 14.60 | 17.20 | 11.41 | 15.66 | 10.40 |
| ab | 25.18 | 10.67 | 24.20 | 31.06 | 24.29 | 27.08 | 32.07 | 31.31 | 30.72 |
| an | 18.90 | 11.35 | 32.41 | 22.15 | 20.62 | 17.04 | 21.44 | 20.21 | 23.94 |
| c | --- | --- | --- | --- | --- | --- | --- | --- | --- |
| ne | 5.16 | 11.13 | --- | 2.79 | --- | --- | --- | --- | --- |
| di | 10.34 | 23.82 | 13.54 | 7.70 | 13.71 | 15.59 | 12.01 | 7.58 | 6.86 |
| hy | --- | --- | 9.63 | 14.19 | --- | 7.17 | 12.66 | 17.66 | 16.36 |
| ol | 14.02 | 6.77 | 6.65 | 8.98 | 4.05 | 9.06 | 3.04 | --- | --- |
| mt | 2.94 | 2.77 | 2.49 | 2.51 | 2.97 | 2.45 | 2.64 | 2.71 | 2.44 |
| il | 3.63 | 3.82 | 2.53 | 3.82 | 3.72 | 2.73 | 3.48 | 2.64 | 2.68 |
| ap | 1.88 | 1.71 | 0.86 | 2.20 | 1.85 | 1.67 | 1.25 | 0.79 | 0.86 |

Table 2 con't.

| Site # | 42(c) | 41 | JN | 35 | 5(c) | 5 | 44 | JN | 27 |
|---|---|---|---|---|---|---|---|---|---|
| USGS ID | 7J138 | 7J137 | JN190A | 5H102 | 5H016 | 5H014 | 7J154 | JN161 | 5H082 |
| SiO2 | 57.16 | 59.13 | 60.78 | 64.58 | 65.21 | 67.76 | 68.92 | 69.88 | 70.15 |
| Al2O3 | 16.42 | 17.15 | 16.31 | 16.35 | 15.99 | 15.78 | 15.42 | 15.88 | 15.63 |
| Fe2O3 | 1.59 | 1.23 | 1.32 | .91 | .90 | .70 | .60 | .48 | .46 |
| FeO | 5.74 | 4.42 | 4.75 | 3.27 | 3.24 | 2.53 | 2.16 | 1.74 | 1.67 |
| MgO | 3.57 | 4.27 | 3.60 | 1.88 | 2.08 | 1.32 | 1.24 | .77 | .64 |
| CaO | 4.66 | 2.85 | 5.52 | 3.65 | 3.27 | 2.96 | .98 | 1.23 | 1.43 |
| Na2O | 4.34 | 5.24 | 3.38 | 4.33 | 4.10 | 3.99 | 4.79 | 4.41 | 4.70 |
| K2O | 4.07 | 4.42 | 3.00 | 3.88 | 4.17 | 4.17 | 5.20 | 4.95 | 4.69 |
| TiO2 | 1.71 | .97 | .99 | .76 | .76 | .59 | .50 | .40 | .38 |
| P2O5 | .60 | .21 | .25 | .32 | .22 | .17 | .14 | .14 | .15 |
| MnO | .13 | .13 | .10 | .07 | .07 | .04 | .05 | .11 | .10 |
| LOI | 4.51 | 4.40 | 2.20 | 1.69 | 2.80 | 4.31 | 1.72 | .65 | .69 |
| TOTAL | 100.00 | 100.00 | 100.00 | 100.00 | 100.00 | 100.00 | 100.00 | 100.00 | 100.00 |

CIPW Norms

| | | | | | | | | | |
|---|---|---|---|---|---|---|---|---|---|
| q | 0.97 | --- | 11.47 | 13.44 | 14.46 | 19.48 | 16.35 | 20.83 | 20.24 |
| or | 24.05 | 26.12 | 17.73 | 22.93 | 24.64 | 24.64 | 30.73 | 29.25 | 27.72 |
| ab | 36.72 | 44.34 | 28.60 | 36.64 | 34.69 | 33.76 | 40.53 | 37.32 | 39.77 |
| an | 13.30 | 10.22 | 20.47 | 13.72 | 12.91 | 12.83 | 3.95 | 5.19 | 6.11 |
| c | --- | --- | --- | --- | --- | --- | 0.47 | 1.37 | 0.58 |
| ne | --- | --- | --- | --- | --- | --- | --- | --- | --- |
| di | 4.83 | 2.07 | 4.32 | 1.89 | 1.54 | 0.61 | --- | --- | --- |
| hy | 13.17 | 7.31 | 13.04 | 7.88 | 8.51 | 6.15 | 5.83 | 4.26 | 3.84 |
| ol | --- | 5.85 | --- | --- | --- | --- | --- | --- | --- |
| mt | 2.31 | 1.78 | 1.91 | 1.32 | 1.30 | 1.01 | 0.87 | 0.70 | 0.67 |
| il | 3.25 | 1.84 | 1.88 | 1.44 | 1.44 | 1.12 | 0.95 | 0.76 | 0.72 |
| ap | 1.39 | 0.49 | 0.58 | 0.74 | 0.51 | 0.39 | 0.32 | 0.32 | 0.35 |

Table 2 con't.

| Site # | 43 | 36 | 17 | 19 | JN | 39 |
|---|---|---|---|---|---|---|
| USGS ID | 7J149 | 5H105 | 5H050 | 5H056 | JN190B | 7J081 |
| SiO2 | 70.24 | 72.41 | 72.60 | 73.11 | 73.59 | 73.81 |
| Al2O3 | 14.99 | 14.46 | 14.17 | 13.92 | 14.20 | 14.35 |
| Fe2O3 | .54 | .38 | .41 | .34 | .36 | .30 |
| FeO | 1.94 | 1.39 | 1.49 | 1.22 | 1.30 | 1.08 |
| MgO | 1.09 | .60 | .70 | .48 | .60 | .35 |
| CaO | .84 | 1.56 | 1.56 | 1.80 | 1.23 | .77 |
| Na2O | 4.63 | 4.45 | 3.55 | 3.35 | 3.07 | 3.61 |
| K2O | 5.14 | 4.32 | 5.09 | 5.40 | 5.24 | 5.49 |
| TiO2 | .44 | .34 | .32 | .29 | .30 | .24 |
| P2O5 | .12 | .06 | .07 | .06 | .08 | .00 |
| MnO | .04 | .04 | .03 | .02 | .02 | .00 |
| LOI | 1.53 | 1.60 | 2.09 | 2.54 | 2.42 | 1.95 |
| TOTAL | 100.00 | 100.00 | 100.00 | 100.00 | 100.00 | 100.00 |

CIPW Norms

| | 43 | 36 | 17 | 19 | JN | 39 |
|---|---|---|---|---|---|---|
| q | 19.43 | 25.26 | 27.40 | 28.19 | 31.63 | 29.02 |
| or | 30.38 | 25.53 | 30.08 | 31.91 | 30.97 | 32.44 |
| ab | 39.18 | 37.66 | 30.04 | 28.35 | 25.98 | 30.55 |
| an | 3.38 | 6.72 | 7.28 | 7.00 | 5.58 | 3.82 |
| c | 0.58 | --- | 0.15 | --- | 1.43 | 1.07 |
| ne | --- | --- | --- | --- | --- | --- |
| di | --- | 0.52 | --- | 1.28 | --- | --- |
| hy | 5.18 | 2.99 | 3.67 | 2.07 | 3.13 | 2.21 |
| ol | --- | --- | --- | --- | --- | --- |
| mt | 0.78 | 0.55 | 0.59 | 0.49 | 0.52 | 0.43 |
| il | 0.84 | 0.65 | 0.61 | 0.55 | 0.57 | 0.46 |
| ap | 0.28 | 0.14 | 0.16 | 0.14 | 0.19 | --- |

Analytical Results

The geochemical data are graphically summarized in figure 8 (A-I). Correlation coefficients (r) were _calculated for these data via linear regression and are also shown in figure 8. Silica varies from 50-74 wt% in dike samples from the Mohave Mountains. Covariant, linear trends are defined by iron, magnesium, calcium, titanium, and manganese oxides, decreasing as silica increases. Their negative correlation coefficients are significant at the 95% confidence limit, where $r \geq |0.40|$ is significant at the 95% confidence limit for n=24 (Marsal, 1987). In contrast to these oxides, phosphorus and alumina decrease in a non-linear fashion; the curvature in these trends reduces their negative correlation coefficients to $r=-0.89$ and $-0.64$, respectively, but they are still significant at the 95% confidence level. Sodium does not vary in a systematic fashion, which is reflected in its low and statistically insignificant correlation coefficient of $r=+0.24$. Potassium is positively correlated with silica, with $r=+0.79$. It is apparent that the data from the Standard Wash block contribute to much of the scatter associated with potassium; if these samples are ignored, a better-defined positive correlation with silica exists. The correlation of sodium with silica is not improved when samples from the Standard Wash block are excluded.
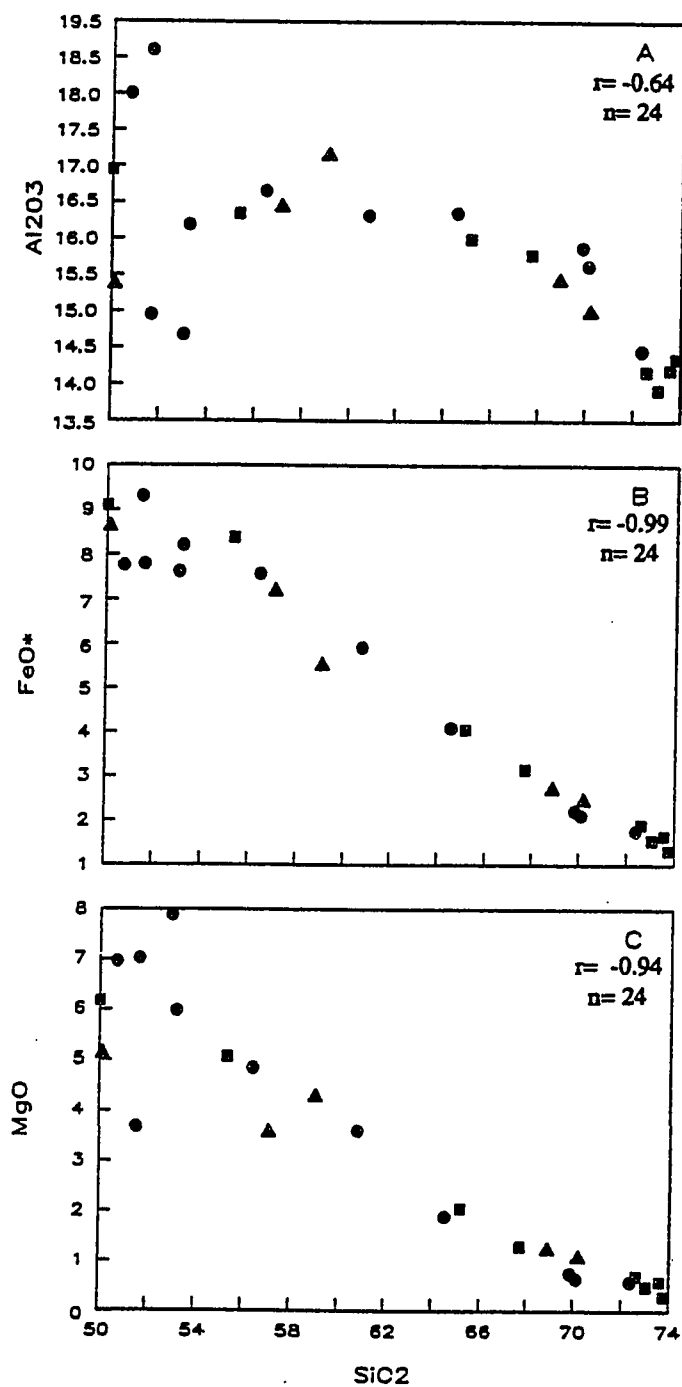
Figure 8. Major element oxide variation against SiO₂.
Circles = Crossman Block samples; squares = samples from
J. Nakata; triangles = Standard Wash Block samples.
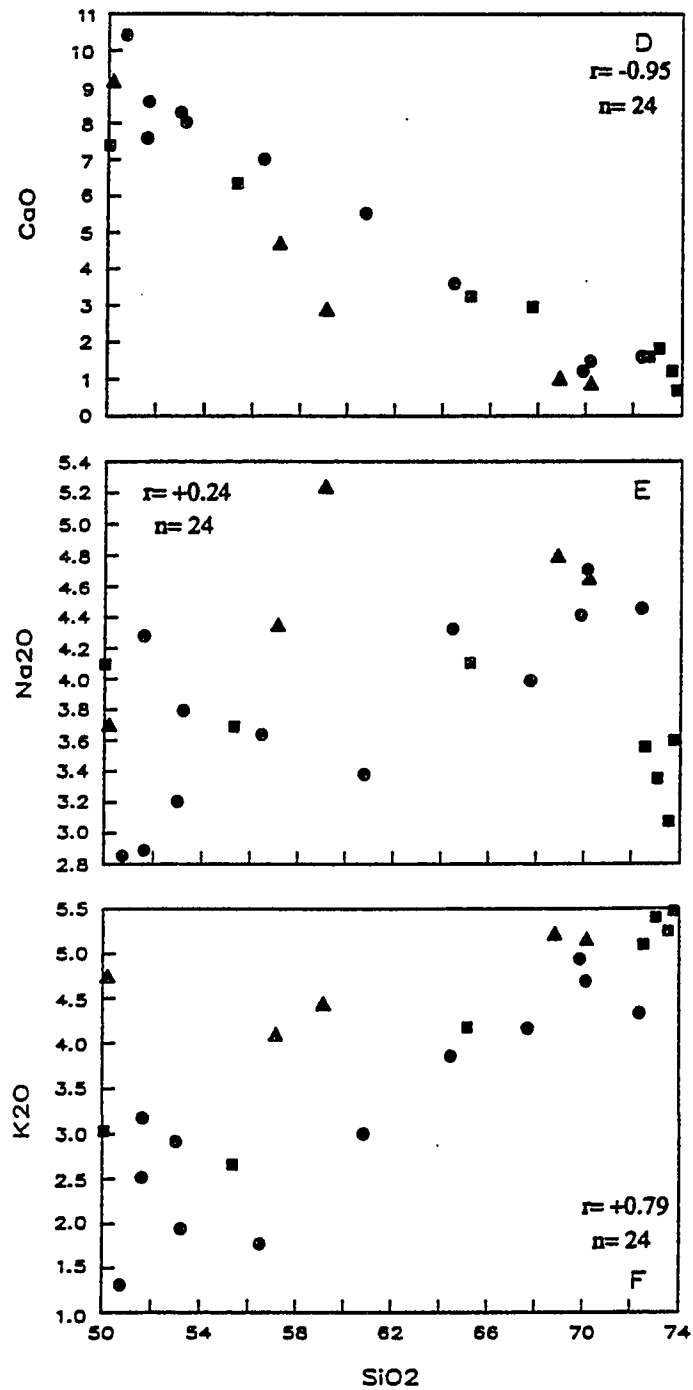
Figure 8 con't.
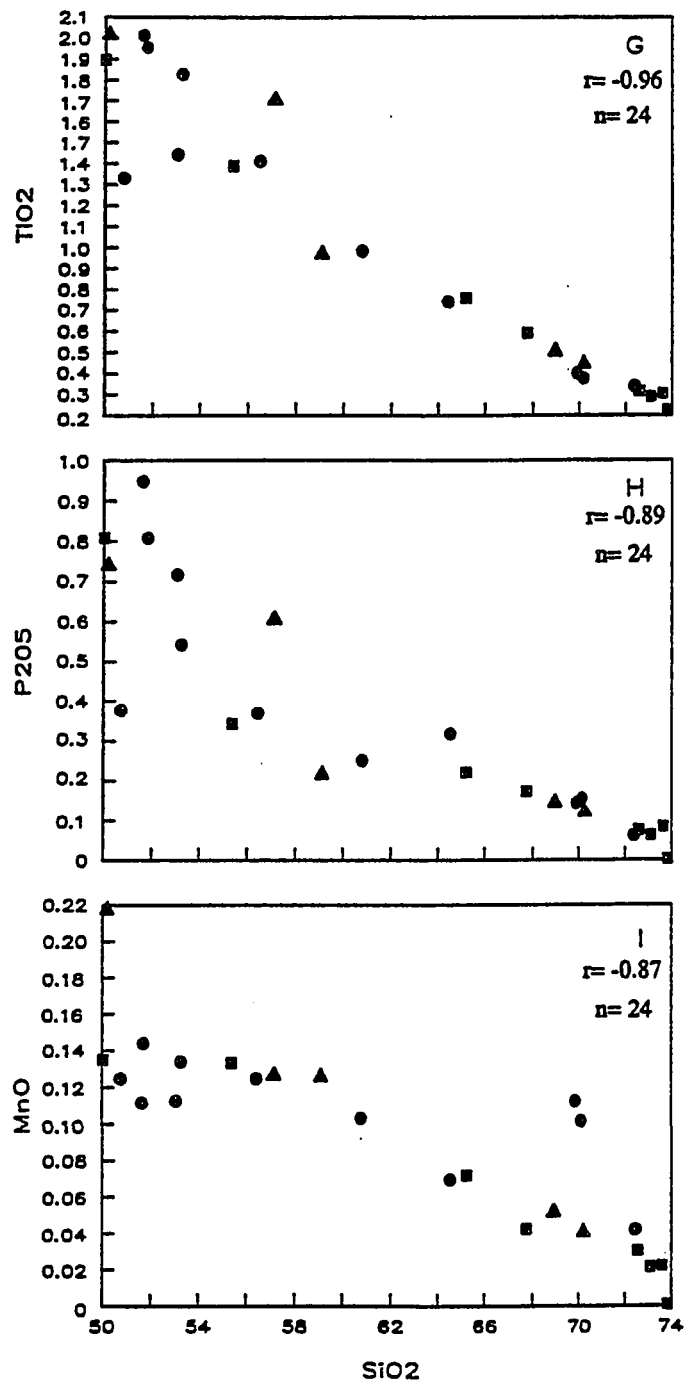
Figure 8 con't.

Most of the samples are altered to varying degrees. High loss-on-ignition values (LOIs) substantiate the degree of alteration noted in the petrographic descriptions (table 2). In particular, the highest LOIs coincide with samples in which feldspars are most strongly saussuritized. In general, samples from the Standard Wash block have higher LOI values than those from the Crossman block, in agreement with the inferred higher degree of alteration in the former area.

On a total alkalis versus silica plot (fig. 9) samples from the dike swarm of the Mohave Mountains span the basalt, basaltic trachyandesite, andesite, trachyandesite, trachydacite, and rhyolite fields of LeBass et al. (1986). High total alkali values for samples from sites 9, 41, 42, 45, and 46 suggest that these samples may be more altered than the rest of the sample suite, though this is not substantiated petrographically. The chemical analyses from the dike swarm define a calcalkaline trend (fig. 10).

## Discussion

### Within Suite Variation

Significant major-element variation in the basaltic samples from the Mohave Mountains (fig. 8, sites 9, 37, 45, 46, 47) suggests that these samples have been variably altered or contaminated. Petrographic observations indicate that sites 45, 46, and 47 are relatively unaltered. In
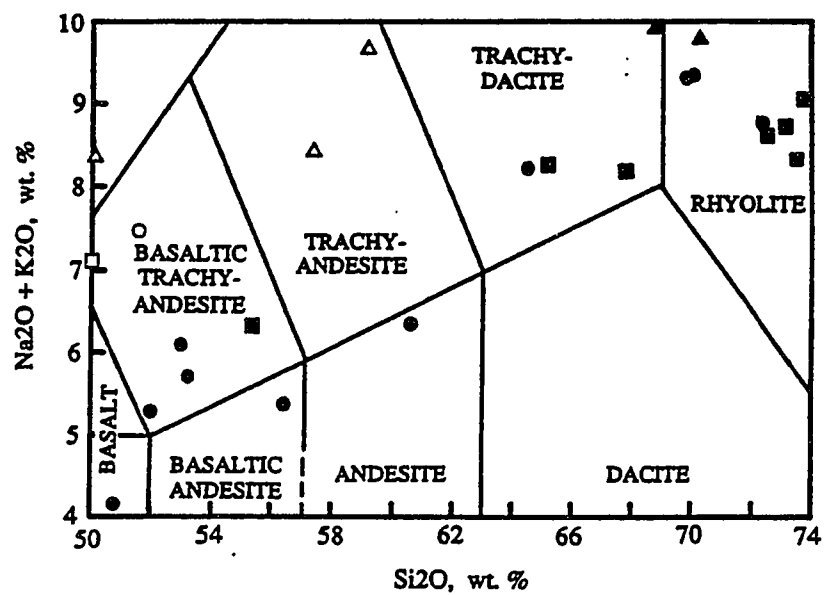
Figure 9. Alkalis against $SiO_2$. Symbols the same as in Fig. 8; open symbols may be altered. Figure after LeBass et al. (1986).
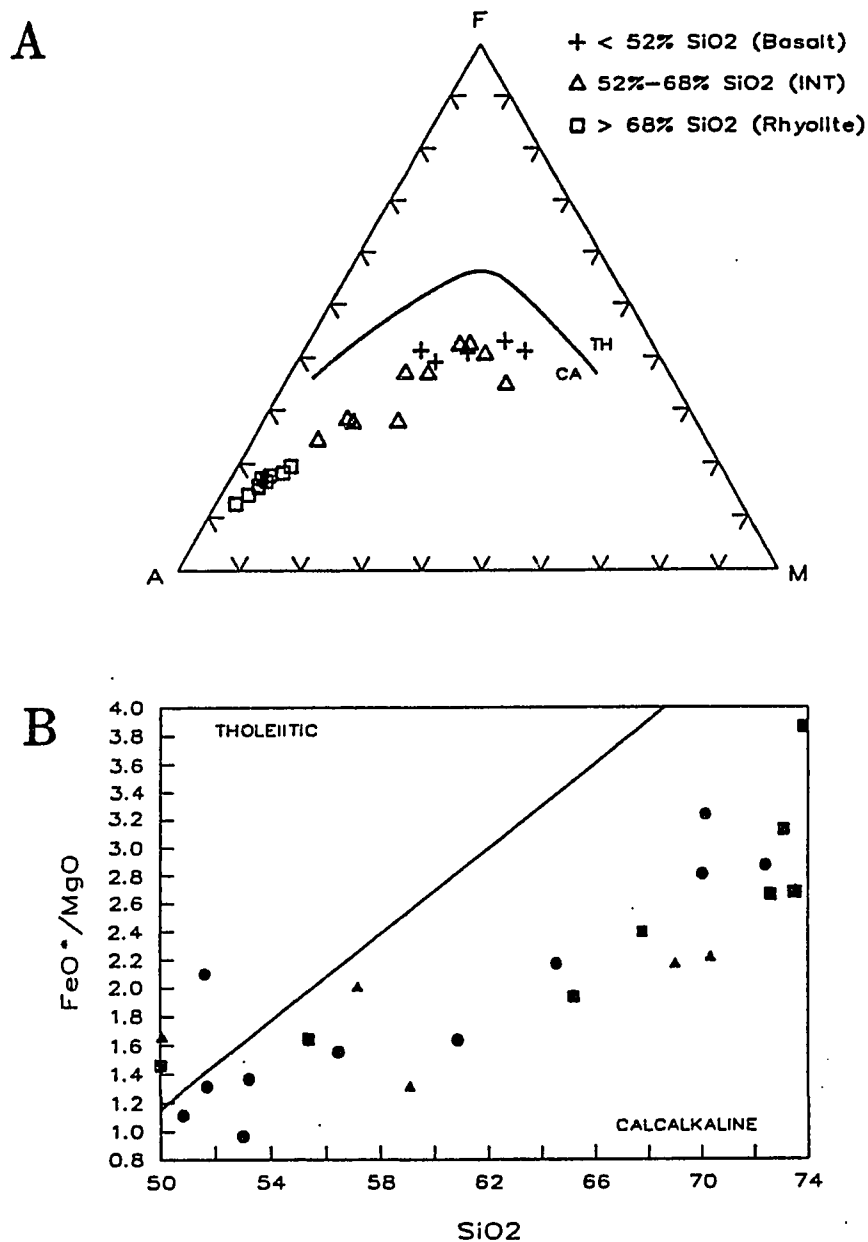
Figure 10. A) AFM diagram: A=Na$_2$O+K$_2$O, F=FeO*, M=MgO. Solid line separates tholeiitic (TH) from calcalkaline (CA) suites (Irvine and Baragar, 1971). B) Differentiation of tholeiitic versus calcalkaline compositions after Miyashiro (1974). Symbols are the same as in Fig. 8

order to further evaluate the possibility of contamination, major element oxides where plotted against MgO/FeO* + MgO (fig. 11). FeO*, MgO, $SiO_2$, $P_2O_5$, and $TiO_2$ should be least susceptible to remobilization during secondary alteration. A grouping distinct from the fractionation trend is defined by all of these elements, with the possible exception of MgO. This group appears fundamentally distinct from the rest of the suite in that it is richer in FeO*, $P_2O_5$, $TiO_2$, and possibly MgO. This variation suggests that 1) these samples were the result of a lesser degree of partial melting than the more primitive (higher MgO/FeO* + MgO ratio) samples and their evolved equivalents, or 2) that they were subjected to a greater amount of crustal contamination than the samples which define the fractionation trend. The non-systematic variation of the major-element oxides for these samples, e.g.- high $P_2O_5$ in site 9, high $TiO_2$ and $K_2O$ in site 45, would seem to argue against uniform crustal contamination. Isotopic and trace-element studies are needed to determine more definitively whether partial melting or crustal contamination was the dominant process involved in generating this variation.

The overall linear patterns of oxide variations in figures 8 and 11 can generally be explained by fractional crystallization. The hyperbolic decrease in phosphorus in figure 8 may indicate early crystallization of apatite and the variation of alumina probably reflects the onset and
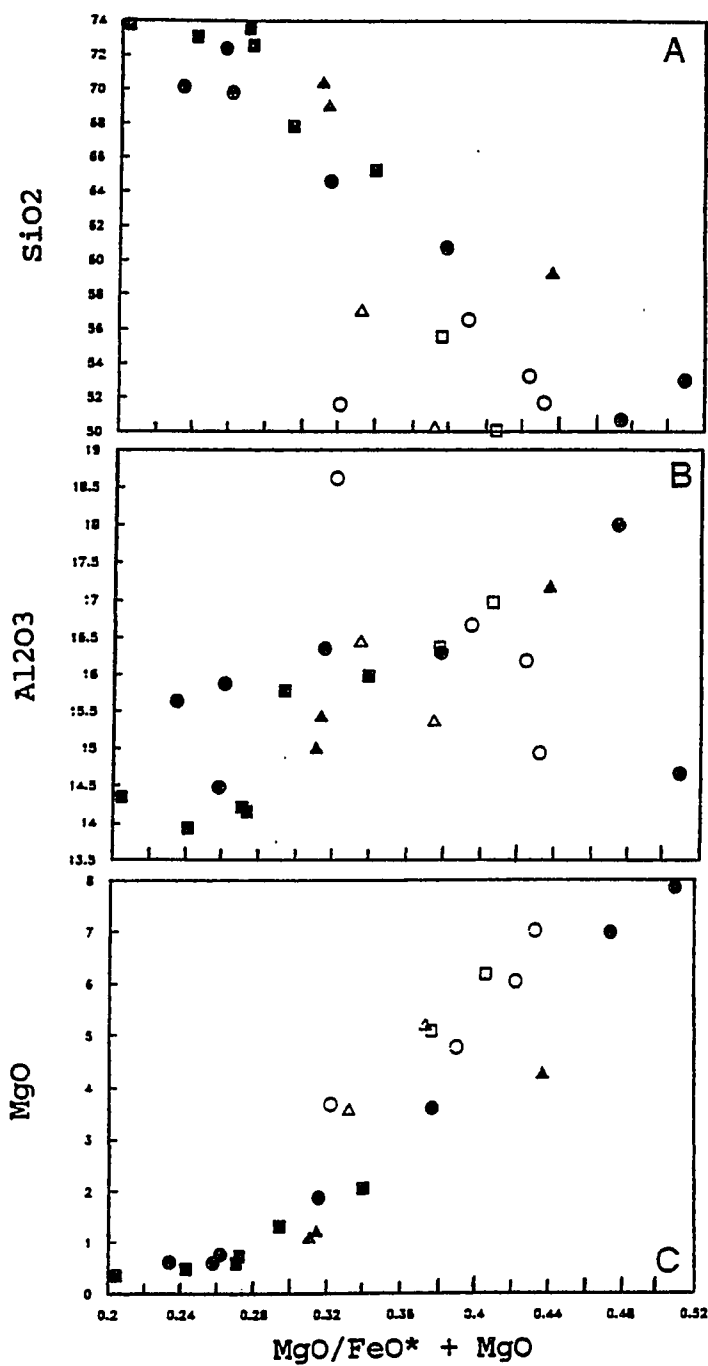
Figure 11. MgO/FeO$^*$ + MgO versus SiO$_2$. Symbols are the same as in Fig. 8; open symbols show the group of samples enriched in MgO, FeO$^*$, P$_2$O$_5$, and TiO$_2$.
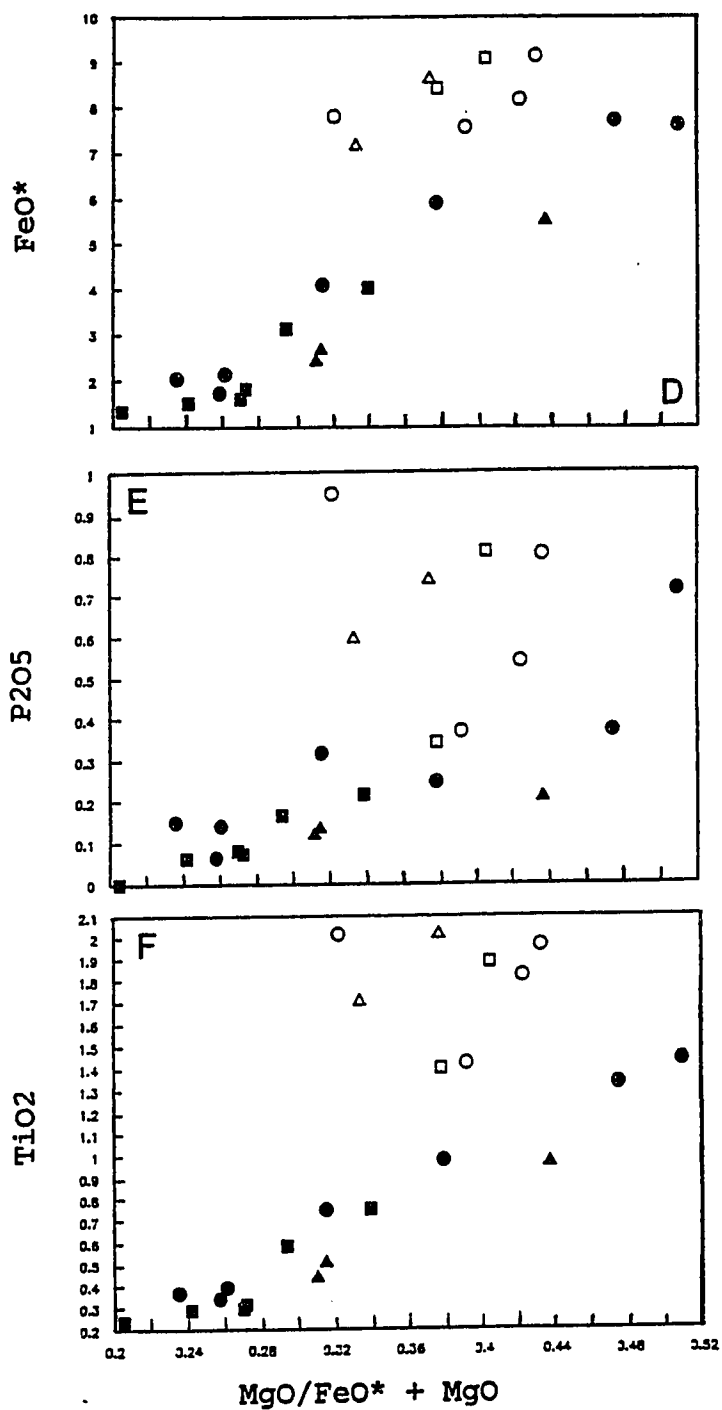
Figure 11 con't.
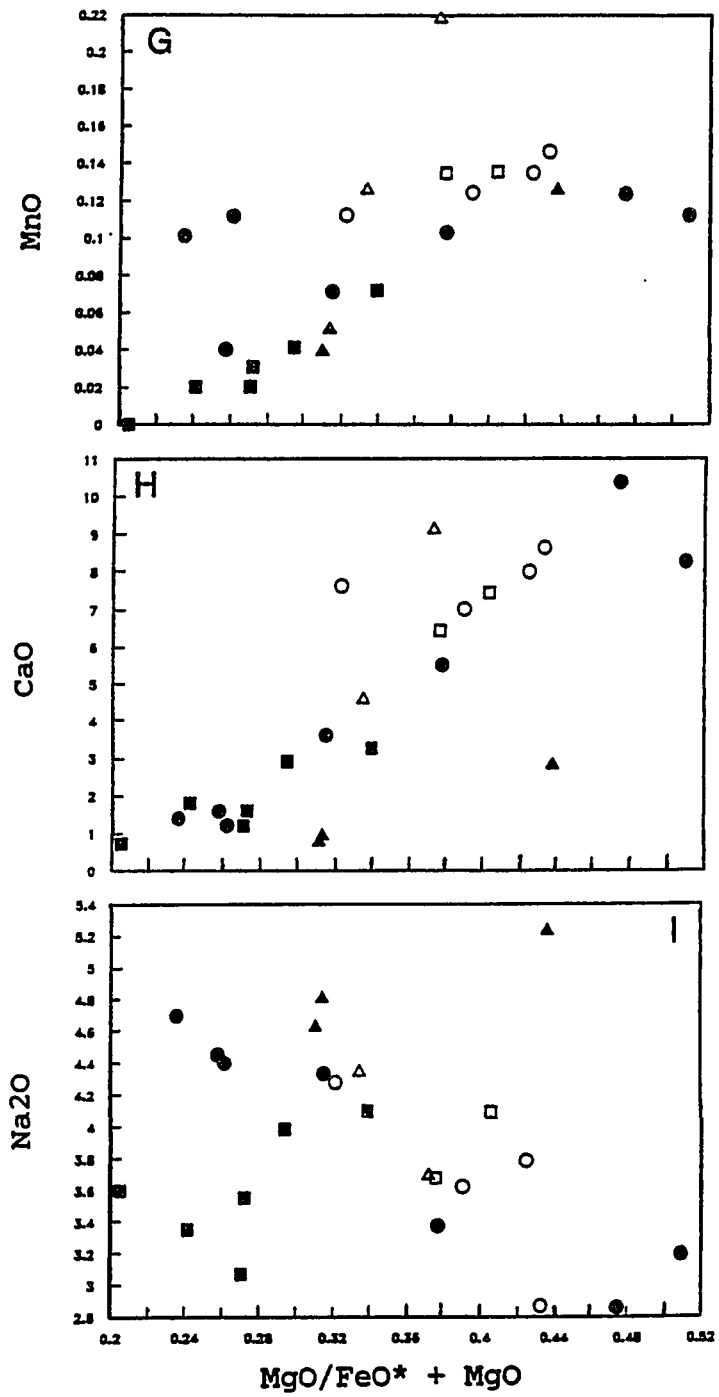
Figure 11 con't.
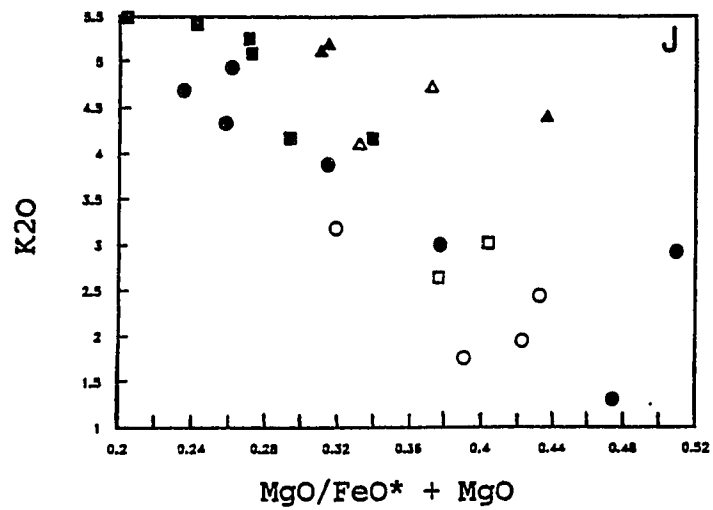
Figure 11 con't.

continued crystallization of plagioclase. The negative correlation of the Fe, Ti, Mg, and Mn oxides in figure 8 further suggests the early crystallization of a mafic phase(s); Fe-Ti oxides, augite, and hornblende are the dominant, early crystallization products in thin-sections. It is interesting that the alteration associated with these samples appears to affect sodium more than potassium or the other oxides. The trend of sodium is difficult to explain under normal fractionation processes and is probably related to hydrothermal alteration.

Potassic Metasomatism

Brooks (1986) and Glazner (1988) documented K-metasomatism in Tertiary volcanic rocks associated with detachment faulting in Arizona. Nielson and Beratan (1990) presented geochemical data from the extrusive equivalents of Mohave Mountain dikes and documented potassium and silica enrichment which they also attributed to metasomatic alteration. The Miocene dike samples of the Mohave Mountains, however, have $K_2O:Na_2O$ ratios typical of isochemical rocks, ranging from 0.7 to 1.7 in basalt to rhyolite, respectively (Brooks, 1986). In figure 12, geochemical data from the dike swarm of the Mohave Mountains have been added to a modified version of a ternary plot of Nielson and Beratan (1990). Olivine normative values have been plotted as negative quartz to illustrate linear trends
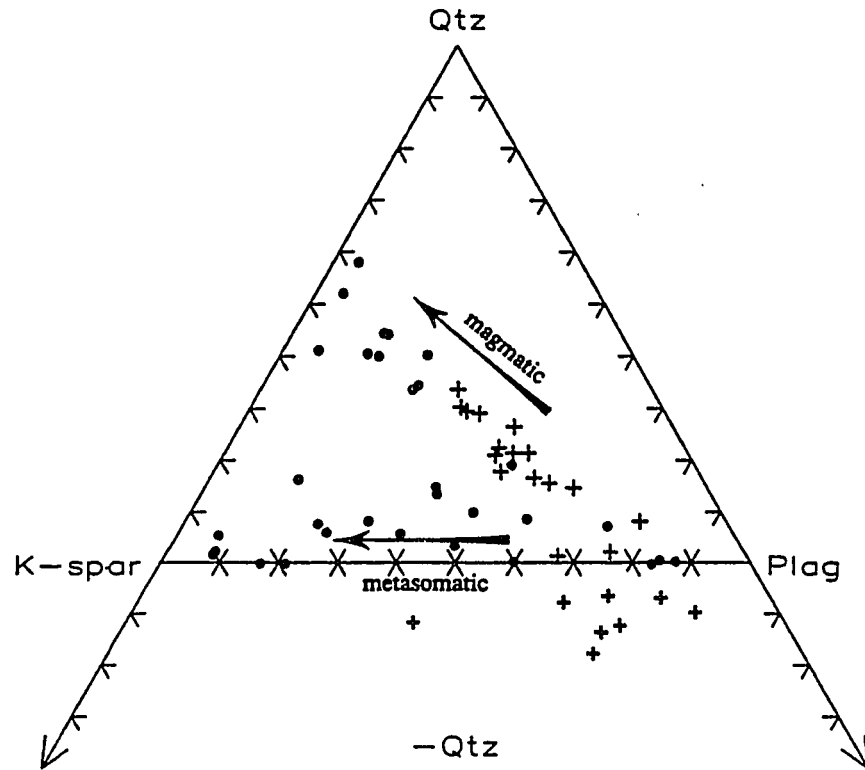
Figure 12. QAP diagram of calculated norms of Miocene lava flows and intrusive rocks. Circles are data from Nielson and Beratan (1990); crosses are analyses from the dikes presented in this study.

in the data set. Two apparent trends are defined by the dike samples. One is consistent with magmatic fractionation patterns and complements the data of Nielson and Beratan (1990). The other trend is defined by the olivine normative samples. The olivine normative samples, with the exception of site 41 and one analysis from Nakata, belong to the group enriched in $FeO^*$, $TiO_2$, and $P_2O_5$ (fig. 11). As discussed above, the variation of the data in this group may be due to crustal contamination or to variable degrees of partial melting in the source region. These samples do not reflect the extreme potassic metasomatic enrichment noted by Nielson and Beratan (1990), Glazner (1988), or Brooks (1986); however, the possibility that some of these samples may record a small degree of potassic metasomatism cannot be discounted.

Chamber's Well Dike Swarm

Howard et al. (1982) suggested that the dike swarm of the Mohave Mountains may be correlative with the Chamber's Well dike swarm of the Whipple Mountains to the SW (fig. 1). The range of rock types within the Chamber's Well dike swarm is somewhat bimodal with high-K, calcalkaline andesites and dacites predominating over younger olivine normative, tholeiitic diabases (Davis et al., 1982; Anderson and Cullers, 1990). Strontium isotopic data from Davis et al. (1982) suggest that the andesite-dacite fractionation series

from the Whipple Mountains has experienced a significant amount of crustal contamination and that it is not comagmatic with the diabase.

In figure 13, representative geochemical data from the Tertiary dike swarm of the Mohave Mountains is compared to data from the Chamber's Well dike swarm. Anderson and Cullers (1990) did not analyze for phosphorus so a comparison to the data reported here is not exact. However, $P_2O_5$ makes up a small percentage (<1.0%) of the dike samples from the Mohave Mountains, thus the data from the Chamber's Well dike swarm lie within the natural variation of the Mohave Mountain data set; this is true for all of the major elements, though only FeO*/FeO* + MgO is shown here.

The major-element chemistry from the Chamber's Well dike swarm is comparable to that of the dike swarm from the Mohave Mountains. The determination of a conclusive cogenetic relationship cannot be made without isotopic and trace-element analyses. If these two suites are related, the lack of calcalkaline basalts and the apparent "bi-modality" of the andesites and dacites of the Chamber's Well suite need to be explained.

Summary

1. The greater amount of scatter in the major-element oxide data (especially the alkali's) and the relatively high LOI values from the Standard Wash block suggests that this
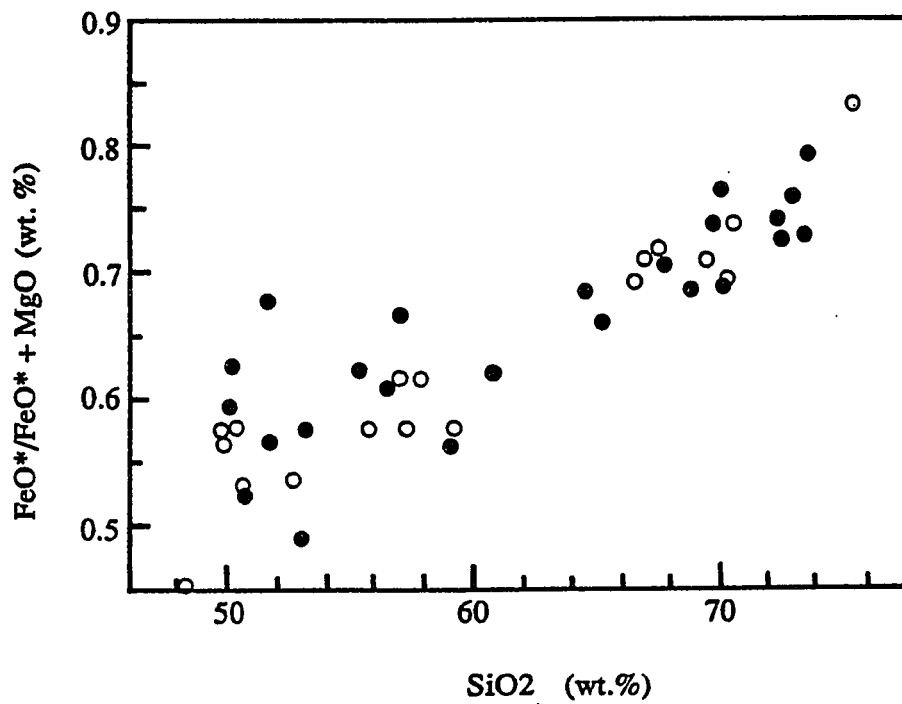
Figure 13. FeO$^*$/Feo$^*$ + MgO versus SiO$_2$. Open symbols = Chamber's Well Dike Swarm (from Anderson and Cullers, 1990); closed symbols = dike swarm of the Mohave Mountains (this study).

block has been more altered than the Crossman block. This
interpretation is also supported by petrographic studies.

2. In general, samples from the dike swarm of the
Mohave Mountains do not appear to have been affected by
extensive potassic metasomatism, in contrast to their
extrusive equivalents.

3. Samples from the dike swarm of the Mohave Mountains
range from basalt to rhyolite and define a calcalkaline
trend. This is interpreted to be a natural magmatic
differentiation trend dominated by crystal fractionation.
Significant oxide variation within the basaltic data
suggests that some samples have experienced variable degrees
of crustal contamination or partial melting.

4. Major-element oxide data from the Chamber's Well
dike swarm of the Whipple Mountains is similar to that
from the dike swarm of the Mohave Mountains.

# GEOCHRONOLOGY

Previous geochronological work in the Mohave Mountains has been summarized by Nakata et al. (in press). Ages from the dike swarm of the Mohave Mountains are poorly resolved, ranging from ≈10 to ≈350 Ma, clustering around 20 ± 1 m.y. These ages were determined on whole-rock and biotite and hornblende mineral separates using conventional K-Ar methods. Nakata et al. have suggested that the poor resolution of the age of the dike swarm may be due to the presence of extraneous (excess) argon, as the older dates are not in agreement with ages inferred from geologic evidence. Nakata and co-workers believe that the Mohave Mountains dike swarm is about 20 Ma based on 1) concordant biotite ages from dacitic dikes, and 2) intrusive relationships between the dikes and the base of the extrusive Tertiary volcanic section, which is 19-23 Ma (Sequence I of Nielson and Beratan, 1990).

In principle, the $^{40}Ar/^{39}Ar$ incremental heating technique of Merrihue and Turner (1966) is capable of distinguishing between undisturbed and disturbed samples, identifying the presence of excess argon, and of recovering the crystallization age or reheating age of a sample that has experienced a thermal or chemical perturbation if argon loss is less than 15-20% (Harrison, 1983). This technique has been applied to samples from the dike swarm of the

Mohave Mountains for several reasons. First, it is an attempt at high precision age determinations for the dikes by establishing whether or not excess radiogenic argon is present in the samples. Ideally, excess radiogenic argon will be released at low temperatures, while the high temperature portion of the age spectra will record the crystallization age of the sample. Second, it is an attempt to gain some information about the thermal history of the dikes by applying this technique to 1) minerals with different closure temperatures for intracrystalline retention of argon (biotite and hornblende), and 2) samples representing shallower and deeper levels of the upper crust, from west to east, respectively. Consequently, some comparison regarding the extent to which the thermal history of the dikes reflects the uplift and cooling history of the Mohave Mountains as summarized by Foster et al. (1990) have been made.

## Sampling and Analytical Techniques

Ten samples of dikes and one sample of basement gneiss were collected for isotopic dating using the $^{40}Ar/^{39}Ar$ incremental heating technique. This sampling reflected the compositional variation and areal distribution of the Mohave Mountains dike swarm within the Crossman block. After petrographic evaluation, only seven of these eleven samples were considered fresh enough to analyze. Of these seven,

one sample was lost due to operator error during measurement
on the mass spectrometer. The six remaining samples, their
locations, and the mineral phases dated are summarized in
table 1.

Mineral separations and $^{40}Ar/^{39}Ar$ incremental heatings
were done at the U.S. Geological Survey, Menlo Park,
California. Pure (>99%) hornblende and biotite mineral
separates were prepared from crushed and sized rock powders
using heavy liqiud, magnetic, electrostatic, sonic, and
hand-picking techniques. The sample size used for dating
biotites was 150 mg of U.S. standard sieve fraction 60-140
mesh and was 250 mg of 100-230 mesh for hornblende.

Five of the six mineral separates (samples from sites
26, 35, 37, and two from 47) were wrapped in aluminum-foil
packets, encapsulated in sealed quartz vials, and irradiated
in the central thimble position of the U.S. Geological
Survey TRIGA reactor in Denver, Colorado. Details on
monitor minerals, flux characteristics of the TRIGA reactor,
activity predictions, etc., are presented by Dalrymple et
al. (1981). These five samples were heated incrementally
until fusion in a conventional argon extraction system
(Dalrymple and Lanphere, 1969). Each heating step was
maintained for ≈40 minutes. Temperatures are accurate to
±15°C. Each increment of purified gas was isotopically
analyzed using a six-inch Nier-type mass spectrometer. The
measured isotopic ratios were corrected for the effects of

mass discrimination and the interfering isotopes produced during irradiation using the factors reported by Dalrymple et al. (1981). Apparent $^{40}Ar/^{39}Ar$ ages were calculated using the decay constants specified by Dalrymple et al. (1981). The plateau increments were weighted according to the inverse of their estimated variance. Isochron correlations were derived after York (1969). The reported errors are estimates of the standard deviation of analytical precision (Dalrymple et al., 1981).

One hornblende sample (site 16) yielded less than 200 mg of the 100-230 mesh sieve fraction, consequently this sample was analyzed using a continuous laser system which requires a much smaller amount of sample. This continuous laser system (GLM) is described in detail in Dalrymple and Duffield (1988). The amount of sample needed for dating using the GLM can be quite small (submilligram). Of the ≈50 mg of sample sent for irradiation, only ≈10 mg were used in generating the age spectra. The correction factors and decay constants used in generating these data are the same as above.

Lanphere and Dalrymple (1978) have defined four criteria to distinguish undisturbed from disturbed samples. These criteria are 1) a well-defined high-temperature plateau for >50% of the total $^{39}Ar$ released, 2) a well-defined isochron for the plateau gas fractions, 3) concordant plateau and isochron ages, and 4) a $^{40}Ar/^{36}Ar$

intercept not significantly different from 295.5. An isochron was determined if three or more steps in the $^{39}$Ar release spectra were concordant. An isochron is considered good if the value for SUMS/(N-2)$^{1/2}$ $\leq$ 2.5 (Brooks et al., 1972); this value is only a rough indication of "goodness-of-fit" as replicate analysis to determine the precision of individual gas fractions were not possible. The $^{40}$Ar/$^{36}$Ar intercept value of 295.5 defines an atmospheric argon reservoir. Magmatic argon reservoirs may have different intercept values, thus the assumption of atmospheric $^{40}$Ar/$^{36}$Ar values may be erroneous (for example, Heizler and Harrison, 1988). A sample is considered "disturbed" if it fails to meet any of the above criteria. Argon isotopic data from the dike samples of the Mohave Mountains are presented in table 3 and are discussed and evaluated below.

## Analytical Results

Of the three biotite separates analyzed, only that from site 35 is regarded as an undisturbed sample. The release curve and isochron of the biotite from this dacite dike are shown in figure 14. This sample is concordant for 100% of the $^{39}$Ar released. It has a well-defined isochron with Sums/(N-2)$^{1/2}$ = 2.1. The $^{40}$Ar/$^{36}$Ar intercept is 309.4 ± 14.2. This value indicates that an atmospheric composition for $^{40}$Ar/$^{36}$Ar in the dike swarm is a valid assumption. The

Table 3.    Summary of Argon Isotopic Data

| TEMP (°C) | $^{40}Ar/^{39}Ar$ [1] | $^{37}Ar/^{39}Ar$ | $^{36}Ar/^{39}Ar$ | $^{36}Ar$ [2] (%) | $^{40}Ar$ [3] (%) | $^{40}Ar$ [4] (%) | $^{39}Ar$ (% of total) | Apparent Age [5] (m.y.) |
|---|---|---|---|---|---|---|---|---|
| SITE 35 (5H102) | BIOTITE | J=0.005370 | | | | | | |
| 600* | 3.640 | 0.03311 | 0.005442 | 0.2 | 0.2 | 55.7 | 17.2 | 19.55 ± 0.32 |
| 650* | 2.539 | 0.01269 | 0.001908 | 0.2 | 0.2 | 77.6 | 12.1 | 18.99 ± 0.43 |
| 700* | 2.465 | 0.01623 | 0.001968 | 0.2 | 0.2 | 76.2 | 10.1 | 18.11 ± 0.51 |
| 750* | 2.516 | 0.02887 | 0.002017 | 0.4 | 0.2 | 76.2 | 11.2 | 18.47 ± 0.46 |
| 800* | 2.486 | 0.03181 | 0.001490 | 0.6 | 0.2 | 82.2 | 14.8 | 19.68 ± 0.35 |
| 850* | 2.433 | 0.05350 | 0.001503 | 0.9 | 0.2 | 81.7 | 15.3 | 19.15 ± 0.34 |
| 900* | 2.335 | 0.09825 | 0.001006 | 2.6 | 0.2 | 87.4 | 15.8 | 19.65 ± 0.33 |
| 950* | 2.555 | 0.3957 | 0.001652 | 6.3 | 0.2 | 81.9 | 3.5 | 20.16 ± 1.42 |
| | | | Recalculated total fusion age | = | | | | 19.21 ± 0.18 |
| | | | Weighted mean plateau age | = | | | | 19.25 ± 0.17 |
| SITE 26 (5H077) | BIOTITE | J=0.005620 | | | | | | |
| 550 | 3.757 | 0.07331 | 0.007391 | 0.3 | 0.2 | 41.9 | 34.2 | 15.88 ± 0.51 |
| 600 | 3.539 | 0.05920 | 0.006554 | 0.2 | 0.2 | 45.3 | 15.5 | 16.17 ± 1.06 |
| 650 | 3.693 | 0.04488 | 0.008658 | 0.1 | 0.2 | 30.7 | 11.6 | 11.44 ± 1.45 |
| 700 | 3.212 | 0.03449 | 0.004718 | 0.2 | 0.2 | 56.5 | 21.5 | 18.30 ± 0.78 |
| 750 | 3.527 | 0.06137 | 0.006719 | 0.2 | 0.2 | 43.7 | 11.8 | 15.56 ± 1.40 |
| 800 | 6.634 | 0.3392 | 0.01719 | 0.5 | 0.1 | 23.7 | 3.4 | 15.89 ± 4.91 |
| 850 | 9.271 | 2.365 | 0.03590 | 1.7 | 0.1 | -12.5 | 1.0 | -11.79 ± 16.05 |
| 900 | 14.46 | 5.002 | 0.05750 | 2.3 | 0.0 | -14.9 | 0.5 | -21.99 ± 35.00 |
| 1100 | 19.26 | 2.718 | 0.06116 | 1.2 | 0.0 | 7.2 | 0.5 | 14.13 ± 33.16 |
| | | | Recalculated total fusion age | = | | | | 15.42 ± 0.51 |

Table 3 con't.

| TEMP (°C) | $^{40}Ar/^{39}Ar_1$ | $^{37}Ar/^{39}Ar$ | $^{36}Ar/^{39}Ar$ | $^{36}Ar_2$ (%) | $^{40}Ar_3$ (%) | $^{40}Ar_4$ (%) | $^{39}Ar$ (% of total) | Apparent Age 5 (m.y.) |
|---|---|---|---|---|---|---|---|---|
| SITE 47 (7J168G) | | BIOTITE  J=0.005530 | | | | | | |
| 550 | 13.10 | 0.09866 | 0.04646 | 0.1 | 0.0 | -4.8 | 0.3 | -6.22 ± 17.19 |
| 600 | 4.739 | 0.02441 | 0.006987 | 0.1 | 0.1 | 56.4 | 7.7 | 26.45 ± 0.75 |
| 630 | 3.369 | 0.01124 | 0.001918 | 0.2 | 0.2 | 83.0 | 20.2 | 27.70 ± 0.30 |
| 660 | 3.217 | 0.004791 | 0.001143 | 0.1 | 0.2 | 89.3 | 16.8 | 28.45 ± 0.36 |
| 720 | 3.330 | 0.01359 | 0.002286 | 0.2 | 0.2 | 79.6 | 8.4 | 26.24 ± 0.69 |
| 750 | 3.424 | 0.02450 | 0.004142 | 0.2 | 0.2 | 64.1 | 3.6 | 21.77 ± 1.60 |
| 850 | 3.230 | 0.008066 | 0.000959 | 0.2 | 0.2 | 91.1 | 33.3 | 29.11 ± 0.21 |
| 900 | 2.208 | 0.01172 | 0.001286 | 0.2 | 0.3 | 82.6 | 9.2 | 18.09 ± 0.63 |
| 1000 | 4.498 | 0.2289 | 0.01338 | 0.5 | 0.1 | 12.4 | 0.6 | 5.56 ± 9.83 |
| | | | | | Recalculated total fusion age = 26.74 ± 0.22 | | | |
| SITE 47 (7J168) | | HORNBLENDE  J=0.005490 | | | | | | |
| 600 | 32.90 | 2.705 | 0.07493 | 1.0 | 0.0 | 33.3 | 2.8 | 105.60 ± 10.90 |
| 650 | 14.64 | 1.196 | 0.06464 | 0.5 | 0.0 | -29.8 | 0.8 | -43.85 ± 20.19 |
| 700 | 10.59 | 1.782 | 0.02695 | 1.7 | 0.1 | 26.1 | 0.9 | 27.17 ± 34.54 |
| 750 | 9.251 | 7.191 | 0.03480 | 5.5 | 0.1 | -5.1 | 1.8 | -4.74 ± 17.86 |
| 780 | 7.382 | 6.080 | 0.03091 | 5.2 | 0.1 | -17.4 | 1.8 | -12.79 ± 18.30 |
| 810 | 6.128 | 5.610 | 0.01996 | 7.4 | 0.1 | 10.8 | 4.3 | 6.56 ± 7.60 |
| 840 | 3.525 | 6.303 | 0.008623 | 19.3 | 0.2 | 41.5 | 11.9 | 14.49 ± 2.72 |
| 900 | 2.732 | 6.295 | 0.003674 | 45.2 | 0.2 | 78.0 | 53.4 | 21.07 ± 0.61 |
| 910 | 3.556 | 6.329 | 0.01004 | 16.6 | 0.2 | 30.3 | 7.2 | 10.69 ± 4.52 |
| 930 | 3.382 | 6.169 | 0.007470 | 21.8 | 0.2 | 48.8 | 13.7 | 16.34 ± 2.35 |
| 1000 | 8.444 | 5.922 | 0.04886 | 3.2 | 0.1 | -65.6 | 1.5 | -55.92 ± 11.41 |
| | | | | | Recalculated total fusion age = 18.14 ± 1.00 | | | |

Table 3 con't.

| TEMP (°C) | $^{40}Ar/^{39}Ar$ [1] | $^{37}Ar/^{39}Ar$ | $^{36}Ar/^{39}Ar$ | $^{36}Ar$ [2] (%) | $^{40}Ar$ [3] (%) | $^{40}Ar$ [4] (%) | $^{39}Ar$ (% of total) | Apparent Age [5] (m.y.) |
|---|---|---|---|---|---|---|---|---|
| SITE 37 (5H108) | HORNBLENDE | J=0.005410 | | | | | | |
| 600 | 173.9 | 0.01077 | 0.4657 | 0.0 | 0.0 | 20.8 | 0.0 | 322.9 ± 748.0 |
| 700 | 159.6 | 0.9046 | 0.1628 | 0.1 | 0.0 | 69.9 | 0.1 | 852.3 ± 234.3 |
| 750 | 11.74 | 1.076 | 0.02518 | 1.1 | 0.0 | 37.3 | 1.1 | 42.22 ± 20.31 |
| 800 | 7.834 | 1.727 | 0.04136 | 1.1 | 0.1 | -54.3 | 0.7 | -42.08 ± 32.52 |
| 850 | 4.924 | 3.821 | 0.007287 | 13.8 | 0.1 | 62.2 | 30.4 | 29.72 ± 0.79 |
| 880 | 3.381 | 4.546 | 0.003608 | 33.3 | 0.2 | 78.8 | 21.1 | 25.89 ± 1.12 |
| 910 | 3.361 | 4.818 | 0.003358 | 37.9 | 0.2 | 81.5 | 24.4 | 26.62 ± 0.97 |
| 940 | 3.261 | 4.622 | 0.005443 | 22.4 | 0.2 | 61.6 | 17.0 | 19.54 ± 1.39 |
| 990 | 4.189 | 4.590 | 0.000815 | 148.7 | 0.1 | 102.7 | 2.5 | 41.62 ± 9.22 |
| 1100 | 4.314 | 4.651 | 0.004734 | 25.9 | 0.1 | 75.9 | 2.6 | 31.75 ± 8.98 |
| | | | | Recalculated total fusion age = | | | | 27.15 ± 0.76 |
| SITE 16 (5H047) | HORNBLENDE | J=0.010295 | | | | | | |
| 0.5W | 16.56 | 1.184 | 0.02276 | 1.4 | 0.0 | 59.9 | 0.9 | 175.6 ± 34.50 |
| 1.0W | 5.323 | 1.239 | 0.01064 | 3.1 | 0.0 | 42.7 | 2.0 | 41.80 ± 17.43 |
| 2.0W | 4.805 | 1.047 | 0.006693 | 4.1 | 0.0 | 60.5 | 3.0 | 53.26 ± 11.54 |
| TFUS | 2.170 | 4.132 | 0.002410 | 45.3 | 0.1 | 82.0 | 94.0 | 32.82 ± 0.39 |
| | | | | Recalculated total fusion age = | | | | 35.02 ± 0.73 |

Footnotes: 1= corrected for $^{37}Ar$ decay, half-life=35.1 days; 2= calcium-derived argon; 3= potassium-derived argon; 4= radiogenic argon; 5= Lambda E=0.581E-10/yr, Lambda B=4.692E-10/yr; *= temperature increments used in calculating weighted mean apparent plateau ages. Errors are estimates of the standard deviation of analytical precision (Dalrymple et al., 1981). For site 16, W = Watts.
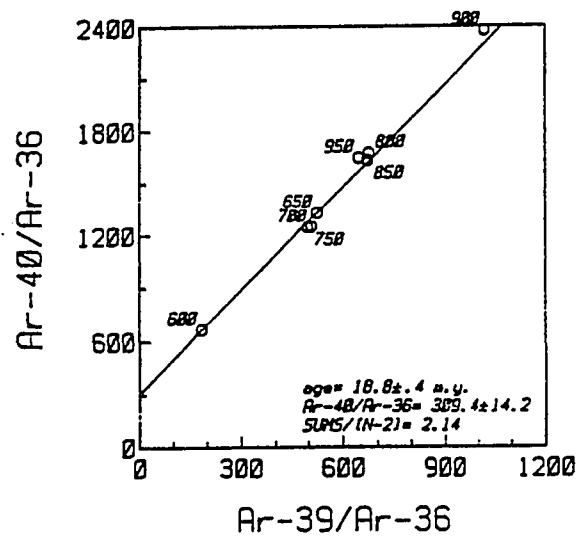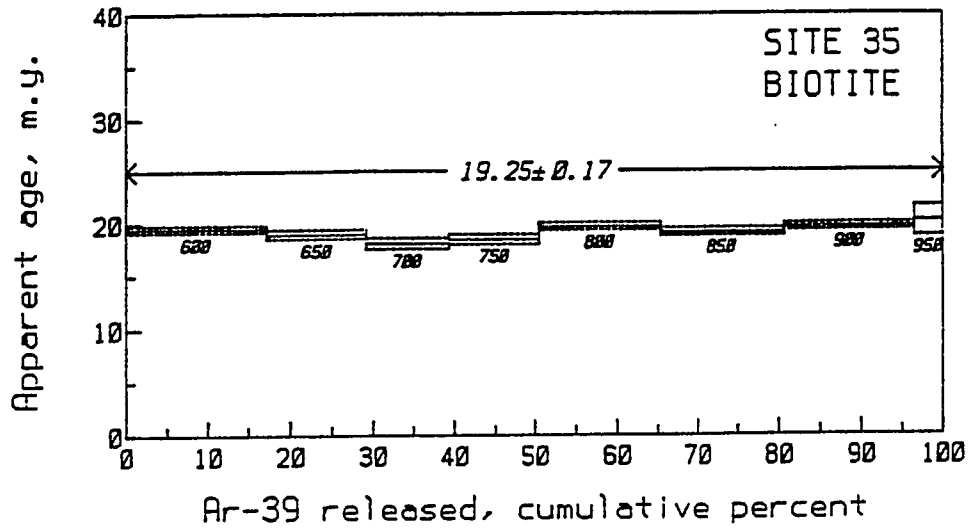
Figure 14. $^{40}Ar/^{39}Ar$ age spectra and isochron (with $1\sigma$ errors).

plateau and isochron ages are concordant. The weighted mean
standard deviation age of 19.25 ± 0.17 m.y. is interpreted
as the crystallization age of this dike. This is in
agreement with the data of Nakata et al. (in press).

The biotite sample from the leucocratic dike at site 26
has a complex $^{39}$Ar age spectra (fig. 15). This sample
displays a concordant release curve from 550-600°C. The
apparent plateau age of these two steps is 16.1 ± 0.94 m.y.
This portion of the release curve involves 49.7% of the
total $^{39}$Ar released, but because it contains only two
heating increments it cannot be evaluated for an isochron
age. An isochron calculated using all of the heating
increments indicates that this is a disturbed sample: The
value of SUMS/(N-2)$^{1/2}$ indicates a poor line-fit and the
$^{40}$Ar/$^{36}$Ar intercept value suggests argon-loss may have
occurred.

The discordance of the 650°C increment in the release
spectra may be due to a phase change. In biotite, such a
phase change is usually the result of dehydration, not
exsolution homogenization (Harrison, 1983). Any
chloritization of the sample might result in a discordant
age spectrum. Biotite was absent from the thin-section of
this sample (Appendix A), perhaps due to its low modal
abundance in hand-sample (≈1%), so this possibility could
not be assessed. It is unlikely that the discordance is the
result of $^{39}$Ar loss due to recoil of $^{39}$K, as this is usually
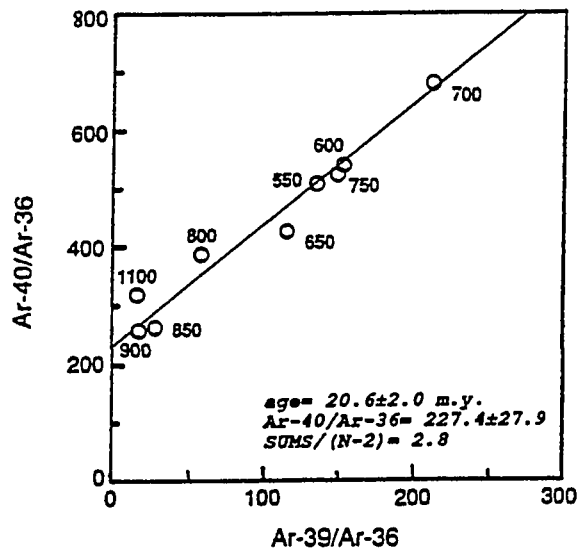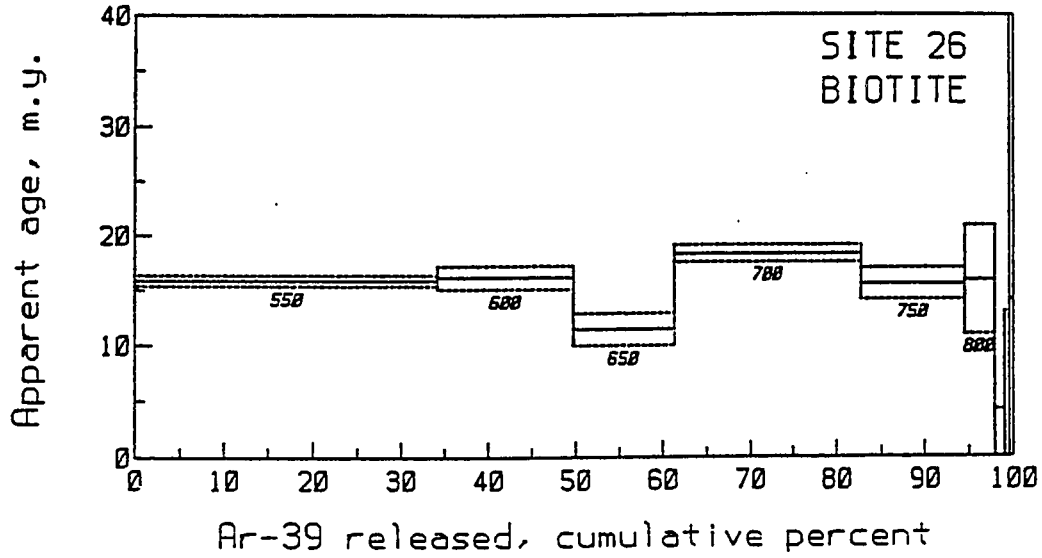
Figure 15. $^{40}Ar/^{39}Ar$ age spectra and isochron (with $1\sigma$ errors).

associated with fine-grained samples and results in an older
apparent age (contrast the 11.5 m.y. age of the 650°C
heating increment with the 16 m.y. apparent age of the
550-600°C heating increments or the 19 m.y. age from site
35). It is interesting to speculate that if the 650°C step
is discordant because of a dehydration reaction and is
disregarded, the overall release spectra for this sample is
suggestive of Ar loss (Lanphere and Dalrymple, 1971). If
this were the case, the 700°C step would represent a minimum
age of 18.3 ± 0.8 m.y. for the sample. This would be in
agreement with the crystallization age for biotite from site
35. The extrusive rocks in the Mohave Mountains, however,
range from ≈10-23 m.y. old and if the dikes are feeders to
these flows, there is no reason to assume a priori that the
dikes will yield a single age. In short, this complex
release spectrum is difficult to resolve.

At site 47 a mafic dike intrudes Precambrian biotite
gneiss. A biotite sample was obtained from the gneiss
directly adjacent to the dike in order to evaluate the
extent to which the country rock was reheated by the dike.
A hornblende sample was collected from the dike. The
biotite has a complex release curve (fig. 16). None of the
heating increments is concordant and the release spectra
cannot, therefore, be evaluated for an isochron age (this is
substantiated by the poor line-fit generated when
calculating an isochron using most of the data; fig. 16).
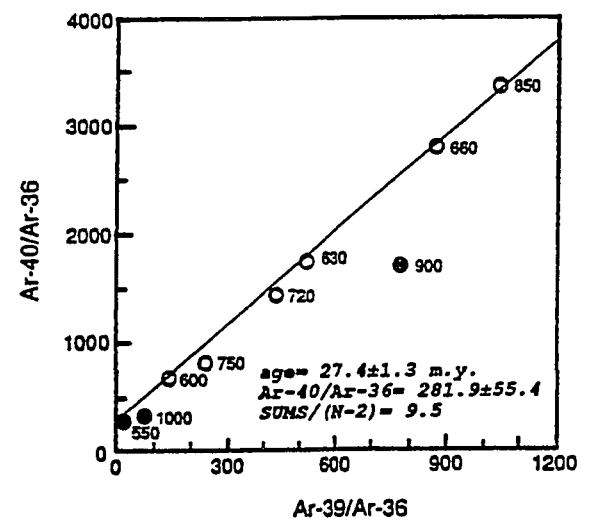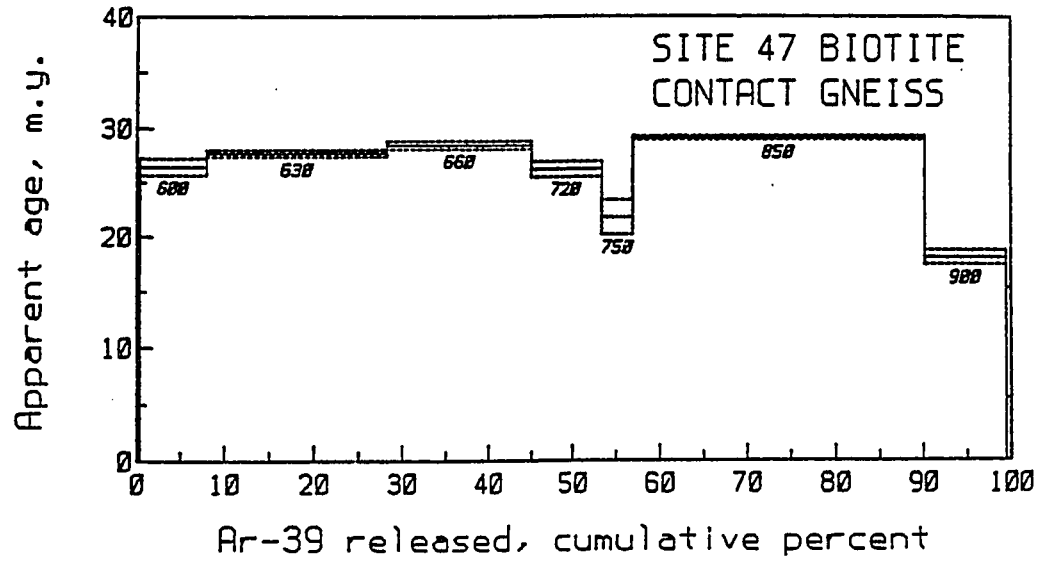
Figure 16.  $^{40}Ar/^{39}Ar$ age spectra and isochron (with 1σ errors).  Solid dots not used in regression.

The discordance of the 720-750°C increments may reflect a dehydration phase transition associated with chloritization of the biotite. This could not be evaluated, however, because a thin-section was not made of the gneiss. If the 720-750°C heating increments are the result of a phase transition and are disregarded, the release spectra define a pattern of Ar loss (Lanphere and Dalrymple, 1971).

It is difficult to determine whether Ar loss associated with this sample is due to the intrusion of the dike or to the slow-cooling and uplift of the Mohave Mountains. Foster et al. (1990), using $^{40}Ar/^{39}Ar$ thermochronology, have determined that the Precambrian crystalline basement of the Mohave Mountains experienced a period of post-orogenic cooling and uplift between 65-35 Ma, after the emplacement of Late Cretaceous batholiths. Site 47 is located in the northeastern Mohave Mountains (fig. 2), which represents the deepest structural level exposed in this range and was at temperatures in excess of 300°C between 65-35 Ma. By 22-20 Ma the NE Mohave Mountains had cooled to below 300°C. If Ar loss in the biotite gneiss sample is related to slow cooling, then the apparent age of 29.1 ± 0.2 m.y. from the 850°C heating increment may reflect the age of uplift of the crystalline basement in the eastern side of the Mohave Mountains.

Alternatively, this age may represent Ar loss due to reheating associated with the intrusion of the dike. If

this is the case, the reheating event did not reset the age
of the biotite gneiss to the age of the dike, but to some
intermediate value. This implies that either 1) the biotite
gneiss was heated to the biotite closure temperature for the
retention of argon ($\approx$300°C; Harrison et al., 1985), but that
it was not held at this temperature for a long enough period
of time to allow for the thorough rehomogenization of argon;
or 2) that the biotite was thoroughly degassed of argon and
as it cooled it picked up extraneous argon from the
(partially degassed?) Precambrian crystalline rocks. In
either case, the apparent age of 29.1 ± 0.2 m.y. has no
geologic significance.

The incremental heating release spectra for the
hornblende sample from the mafic dike at site 47 is shown in
figure 17. The lowest temperature heating increment from
this sample yields a geologically unreasonably old age of
$\approx$100 m.y. (table 3). This type of discordant release
spectra has been cited by other workers as evidence for
extraneous (excess) argon (Dallmeyer and Rivers, 1983;
Harrison and McDougall, 1981; Dalrymple et al., 1975).
Isotopic ratios are also shown in figure 17. It is notable
that the oldest ages are associated with the most radiogenic
gas increments. The Precambrian crystalline basement in the
Mohave Mountains is a likely source for the older radiogenic
argon. The 650-780°C heating increments involve small
amounts of gas, have associated large errors, and yield
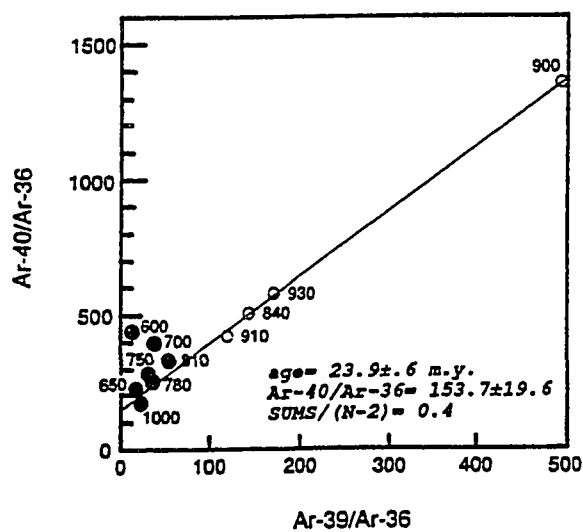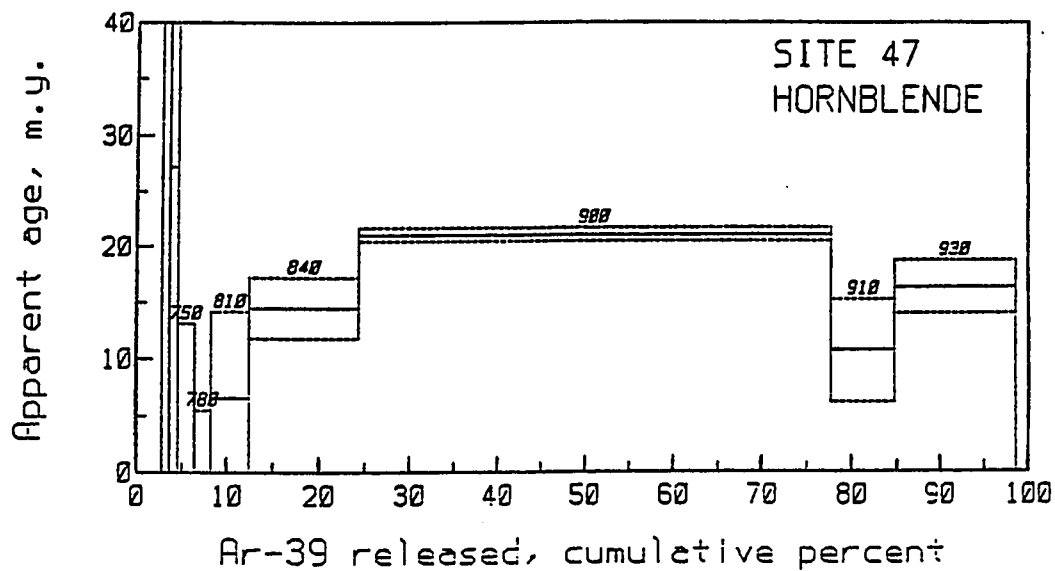
Figure 17. $^{40}Ar/^{39}Ar$ age spectra and isochron (with $1\sigma$ errors). Solid dots not used in regression.

meaningless ages.

In contrast, the heating increments greater than 750°C
define a $^{39}$Ar release pattern suggestive of Ar loss
(Lanphere and Dalrymple, 1971). An isochron calculated for
the 840-930°C increments supports this interpretation
($^{40}$Ar/$^{36}$Ar intercept of 153.7 ± 19.6). It is difficult to
determine whether this apparent Ar loss was due to reheating
or to slow-cooling of the dike. This site was located in a
dense swarm of dikes and thus the hornblende may have been
reheated by subsequent intrusions or subjected to a
protracted cooling history as a result of multiple intrusive
phases.

A lack of detail in the heating schedule for this
sample resulted in the 900°C increment containing 53.4% of
the total $^{39}$Ar released. The data from this sample cannot,
therefore, be legitimately evaluated for an isochron age.
The 900°C increment has an apparent age of 21.1 ± 0.6 m.y.
Specific details in the release spectra associated with
temperatures from 840-900°C may have been obscured, thus any
interpretation of this age may be erroneous. For example,
the 900°C heating increment may have averaged younger and
older gas fractions, resulting in an apparent age for this
increment which was younger than the older gas fraction. It
is also possible, however, that this age actually represents
the minimum crystallization age for hornblende. The age is
compatible with the data of Nakata et al. (in press) and is

within the age limits of the overlying volcanic extrusive equilvalents.

The release curve for hornblende from a basaltic andesite dike at site 37 is shown in figure 18. The low-temperature heating increments yield geologically unreasonably old ages of 42-852 m.y. (table 3). These old ages, combined with the older age from the 940°C heating increment, define a "saddle-shaped" $^{39}$Ar release curve typically associated with presence of extraneous argon (Dallmeyer and Rivers, 1983; Harrison and McDougall, 1981; Dalrymple et al., 1975). Isotopic ratios for each heating increment are also shown in figure 18. The radiogenic 600-750°C steps, coincident with their extremely old ages, also suggests that excess radiogenic argon is present. Furthermore, the high $^{40}$Ar/$^{36}$Ar ratio (385.0 ± 18.9) of an isochron calculation using the 850-910°C release increments indicates excess argon (fig. 18). The presence of excess argon results in apparent ages which are older than the age of crystallization of a mineral, thus the age of 19.5 ± 1.4 m.y. from the 940°C increment is the maximum age for the crystallization of hornblende in this sample.

The hornblende sample from site 16 was analyzed using the GLM of the U.S. Geological Survey (Dalrymple and Duffield, 1988). The release curve for this sample is shown in figure 19. The "heating increments" in this case are actually increments of increased wattage. Temperature
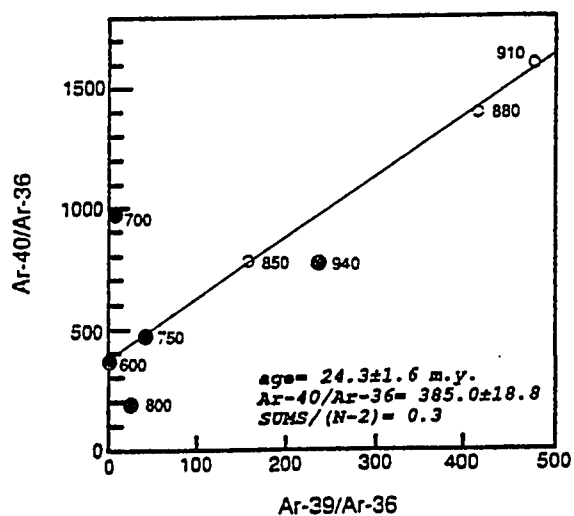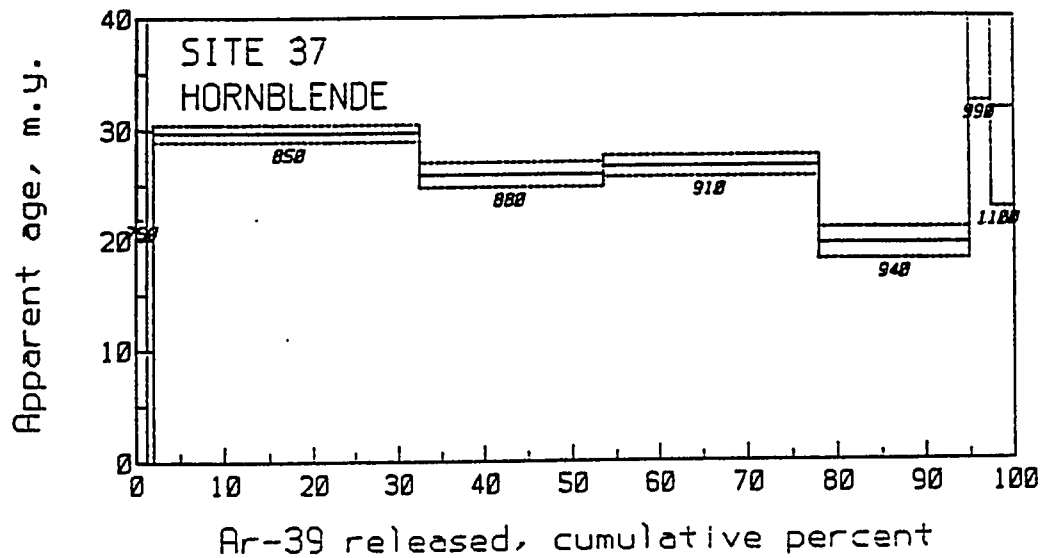
Figure 18. $^{40}Ar/^{39}Ar$ age spectra and isochron (with 1σ errors). Solid dots not used in regression.
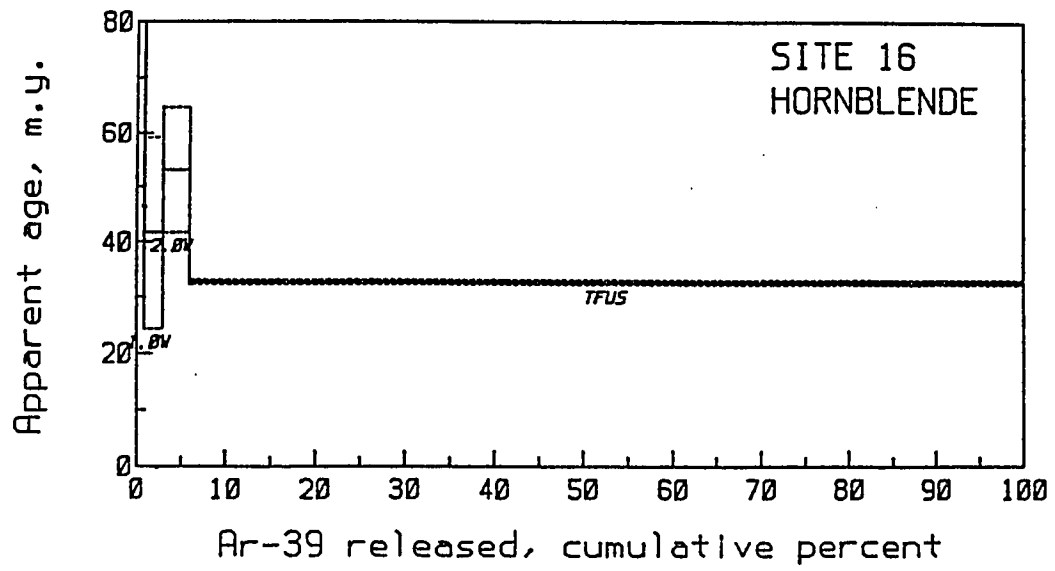
Figure 19.  Laser $^{40}Ar/^{39}Ar$ age spectra with $1\sigma$ errors.

control in this system is semi-quantitative in as much as an increase in wattage results in an increase in temperature. Ninety percent of the total $^{39}$Ar in this sample was released during fusion. Once again, the "low-temperature" portion of the release curve generates geologically unreasonably old ages of 53-175 m.y.(table 3), suggesting extraneous radiogenic argon is present. The resulting age associated with fusion of the sample is 32.8 ± 0.4 m.y. and is regarded as a maximum age for the crystallization of hornblende.

Discussion

The number of reliable age data presented in this investigation does not allow for a conclusive evaluation of the thermal history of the dike swarm in the Mohave Mountains. However, in as much as the apparent ages of crystallization of hornblende at site 37 (19.5 ± 1.4 m.y.) and site 47 (21.1 ± 0.6 m.y.) may have geologic significance, they are not very different from the biotite age at site 35 of 19.2 ± 0.2 m.y. The closure temperature for the retention of argon in biotite is ≈300°C (Harrison et al., 1985) and is ≈500°C in hornblende (Harrison, 1981). If the errors associated with these ages are interpreted to maximize the amount of time between biotite and hornblende closure temperatures, these data suggest that the dikes of the Mohave Mountains must have cooled from 500°C to 300°C very quickly (within about 2 m.y.?). There are no reliable

ages presented in this investigation of samples from the western side of the Mohave Mountains. K-Ar age data on biotite in dacite dikes in the western side of the range, however, yield similar ages (Nakata et al., in press). Thus, it can be argued that the entire dike swarm has a single age. If this is the case, the dike swarm must have cooled to below 300°C relatively quickly.

Volcanic rocks with compositions ranging from basalt to rhyolite alternately erupted throughout the interval of about 23 to 10 Ma (Nielson and Beratan, 1990). If the dike swarm is ≈20 m.y. old, the absence of dikes associated with the 10 m.y. old volcanic flows suggests that the style of volcanism in the Mohave Mountains changed after about 20 Ma from one of widespread diking to one of localized volcanic centers. This may have resulted as magma ultimately found avenues through the crust to the surface, or it may be related to a change in the stress regime of the upper crust associated with ongoing detachment faulting and the continued rotation of the Crossman block.

## Summary

1. A single undisturbed $^{40}Ar/^{39}Ar$ age of 19.25 ± 0.17 m.y. (1σ) was obtained from biotite in a dacite dike.

2. Release curves in two of the three biotite samples were discordant. Discordant release curves could result from chloritization of biotite. These two samples were not

evaluated petrographically for chloritization, but
chloritization of the dikes in the Mohave Mountains is
common.

   3.   All hornblende separates contain excess radiogenic
argon.   The Precambrian crystalline basement provides a
likely source for excess argon.   Both of the apparent ages
obtained via the conventional incremental heating technique
are in close agreement with each other, though there is no
reason a priori to expect them to be.   These ages are 19.5 ±
1.4 m.y. and 21.1 ± 0.6 m.y.

   4.   The data do not permit a conclusive evaluation of
the thermal history of the dike swarm.   They suggest,
however, that the entire dike swarm of the Mohave Mountains
was intruded over a short period of time about 20 m.y. ago
and that it cooled within a few million years.

   5.   If the dike swarm is 20 Ma, a change in the style
of volcanism from dikes to a localized source must have
occurred after about 20 Ma.   This may have been the natural
evolution of magma ascending to the surface, or it may have
resulted from a change in the stress regime of the crust as
ongoing detachment faulting continued to tilt the Crossman
block.

# PALEOMAGNETISM

Samples were collected for paleomagnetic analysis from the Miocene dike swarm of the Mohave Mountains and their extrusive equivalents in order to test various hypotheses concerning the the geometry and timing of detachment faulting in this area. A fundamental premise of paleomagnetism is that the earth's magnetic field, when averaged over time, closely approximates that of an axial geocentric dipole. Thus, the average magnetic inclination (I) at a site varies according to latitude (L) by the dipole formula, $2 \tan L = \tan I$. Magnetic declination (D) is the deviation of magnetic north from geographic north and can be useful in determining rotations about the vertical axis. (For a discussion of principles and techniques see McElhinny, 1973.) There are some conditions that must be satisfied in order to apply paleomagnetic data to the solution of structural or tectonic problems in geology:

1) Horizontal at the time of magnetization must be known for the rocks being studied.

2) The rocks must be accurate recorders of the geomagnetic field.

3) A stable magnetic direction must be determined.

4) If more than one time unit (flow, bed, etc.) is used, the rocks analyzed must encompass several thousand years in age so that the data average secular variation (the

natural variation of the earth's magnetic field caused by variable electrical currents in the earth's core). If the above conditions are met, deviations from the expected values of I and D at a given location may be attributed to tectonic rotations and translations of crust.

Howard et al. (1982) have proposed that the Precambrian crystalline core of the Mohave Mountains was deformed during Miocene detachment faulting. This deformation involves at least 90° of tilt to the southwest, as recorded by the dip of volcanic flows and sedimentary rocks in unconformable contact with the Precambrian basement. This interpretation is further supported by $^{40}Ar/^{39}Ar$ thermochronologic data which indicate an increasing temperature gradient from west to east of $\approx 200°C$ in the Mohave Mountains since the Cretaceous (Foster et al., 1990). The higher temperatures to the east probably reflect the greater initial depth of this crust prior to uplift and faulting. The southwest tilt of the Tertiary strata and the exposure of deep crustal rocks to the east is consistent with the Crossman block once being a horizontal slab of crust that was tilted and uplifted by detachment processes (fig. 1B). If this model is correct, the eastern part of the Mohave Mountains represents crust which was initially at depths of 10-12 km. This paleomagnetic investigation was undertaken to test the tilt hypothesis. A magnetic direction for the dike swarm of the Mohave Mountains was determined and was then compared

to a Miocene reference direction from the North American craton to test for tilt.

## Sampling and Analytical Techniques

Paleomagnetic samples were collected from dikes and flows in the Crossman block and from dikes in the Standard Wash block of the Mohave Mountains. With the exception of site 39, oriented paleomagnetic samples were collected using portable drilling equipment. The number of cores collected per site varies and is discussed below. In 95% of the samples the azimuths of the core axes were measured using a solar compass with an accuracy of ±1°. The azimuths of the core axes for the remaining samples were measured using a Brunton compass. The solar compass eliminates orientation errors due to local magnetic anomalies. The cores were cut into 2.5 cm lengths, resulting in at least two 2.5 cm specimens per core. Sample locations are summarized in figure 2 and in table 1.

The flows sampled at site 40 were collected from basaltic andesite near the base of the Tertiary section in the Crossman block in hopes of providing a structural reference for the dikes. These rocks are equivalent to sequence I of Nielson (1986). Sequence I flows commonly have red, oxidized baked contacts. They often entrained sedimentary interbeds during their deposition and at the sampling location the entrained sediments are parallel to

the baked contacts. No sedimentary rocks were seen between flows at this location, though Nielson (1986) described them elsewhere within sequence I. This location provided some of the best outcrop of the flows; it was, however, fractured and did not permit extensive sampling. Limited time and exposure restricted the number of samples collected to two or three cores per flow. These cores were spaced at least one meter apart. A total of twenty-four flows were collected over ≈200 m of discontinuous outcrop.

Paleomagnetic samples were also collected from higher in the Tertiary stratigraphic section. Samples from site 49 are from the hydrated (perlitized), basal vitrophyre of sequence IV (Nielson, 1986). This vitrophyre may be autobrecciated (J. Nielson, oral communication, 1989). These ten cores were collected over 30 m of outcrop and were spaced at least one meter apart from each other. Sequences II and III are not well exposed in the Crossman block region and were not sampled.

Forty-two dikes were sampled in the Crossman block. These dikes dikes range from 1 to 20 m in thickness, but are typically 3-6 m thick. The dikes are exposed as resistant ribs cutting the metamorphic fabric of the Precambrian crystalline basement. Generally, three cores were sampled across the thickness of each dike, including the chilled margins where present (Appendix B).

At site 39, a single dike was sampled and seven cores were collected. Two of the seven samples were hand-oriented because the dike was highly fractured. These samples were cored using a drill press at the laboratory and reoriented using a Brunton compass. This dike feeds a rhyolite unit high in the Tertiary section to the west.

In the Standard Wash block five dikes were sampled, with six cores collected per dike. The dikes in this area are generally thicker ($\approx$10 m) and much less fractured than those in the Crossman block. Furthermore, they have a topographic expression similar to the crystalline basement. In this area some of the dikes have single-sided chilled margins, indicating that distinct batches of magma were intruded along the same conduit in this region.

## Demagnetization Treatments

Pilot specimens from the dikes and flows were partially demagnetized using alternating field (AF) and thermal (TH) demagnetization techniques to remove secondary components of magnetization (e.g.- Merrill and McElhinny, 1983). An AF demagnetizer with a reciprocating tumbling specimen holder was used to a maximum peak field of 100 milliTeslas (mT). In this procedure, progressively higher peak fields were applied in 11 steps up to 100 mT. The AF increments were taken at 5 mT intervals from 5 mT to 40 mT and then at 20 mT intervals from 40 mT to 100 mT. Thermal demagnetizations

were performed in a low-field furnace. The specimens were heated in air in an ambient field of less than 5 nanoTeslas. Progressively higher temperatures were produced over 18 heating increments, attaining a maximum temperature of 680°C. The heating steps were taken at 50°C intervals from 100° up to 400° and were then decreased to 30° intervals from 400° to 680°. All measurements were made using a cryogenic magnetometer at the Paleomagnetic Laboratory of the U. S. Geological Survey in Menlo Park, California.

Using the AF and TH pilot demagnetizations from a pair of specimens from a single core per dike, orthogonal projections of the resultant vectors were analyzed to determine components of magnetization. Two or more components of magnetization were identified in the dikes from the Crossman and Standard Wash blocks. AF and TH demagnetization techniques often identified different components of magnetization within the same dike in the Crossman block. The mixed success of AF and TH demagnetization techniques in isolating the same components of magnetization required the application of both techniques to all of the remaining samples. The same detailed demagnetization procedures which were outlined for the pilot investigations were used. This was also true for the vitrophyre of site 49.

A single component of magnetization was isolated in the basaltic andesites of site 40. Both AF and TH

demagnetization techniques were successful at isolating this component, but the TH procedure was more successful at completely demagnetizing the specimen. Only TH demagnetization techniques were applied to the remaining specimens from this site, using the same detailed procedures outlined for the pilot investigations above.

Principal component analysis of the demagnetization data (Kirschvink, 1980) was used to determine the secondary and stable components of magnetization of the majority of specimens (Appendix B). For each site, results from the individual specimens were then averaged together to obtain mean directions of magnetization. The 95% confidence ellipse ($\alpha_{95}$) was calculated about the site mean directions of magnetization according to the statistical model of Bingham (1974) and the values of the minor and major axes are reported. The method of Fisher (1953) was not used in determining the 95% confidence limits because of its inherent assumption of the circular distribution of the data set. Corrections for the tilt of bedding were made by rotating the mean magnetization vector about the strike by the amount of the dip (Appendix C).

## Natural Remanent Magnetization

Figure 20 shows histograms of the logarithmic distribution of natural remanenet magnetization (NRM) intensities for the dikes and flows from the Crossman block

CROSSMAN BLOCK DIKES

N

NRM   (emu/cc)

STANDARD WASH DIKES

N

NRM   (emu/cc)

CROSSMAN BLOCK FLOWS

N

NRM   (emu/cc)
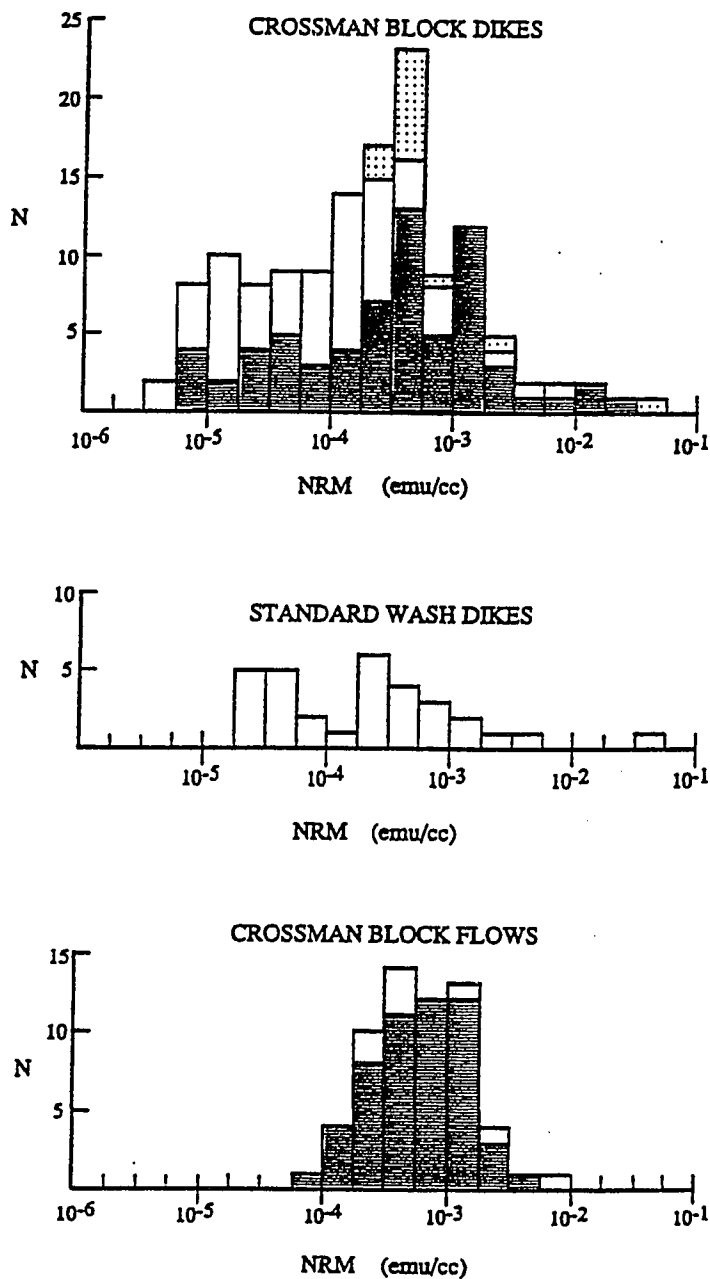
Figure 20. Histogram of NRM intensities divided into two compositional groups; compositions determined visually in the field. Ruled pattern denotes mafic compositions, dots = intermediate compositions, and unpatterned areas are felsic compositions.

and for the dikes from the Standard Wash block. This figure
shows that the mafic dikes and flows have similar
intensities, as would be expected if the dikes are feeders
to the flows. The mean NRM intensity for mafic rocks,
combining the dikes and flows of the Crossman block, is 1.2
x $10^{-3}$ emu/cc (electromagnetic units per cubic centimeter).
The distribution of NRMs from the mafic dikes of the
Crossman block spans a considerably broader range of
intensities than those of the mafic flows. The NRMs from
felsic dikes of the Crossman block are generally skewed
toward lower intensities than those observed from the felsic
flow at site 49, the glassy vitrophyre. The mean NRM
intensity for the combined felsic dikes and flows of the
Crossman block is 5.4 x $10^{-4}$ emu/cc, whereas that of dikes
from the Standard Wash block is 1.6 x $10^{-3}$ emu/cc (though
the number of samples from the Standard Wash block may be
too few to define trends in the NRM distributions).

Secondary Magnetization Induced By Lightning

The removal of a secondary component of magnetization
induced by lightning was anticipated as a problem because
electrical thunder storms are common in this region.
Unusually strong magnetizations and aberrant magnetic
directions are typically found in rocks that have been
affected by lightning. AF demagnetization techniques are
generally more successful than TH treatments at isolating

the characteristic component of magnetization when it has been overprinted by an isothermal remanent magnetization resulting from the strong magnetic fields produced by lightning strikes (Merrill and McElhinny, 1983). Mafic samples with NRM intensities greater than $\approx 1 \times 10^{-2}$ emu/cc and felsic samples with NRM intensities greater than $\approx 1 \times 10^{-3}$ were suspected of being overprinted by a secondary component of isothermal remanent magnetization induced by lightning. The intensity of magnetization induced by lightning strikes can decay with time and the NRM of a dike which was struck by lightning thousands of years ago _may not be_ unusually high. The above values do not allow for the natural decay of magnetic intensity with time of this component and provide only the upper limits for suspecting lightning-induced NRM intensities; because of this, where widely scattered magnetic directions exist without high magnetic intensities, the remanent magnetization was suspected to be overprinted by lightning as well. If a magnetically stable directional endpoint was not isolated for these samples using AF demagnetization techniques, the data were not used in the final site average. TH demagnetization data was regarded as unreliable in the event of suspected lightning-induced isothermal remanent magnetization.

## Analytical Results

Crossman Block

Flows and Vitrophyre. At site 40, after thermal
cleaning, the data from 1 of the 24 flows was discarded
because of the incomplete removal of a secondary component
of magnetization attributed to lightning. An example of the
characteristic and single component of magnetization in the
basaltic andesites is shown in an orthogonal vector diagram
from one of the flows (fig. 21). The magnetization is
thermally stable, with 30-90% of the magnetization remaining
until temperatures between 550° and 650°C are reached (fig.
22). This is within the range of the Curie temperatures of
magnetite (580°C) and titanohematite (up to 680°C), both
resulting from the high-temperature oxidation of
iron-titanium oxides during the emplacement and subsequent
cooling of the flows (Gromme et al., 1969). This
high-temperature oxidation process develops a very stable
thermoremanent magnetization (TRM) in the flows.

The directions of magnetization of specimens from an
individual flow, obtained using principal component
analysis, were averaged. If the angular difference between
the averaged magnetic direction of a flow and the mean
magnetic direction of the 23 averaged flows differed by more
than 30°, the data were rejected (fig. 23). Using this
criteria, the data from 3 of the 23 flows were rejected. The

SITE 40 (8P011)

TH demagnetization

horizontal plane

vertical plane
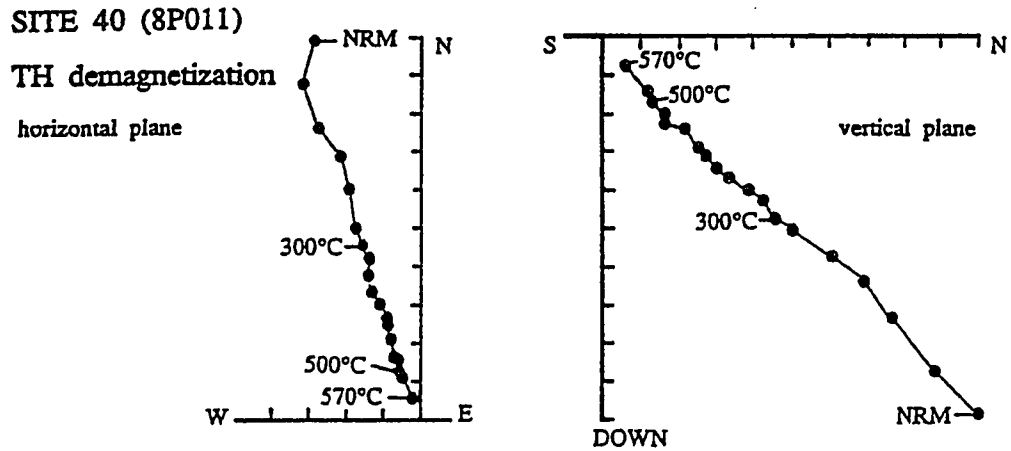
Figure 21. Orthogonal vector diagrams depicting the thermal demagnetization of a flow specimen. Note the stability of the magnetization for the entire range of temperatures. NRM, natural remanent magnetization before demagnetization. Axis units: 1 division = 4.27 x $10^{-2}$ Ampere/meter.
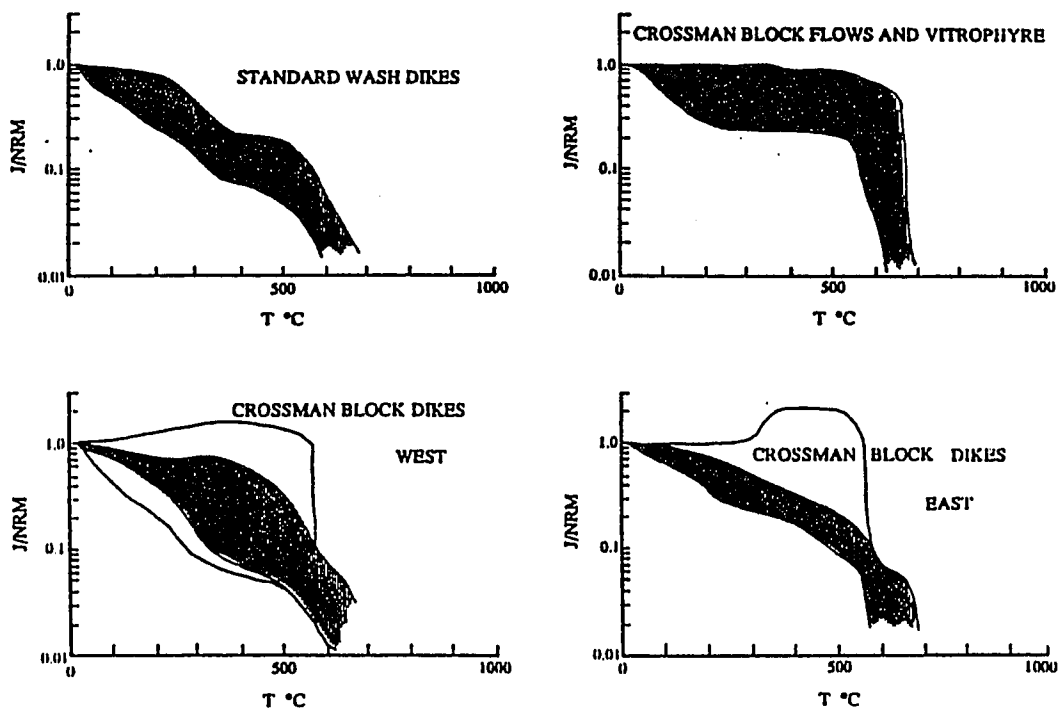
Figure 22. Normalized intensity (J/NRM) versus temperature curves for all samples. The majority of samples fall in the shaded regions.
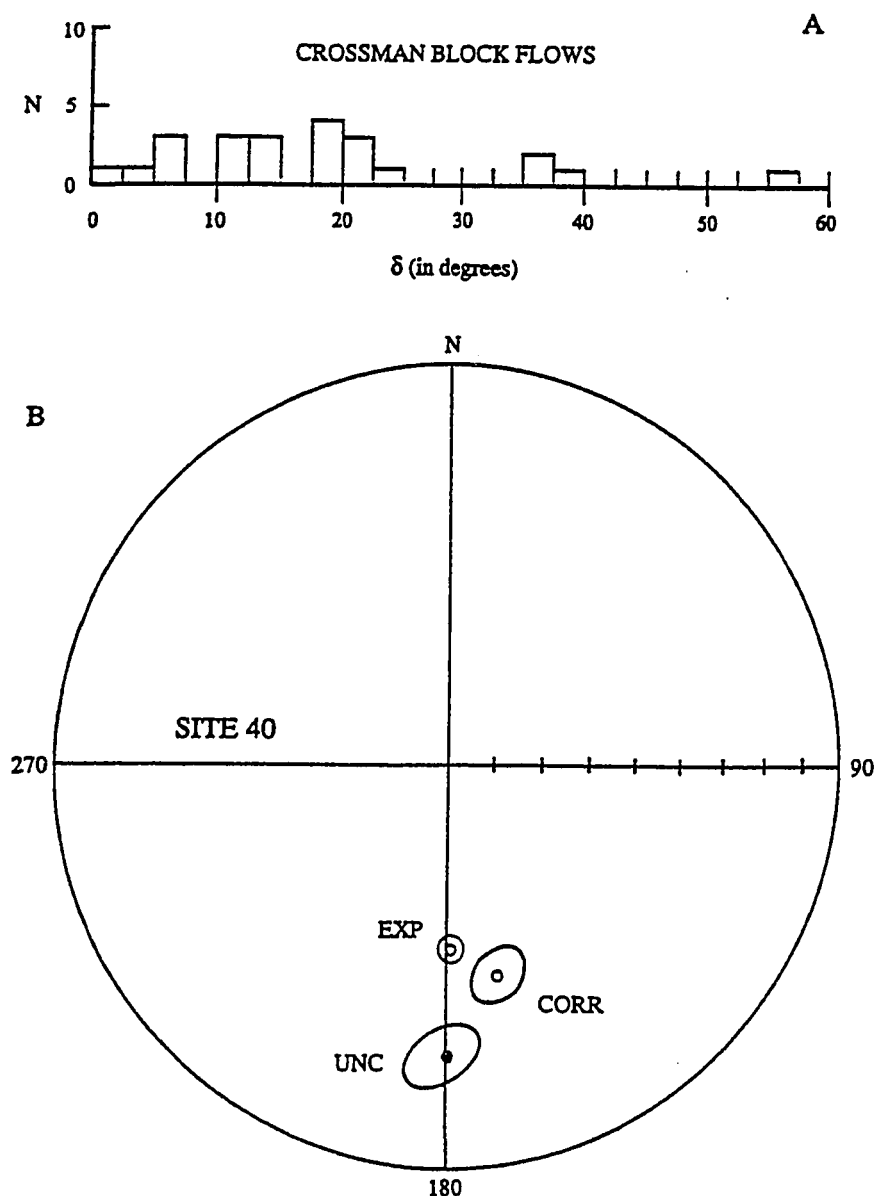
Figure 23. A) Histogram showing angular difference of individual flows from mean direction of flows ($\delta$), prior to data selection. B) Equal-area projection of the site-mean direction of magnetization (dots) and 95% confidence limits (ellipses) for Crossman Block flows. EXP, expected axial dipole direction for Miocene time; UNC, direction of magnetization uncorrected for tilt of bedding; CORR, direction of magnetization corrected for tilt of bedding. Solid symbols = lower-hemisphere projection, open symbols = upper-hemisphere projection.

magnetic directions of the 20 remaining flows were then corrected for tilt using the strikes and dips of the individual flows (Appendix C). The structurally corrected directions of these 20 flows were then averaged together for a combined site mean direction of magnetization with 95% confidence limits (I=-44.8°, D=164.8, $\alpha_{95}$=5.1, 6.3; table 4).

From table 4 and figure 23 it is evident that when the flows from site 40 are corrected for tilt the reversed direction of magnetization does not coincide with the expected Miocene direction for this area of I=-52.8, D=178.0, $\alpha_{95}$=2.6 (Irving and Irving, 1982, 15-20 m.y. window). The observed magnetic inclination is 8° shallower than would be expected for this location in Miocene time, although the discordance may not be significant given the confidence limits. Some possible explanations for the discordant inclination are 1) incomplete removal of secondary magnetization, 2) unrecognized initial dip of the strata, 3) northward movement of the region relative to North American craton, and 4) incomplete averaging of secular variation. In the first case, it is unlikely that this "shallow" inclination is the result of the unsuccessful removal of a secondary magnetization because these flows have only one component of magnetization. This component has a high thermal stability and is most likely the result of deuteric alteration. In the second case, errors in

Table 4. Site means of paleomagnetic data.

| Site # | NLat/ELon | Bedding *1 strike/dip | N/Nc | I | D | $\alpha_{95}$ min/max | $I_c$ | $D_c$ |
|---|---|---|---|---|---|---|---|---|
| Exp | 34.50/245.80 | | | 52.8 | 358.0 | 2.6 | | |
| 40 | 34.49/245.76 | 136.6/96.4 SW | 20/24 | 28.2 | 179.9 | 5.1/6.3 | -44.8 | 164.8 |
| CBL | 34.58/245.79 | 136.6/96.4 SW | 103/134 | 54.4 | 8.0 | 3.7/4.4 | 21.1 | 249.5 |
| CNH | 34.58/245.79 | 136.6/96.4 SW 114.4/34.7 SW 136.6/34.7 SW | 48/134 | 48.5 | 6.4 | 4.0/5.2 | 24.8 77.0 64.6 | 254.7 318.6 315.3 |
| CRH | 34.58/245.79 | 136.6/96.4 SW 114.4/34.7 SW 136.6/34.7 SW | 25/134 | -31.6 | 198.8 | 3.8/5.6 | -43.7 -66.0 -59.3 | 79.9 192.6 175.6 |
| SWL | 34.47/245.84 | 118.0/83.0 SW | 22/31 | 45.5 | 8.7 | 4.5/10.8 | 48.0 | 228.3 |
| SWH | 34.47/245.84 | 118.0/83.0 SW 071.1/56.4 SE | 17/31 | 7.2 | 0.7 | 7.5/12.4 | 62.9 56.0 | 295.8 16.5 |

Note: *= average attitudes of dikes and flows (individual attitudes of flows used for tilt correction of site 40, refer to appendix C); N/N = number of samples averaged/number of samples collected for dikes or number of flows averaged/number of flows collected; I and D= inclination and declination of site mean, in degrees, before tilt correction; $\alpha_{95}$= minimum and maximum axes of the 95% confidence ellipse (Bingham, 1974); $I_c$ and $D_c$= inclination and declination of site mean after correction for tilt; Exp= expected Miocene magnetic direction using 15-20 m.y. window (Irving and Irving, 1982); CBL= Crossman Block dikes, low temperature component (0-300°C); CNH= Crossman Block dikes, normal polarity, high temperature component (400-680°C); CRH= Crossman Block dikes, reversed polarity, high temperature component (400-680°C); SWL= Standard Wash Block dikes, low temperature component (0-300°C); SWH= Standard Wash Block dikes, high temperature component (400-680°C).

magnetic inclination could result if there was an initial
dip to the sub-flow topography. Nielson and Beratan (1990)
have argued that the large variations in stratal dips in
sequences II and III are due to original dips of flows
deposited on uneven topography. This variation is not
present in sequence I flows. They have also proposed that
the basal arkosic deposits of sequence I, which grade
downward into grus zones on pre-Tertiary rocks, record early
Tertiary weathering and erosion under conditions of relative
crustal stability. It is, therefore, unlikely that the
deviation of the flow site-mean magnetic direction from the
expected direction is due to the effects of the sub-flow
topography. In the third case, Cenozoic tectonism and
extensional faulting in this region is characterized by
clockwise and counterclockwise rotations about vertical
axes, but not by northward transport relative to the North
American craton (c.f. Calderone et al., 1990; Wells and
Hillhouse, 1989). It is, therefore, unlikely that this is
the cause for the discordant inclination at site 40. In the
fourth case, because a) the total number of flows used in
determining the average magnetic direction at site 40 is
low, b) the magnetic directions are of a single polarity,
and c) the flows may have erupted during a short time
interval, this apparent magnetic anomaly is likely the
result of magnetic secular variation not having been
sufficiently averaged. Other workers in this region have

found that single stratigraphic sections rarely span enough time to average out variations of the magnetic field from the axial dipole; only when many sections are combined is a true representation of the dipole field obtained (Calderone et al., 1990).

The eight samples from the vitrophyre at site 49 gave poorly grouped directions, suggesting that they were either 1) entirely overprinted by an isothermal remanent magnetization of a high coercivity, or 2) mechanically disturbed (brecciated) after magnetic remanence acquisition. NRM distrbutions (fig. 20) at this site are skewed towards high intensities favoring the former option. Each sample has a single component of magnetization (fig. 24). This component was successfully isolated by both AF and TH demagnetization techniques, though TH procedures were best at unblocking the total magnetization. The intensity of magnetization decreased very little until temperatures greater than 550°C were reached; then the magnetization decreased sharply as the Curie temperature of magnetite was approached (580°C). In all eight samples, 30 to 80% of the magnetization was unblocked between 550° and 580°C. Though each of these samples has a single component of magnetization, they do not form a tight cluster after cleaning. The magnetic directions of samples from this site are scattered before and after local tilt corrections are
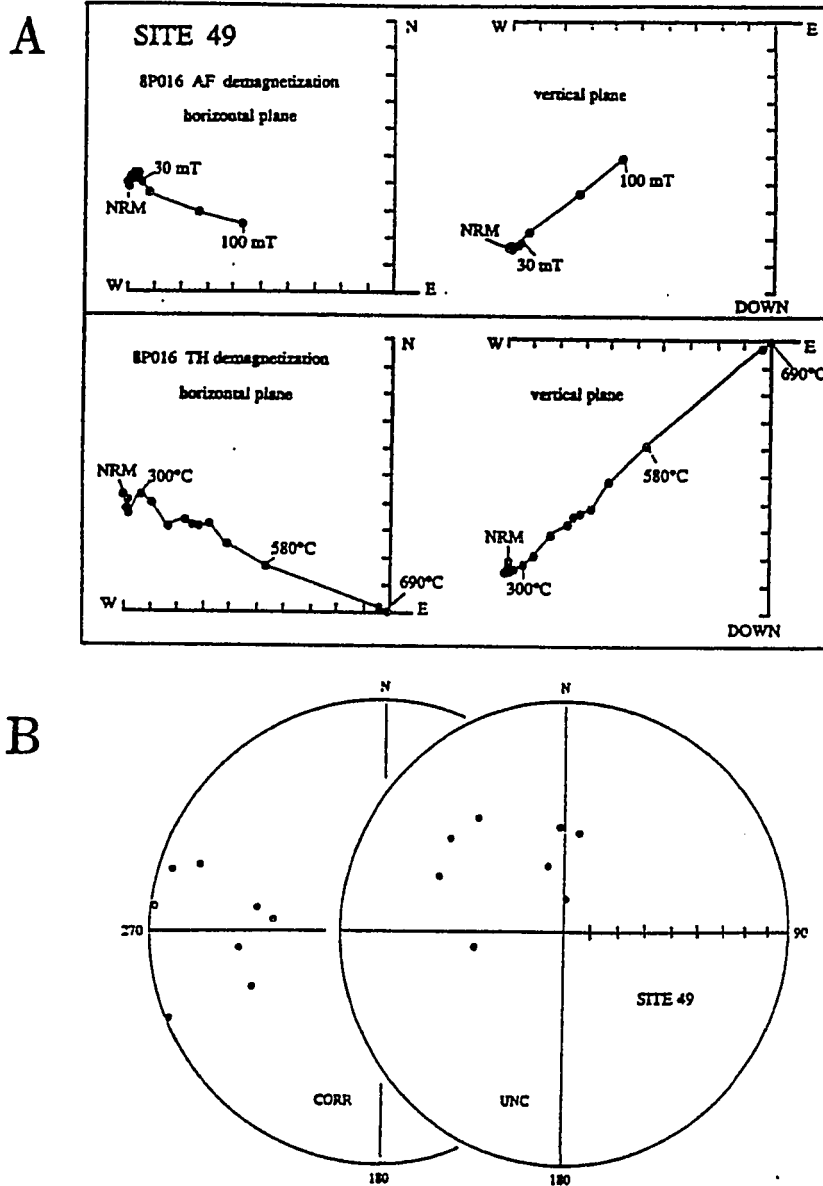
Figure 24. A) Orthogonal vector diagrams depicting AF and TH demagnetizations of a Crossman Block vitrophyre sample. Note the stability of the magnetic direction above 30 mT and 300°C. Axis units: 1 division = 5.38 x $10^{-1}$ Ampere/meter. B) Equal-area projection of directions of magnetization for all samples from the vitrophyre (site 49). Note dispersion before and after correction for tilt of bedding (UNC and CORR, respectively). Symbol convention same as in Fig. 23.

applied (fig. 24). All of the data from this site were rejected.

Dikes. Components of magnetization of normal and reversed polarity were isolated at higher temperatures and coercivities in 55% of the Crossman block samples. The dikes record a complex history of magnetization (fig. 25). Signals of normal and reversed polarity are mixed within different parts of individual dikes and within individual specimens. For example, some cores give stable directions of one polarity after AF demagnetization and then the opposite polarity after TH demagnetization. In other cases, different parts of a single dike yielded stable magnetic directions of opposite polarity. These two components of magnetization have overlapping coercivities and unblocking temperatures. The optimum peak AF intensities for isolating these components generally ranged from 30 to 70 mT. These components are thermally stable from 400 to 580°C, in the range of Curie temperatures for titanomagnetite, magnetite, and titanohematite. As much as 90% of the total magnetization was unblocked at these temperatures (fig. 22).

This complex magnetic behavior meant that the data from specimens of a single dike could not be averaged together. Instead, each specimen was weighted independently and the data set was divided into two populations based on the two stable directions of magnetization isolated. The magnetic

A

SITE 28 (5H084)

TH demagnetization



B
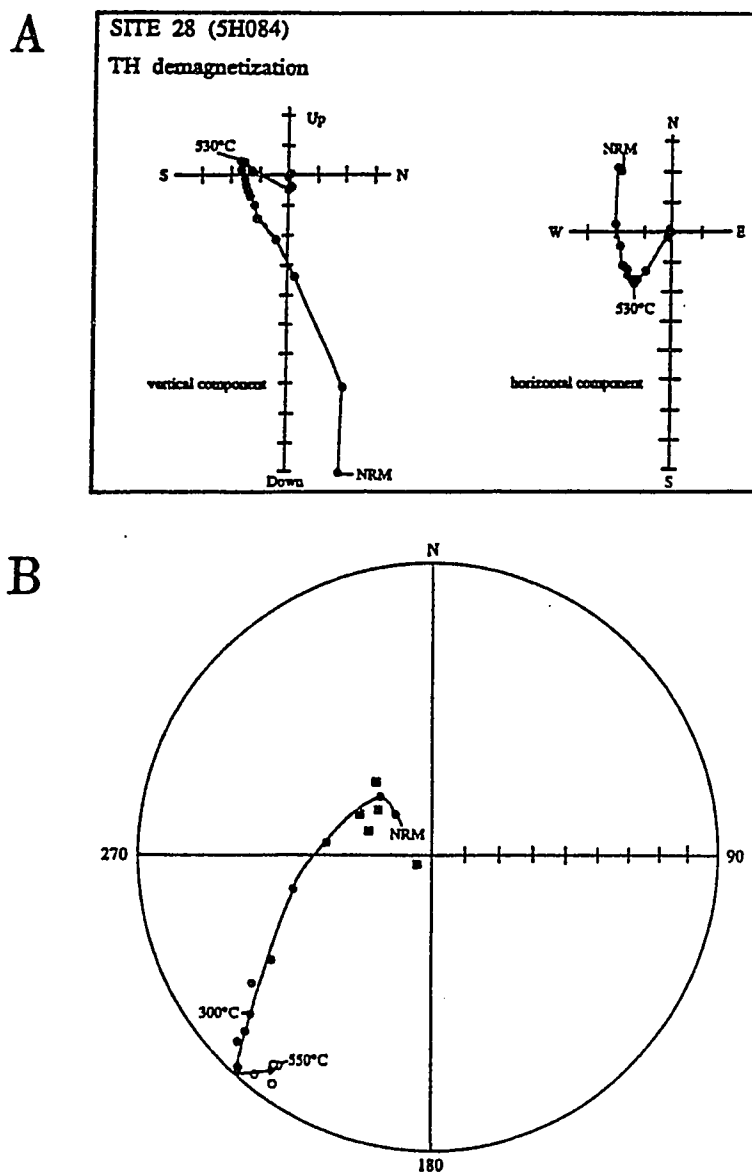
Figure 25.  A) Orthogonal vector diagrams depicting
complex TH demagnetization behavior of a Crossman Block dike
sample.  Axis units: 1 division = 6.83 x 10$^{-3}$ Ampere/meter.
Typical demagnetization behavior is characterized by linear
vector decay into the origin, recording a single magnetic
polarity.  B) Equal-area projection of change in direction
of magnetization with increasing temperature (site 28,
5H084).  Symbol convention same as in Fig. 23; solid squares
= directions associated with >580°C.  Note similarity of
direction of magnetization associated with low and high
unblocking temperatures.

directions of the individual specimens of each of these populations were averaged together to obtain the mean directions of magnetization for normal polarity and reversed polarity groups (table 4). CNH are the specimens of Crossman block dikes which have a normal polarity direction of magnetization in the high-temperature or high-coercivity portion of their demagnetization paths in in-situ co-ordinates. The CNH site-mean direction of magnetization is I=48.5, D=6.4, $\alpha_{95}$= 4.0, 5.2. CRH are the specimens of Crossman block dikes which have a reversed polarity direction of magnetization in the high-temperature or high-coercivity portion of their demagnetization paths in in-situ co-ordinates. The CRH site-mean direction of magnetization is I=-31.6, D=198.8, $\alpha_{95}$= 3.8, 5.6.

Approximately 30% of the specimens in which these high-temperature or high-coercivity components were not identified were overprinted with an isothermal remanent magnetization which was never completely removed (refer to section on secondary magnetization induced by lightning). Approximately 10% of the specimens were magnetically unstable, having very low coercivities and losing 90% of their total magnetization by about 400°C (fig. 22). The remaining 5% of the specimens are from site 39. A stable component of magnetization was determined for each specimen from this site, but because the magnetic directions were scattered and the rocks were highly fractured, the

individual specimens from this site were assumed to have been locally displaced (fig. 26). The data from the above specimens were not included in the group means.

In 77% of the specimens a secondary component of magnetization was identified at temperatures less than 300°C (Appendix B). This low-temperature, normal polarity component has an in-situ direction of magnetization (I= 54.4, D= 8.0, $\alpha_{95}$= 3.7, 4.4; CBL in table 4) indistinguishable from a modern-day magnetic direction. Though this direction is also similar to the expected Miocene direction, the low thermal stability and variable coercivity of this component of magnetization likely reflects its nature as a viscous remanent magnetization (VRM) or a chemical remanent magnetization (CRM). This secondary magnetization may be carried by maghemite, which typically has Curie temperatures around 350°C. Maghemite often occurs as a low-temperature oxidation rim around magnetite. The oxidation of magnetite is visible in thin-section (Appendix A). The in-situ direction of magnetization associated with this VRM or CRM implies that it was acquired after deformation of the dikes.

At temperatures in excess of 580°C, as much as 10% of the total magnetic intensity remained in dike samples from the Crossman block. The magnetic directions associated with these higher temperatures of treatment are similar to the low temperature component (fig. 25). A stable component of
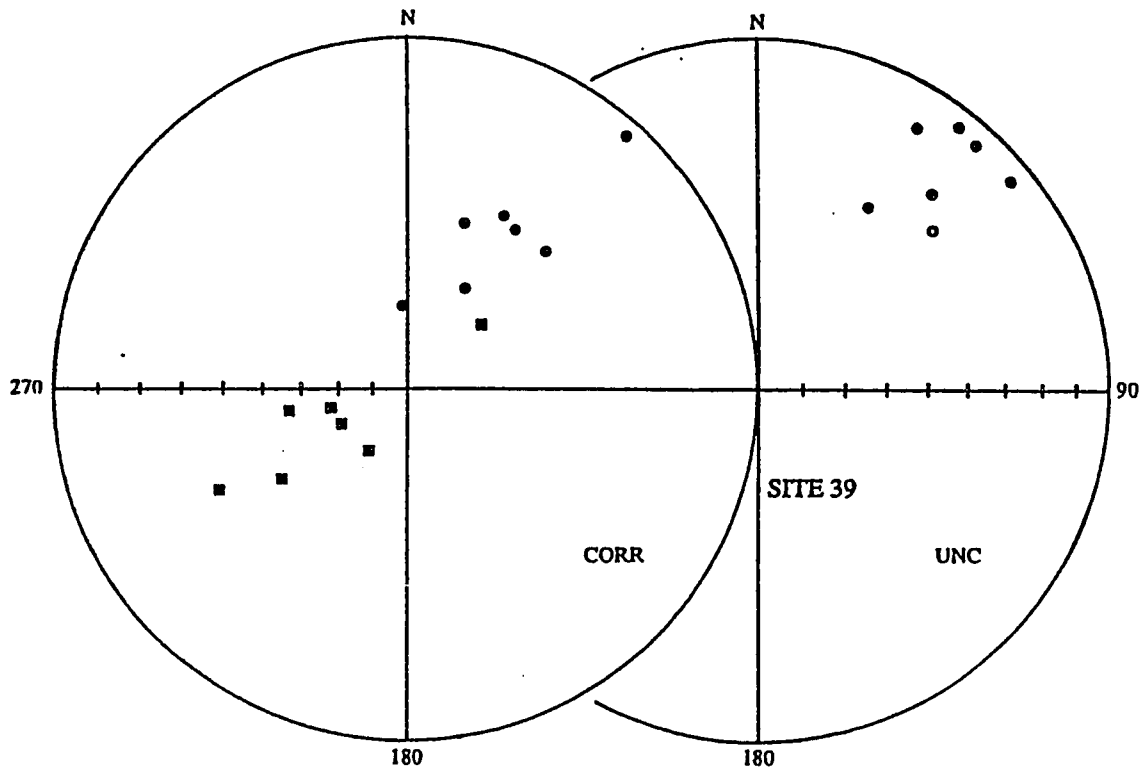
Figure 26. Equal-area projection of directions of magnetization of samples from site 39, before and after corrections for tilt (UNC and CORR, respectively). Symbols same as in Fig. 23. Two structural corrections were applied: dots = restoration of dike to vertical about strike of dike and squares = corrected for tilt by restoring flows to horizontal. Note dispersion of directions of magnetization before and after correction for tilt.

magnetization was not successfully isolated at temperatures of more than 580°C, because so little of the total magnetic intensity remained. It is plausible that the oxidation of titanomagnetite to titanohematite has produced these high unblocking temperatures (>580°C) and that this process has also recorded the same secondary component of magnetization as CBL. The presence of oxidation rims around the principal magnetic carrier can be seen in thin-sections (Appendix A) and lends further support to this hypothesis.

Baked-Contact Test. Samples were collected at site 34, located in the eastern Mohave Mountains, to perform a baked-contact test. This test evaluates the thermal stability of magnetization in an intrusion and its country rock by comparing their directions of magnetization. As distance from the intrusion increases, the effects of reheating of the country-rock resulting from the intrusion will diminish. Ideally, four zones of magnetic direction variation will be defined: 1) The metamorphic zone, where extensive changes in magnetic mineralogy and a total TRM with the direction of magnetization of the intrusion is observed in the country-rock; 2) the heated zone, where minor changes in the magnetic mineralogy occurs and a partial TRM remagnetization with the intrusive magnetic direction is observed in the country-rock; 3) the warmed zone, where minor changes in the magnetic mineralogy occur

and a partial TRM remagnetization of unusual direction is
observed; and 4) the unheated zone, where no change in
magnetic mineralogy or direction of magnetization is
observed.  The intrusion is regarded as having a stable
magnetization if it remagnetizes the country-rock since the
country-rock is of a different age and composition.  The
eastern side of the Mohave Mountains was at a higher
temperature than the western side at the time the dikes were
intruded (about 200°C at 20-22 m.y. ago, Foster et al., in
press); thus the likelihood that the country-rock and the
intrusion would have the same direction of magnetization is
maximized in this area.  A total of 9 cores were collected
at this location.  Of these 9 cores, 5 were from a mafic
dike and 4 were from the adjacent gneiss outcrop collected
at ≈0.5 m intervals away from the dike.

The results of the baked-contact test from site 34 are
shown in figure 27.  Though none of the samples of gneiss
cleaned to stable endpoints, the traces of their
demagnetization paths are shown.  The sample closest to the
dike has a similar magnetic direction to that of the dike
only at the lower unblocking temperatures.  This corresponds
to the heated zone, where the gneiss is partially
remagnetized by the dike.  The metamorphic zone is not
present, suggesting that the dike was intruded under
somewhat wet conditions (Jaeger, 1959; Buchan et al., 1980;
Delaney, 1982; Kristjansson, 1985).  As distance from the
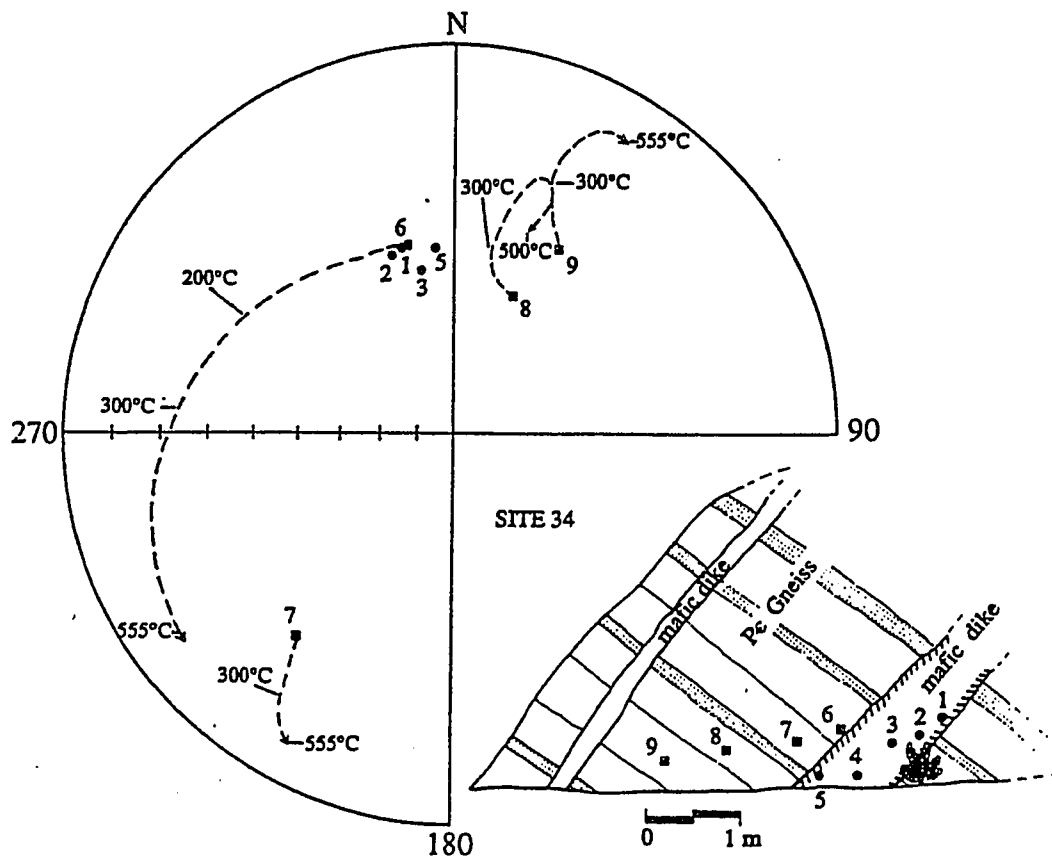
Figure 27. Baked-contact test. Sample distribution and equal-area projection of changes in magnetic direction associated with temperature for these samples. Symbols same as in Fig. 23. One dike sample had no stable endpoint (4) and is not plotted. Gneiss samples never reached stable endpoints, but traces of demagnetization paths are shown.

dike increases, the agreement of the magnetic directions between the dike and the gneiss decreases. The samples farther from the dike appear to be less overprinted and may even be unaffected by the intrusion of the dike (the warmed zone or the unheated zone). In either case, the magnetic direction is distinct from that of the dike. Though the dike was intruded into warm country-rock, the thermal energy from the dike was not great enough to thoroughly remagnetize the country-rock. The dike was able to partially remagnetize the country-rock and displays a thermally stable magnetization. This suggests that the dikes cooled relatively quickly after intrusion into the gneiss.

## Standard Wash Block Dikes

Multiple components of magnetization were isolated in the dike samples from the Standard Wash block. These components are similar to those of the Crossman block in as much as there are two high-temperature/high-coercivity components and a single low-temperature/low-coercivity component (fig. 28). The high-temperature components are thermally stable from 350 to 580°C and by 580°C usually have less than 10% of their total magnetic intensity remaining (fig. 22). These unblocking temperatures are within the range of Curie temperatures for magnetite, titanomagnetite, titanohematite, and maghemite. The optimum peak AF

SITE 45 (7J160)

TH demagnetization
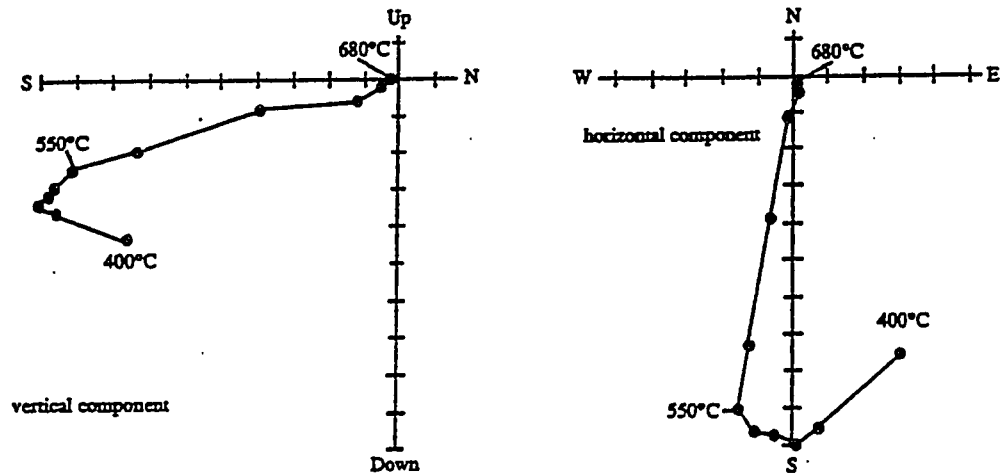


Figure 28. Orthogonal vector diagram depicting the TH demagnetization of a sample from the Standard Wash Block. Note stabilization of magnetization direction at temperatures above 500°C. Axis units: 1 division = 1.80 x 10$^{-5}$ Ampere/meter.

intensities used to isolate these components ranged from 30 to 80 mT.

Two polarities of magnetization are present as high-temperature components, but because one of them is recorded in only three samples the magnetic directions of these two high-temperature components have been averaged into a single population, SWH (Standard Wash high-temperature component). For consistency and ease of comparison with the Crossman block dike data, these samples were also weighted independently and an in-situ combined group mean magnetic direction was obtained (I=7.2, D=0.7, $\alpha_{95}$= 4.5, 10.8; table 4). Due to magnetic instability or the incomplete removal of a secondary component of magnetization, 45% of the samples were rejected.

A low-temperature component of magnetization was also identified in 71% of the samples from the Standard Wash block. This component is stable up to 300°C. The Standard Wash block low-temperature component (SWL) has a stable in-situ magnetic direction of I=45.5, D=8.7, $\alpha_{95}$= 4.5, 10.8. This magnetic direction is indistinguishable from the modern day or Miocene expected directions at the 95% confidence limit; from its low thermal stability, it is likely that the magnetization was acquired as VRM or CRM after the dikes were emplaced. It is possible that this component was the result of the oxidation of magnetite to maghemite.

## Discussion

Magnetic Stability

A typical, unoxidized titanomagnetite from a basaltic dike has a Curie temperature of about 200°C (Ade-Hall et al., 1971). This magnetic phase, however, is highly susceptible to post-consolidation oxidation. This oxidation generally results from deuteric alteration, regional metamorphism, or meteoric-hydrothermal alteration. It is important to know which of these processes has occurred since only deuteric alteration will necessarily be the same age as the dike and the primary magnetization.

Degrees of deuteric oxidation have been defined by Ade-Hall et al. (1968) and the progressive deuteric oxidation of titanomagnetite has been documented by Gromme et al. (1969). One of the important magnetic effects of deuteric oxidation is the production of ilmenite + magnetite from the original titanomagnetite. This compositional change results in an increased Curie temperature for the magnetic phase to as high as 580°C. Further oxidation of these products to titanohematite can result in even higher Curie temperatures (up to 680°C). Magnetic phases with such high Curie temperatures are very stable and generally record the direction of the earth's geomagnetic field at the time of oxidation.

It is clear that the mineral carrying the single magnetic component in the flows is a high-temperature oxidation product which is thermally stable and can be regarded as a TRM acquired at the time of flow deposition. The magnetic mineral(s) responsible for the high-temperature component in the dike samples may be associated with deuteric oxidation, but this is not always clearly defined. Some dikes from the Mohave Mountains record two polarities of magnetization, both with high unblocking temperatures. In these cases, magnetization had to be acquired either 1) over at least the duration of a polarity transition, estimated in one case to be 550 ± 150 years (Mankinen et aL, 1985); or 2) at a later time as a partial remagnetization, possibly a CRM related to later hydrothermal (?) alteration. In spite of these ambiguities, an argument can be made for the primary nature of the high-temperature component of magnetization associated with the Crossman block dikes:  1) The best constrained $^{40}$Ar/$^{39}$Ar data suggest that these dikes cooled relatively quickly about 19 m.y. ago and have not experienced regional reheating to temperatures >300°C since that time.  2) The baked-contact test suggests that the dikes cooled relatively quickly and that metamorphism or hydrothermal alteration after dike emplacement was not pervasive or that it occurred at temperatures <300°C.  3) The major-element chemistry defines a magmatic trend, suggesting that alteration of the dikes may be deuteric

(perhaps late-stage?). 4) If hydrothermal circulation did occur, it probably occurred at temperatures <300°C (the closure temperature for the retention of argon in biotite) after 19 m.y. ago and was unlikely to be very long-lived (<5000 years; see chapter on petrography). Thus, a CRM resulting from hydrothermal alteration is likely to be Miocene in age. If the dikes which record two polarities of magnetization carry a CRM resulting from hydrothermal alteration, the timing of hydrothermal circulation in the Mohave Mountains can be further constrained to have occurred between 550 and 5000 years after dike emplacement. It is, therefore, likely that the high-temperature magnetization of the dikes is a record of the geomagnetic field at the time of dike emplacement and cooling. Assuming this to be the case, further discussion about the structural corrections of paleomagnetic data is presented below.

Crossman Block Dikes

The magnetic directional data from the dikes of the Crossman block are summarized in figure 29 and in table 4. The mean directions of magnetization from the Crossman block, CNH and CRH, are of two polarities but are not antipodal. Though the CNH population has an in-situ direction of magnetization appropriate for the Miocene, the CRH population requires some structural correction to bring it into agreement with the expected Miocene direction. The
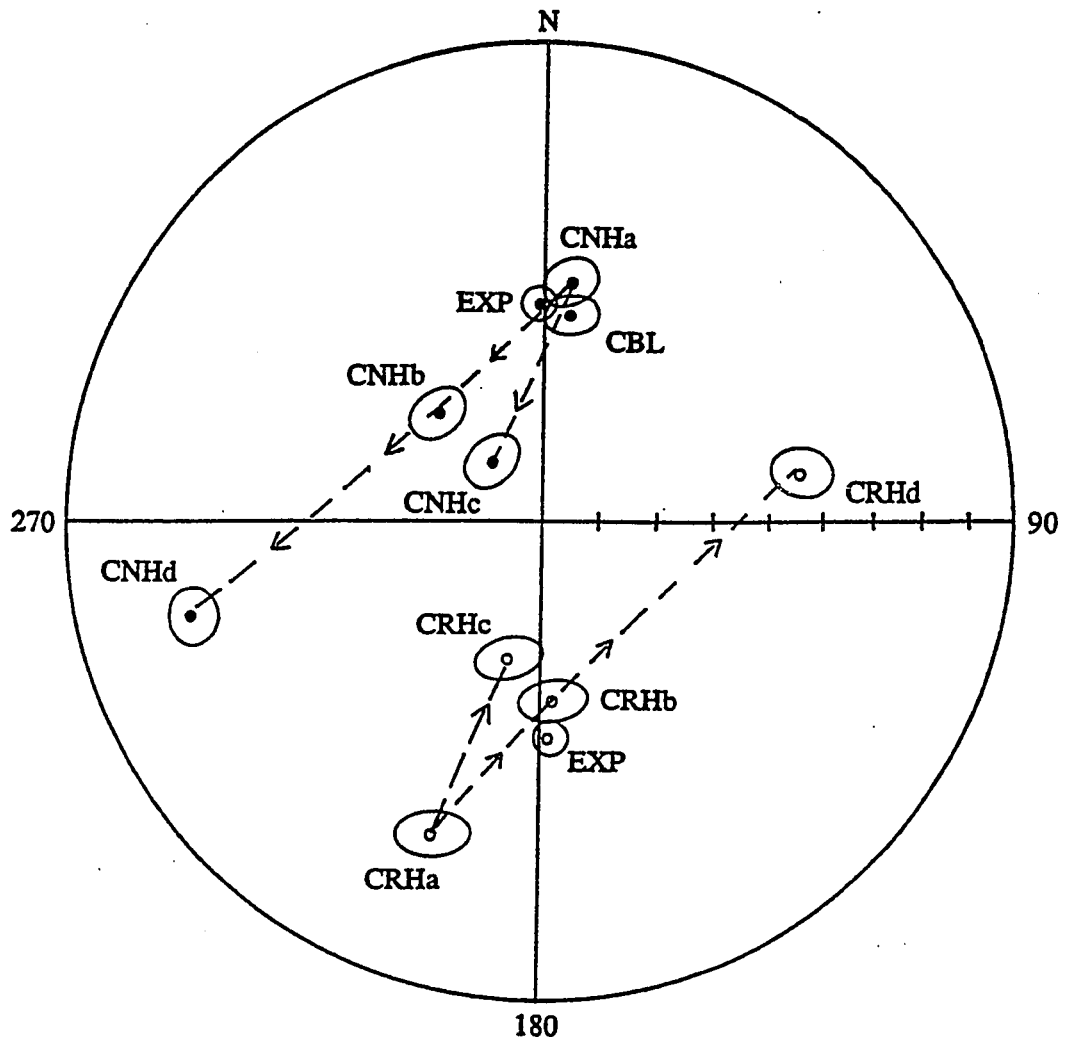
Figure 29. Summary of Crossman Block paleomagnetic
data. EXP, expected axial dipole direction for Miocene
time; CBL, site-mean magnetic direction of Crossman Block
low-temperature component; CNH, site-mean magnetic direction
of Crossman Block normal polarity high-temperature
component; CRH, site-mean magnetic direction of Crossman
Block reversed polarity high-temperature component. Various
structural corrections are applied to the data: a =
uncorrected data, b = dikes restored to vertical about
strike of flows, c = dikes restored to vertical about
strike of dikes, d = corrected for tilt by restoring flows
to horizontal. Symbols same as in Fig. 23.

primary control on paleohorizontal is from the bedded volcanic rocks exposed in the western edge of the study area. The main body of the Crossman block dikes has no primary structural control except the assumption of original verticality. The structural corrections which can most reasonably be applied to this data are 1) to correct these directions about the strike and dip of the regional structure as recorded by the attitudes of the flows of site 40 (136.6°/96.4° SW), 2) to correct these directions by restoring the dikes to their assumed original, near-vertical positions by rotating the dikes 34.7° to the southwest about the average strike of the flows (136.6°), and 3) to correct these directions by restoring the dikes to vertical by rotating the dikes 34.7° to the southwest about the average strike of the dikes (114.4°). There are many possible tilt corrections which would restore the dikes to vertical, but these are the simplest and most consistent with local and regional geology. The tilt corrections were obtained by averaging the poles to the planes defined by the individual attitudes of the flows and dikes (Appendix C) using the statistical method of Fisher (1953) for the distribution of points on a sphere.

In applying the three geologically reasonable structural corrections to the CRH data (fig. 29), it is clear that the regional attitude (136.6°/96.4° SW) over-corrects CRH so that it diverges the greatest amount

from the expected direction. The correction which would restore the dikes to vertical about the average trend of the dikes (114.4°/34.7° SW) gives a direction that is also in poor agreement with the expected direction. The best concordance between the expected direction and CRH is generated by restoring CRH to vertical about the regional trend (136.6°/34.7° SW); this correction results in a slightly steep inclination for CRH, but one that causes the 95% confidence ellipses to just intersect.

The deviation from antipolarity between CRH and CNH can be explained in several ways. First, the CRH component may be contaminated by the incomplete removal of a normal polarity magnetic over-print. However, the westerly deflection of CRH from the expected magnetic direction requires a westerly directed magnetic over-print. The earth's magnetic field has been mostly northerly or easterly since the Miocene so there is no reasonable mechanism for providing this westerly over-print. It is, therefore, unlikely that the magnetic direction of CRH is due to the incomplete removal of a secondary, normal polarity over-print.

Second, the deviation of CRH and CNH from antipolarity may result from both groups not adequately averaging secular variation. In this case, the number of samples averaged to obtain the mean magnetic direction of CRH is too small to represent enough time to have sufficiently averaged the

variation of the earth's magnetic field.  However, the
reasonable amount of scatter in the magnetic directional
data (fig. 30) suggests that secular variation has been
recorded.  The isotopic and hydrothermal modelling data in
the chapters on geochronology and petrography, respectively,
suggest that these dikes probably cooled over hundreds to
thousands of years, thus providing a mechanism for the
acquisition of the complex magnetization.  For these
reasons, it is likely that these samples adequately average
secular variation.

A third alternative is that the magnetization of CRH
was acquired as the Crossman block was tilted and then CNH
was acquired.  In this case, CRH would have been acquired
after 65% of the total tilt of the Crossman block had
occurred, provided the total deformation is indicated by the
slightly overturned southwesterly attitude of the flows.  An
additional 35° of tilt is required after CRH was recorded
and before CNH was recorded.  If this hypothesis is correct,
CRH and CNH would define a small circle about the horizontal
axis of rotation, which in this case should coincide with
the trend of regional structures.

The site-mean magnetic direction for CRH has been
inverted through the origin in figure 31 in order to
determine if CRH and CNH define a small circle path about
the trend of the regional structure.  The regional structure
is defined by the attitude of the flows, which trend
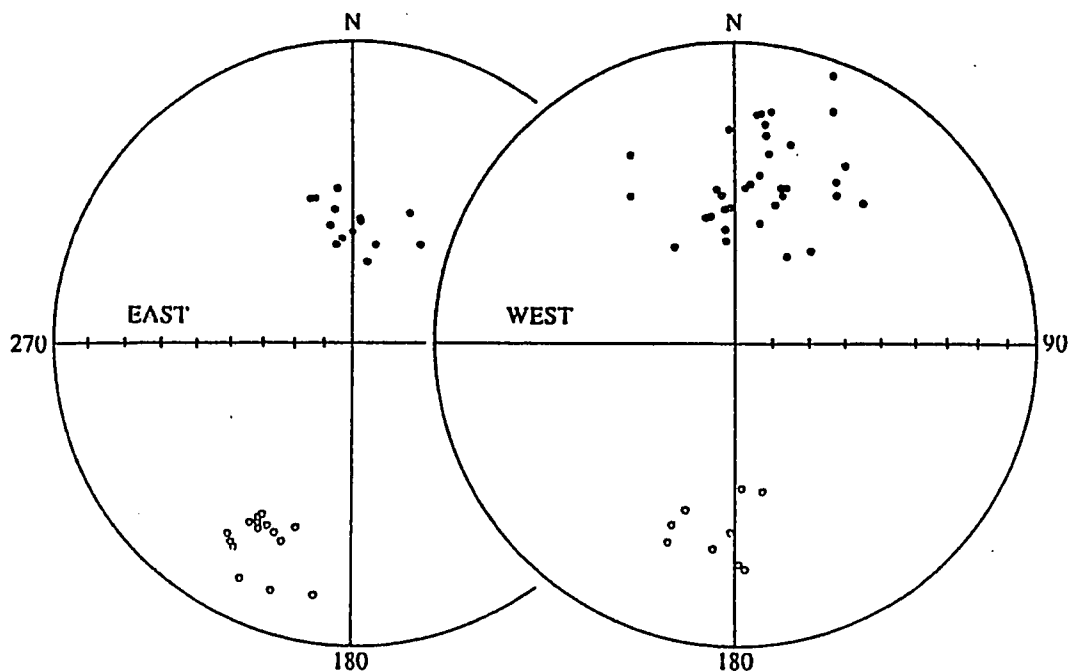
Figure 30. Dispersion and geographic distribution of Crossman Block data. Equal-area projection of directions of magnetization for all samples used in site-mean determinations. Samples are geographically divided according to whether they are east or west of the crest of the Mohave Mountains. Symbols same as in Fig. 23.
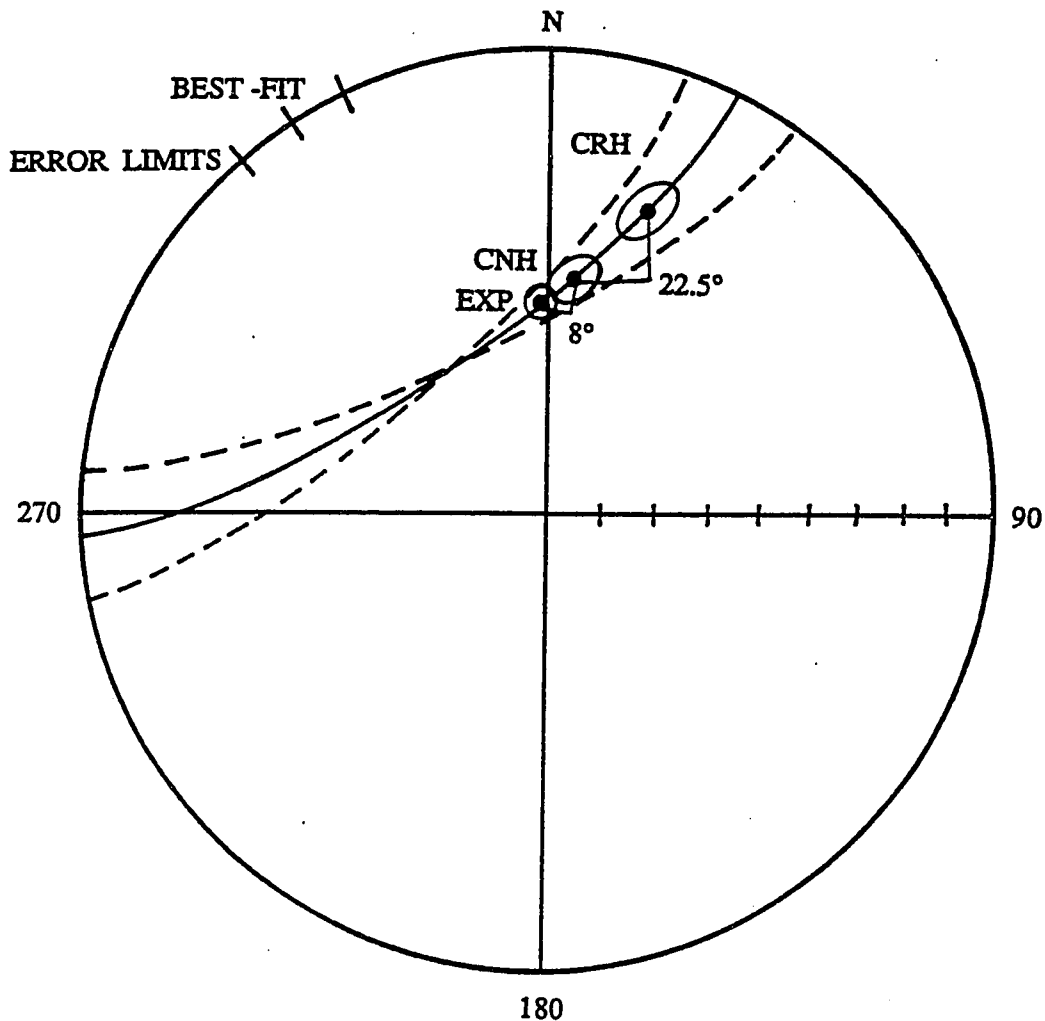
Figure 31. Small circle of rotation associated with Crossman Block data. Abbreviations same as in Fig. 29 and symbols same as in Fig. 23. CRH has been inverted through the origin for graphical representation of small circle fit. Best-fit small circle indicated by solid line through the data and the trend of the axis about which this rotation occurs is perpendicular to it. Error envelope defined by 95% confidence ellipses associated with the data.

northwest-southeast (136.6°). These data define a small circle of rotation; though the best-fit horizontal axis defined by them trends 144°± 8°, the regional trend of 136.6 is within the error limits. This observation is consistent with the hypothesis that the component of magnetization defined by CRH was acquired prior to that of CNH and that CRH has been tilted to a greater extent than CNH about the same horizontal axis.

In order to obtain agreement between the expected direction and CRH at the 95% confidence limit, CRH must be tilted at least 22° but no more than about 40° (fig. 31). This is in agreement with the amount of tilt required to restore the average dike attitude to vertical (34.7°). The correction required to bring CNH into agreement with the expected direction is 0-16° (at the 95% confidence level) and the average attitude of the dikes is not restored to near-vertical orientations. This implies that either 1) CNH dikes have steeper attitudes than CRH dikes, 2) CNH dikes have the same attitudes as CRH dikes, i.e.- CNH and CRH dikes were emplaced at the same time, but that CNH dikes acquired their magnetization after CRH dikes and after most of the deformation had occurred, or 3) that the dikes were not emplaced in near-vertical orientations. The average attitudes of the two populations (CRH and CNH) were obtained by averaging the poles to the individual attitudes according to the statistical method of Fisher (1953). Only the

attitudes of dikes which had magnetizations clearly of a

single polarity were used.

With regards to the first case, the reversed polarity

dikes (CRH) have an average attitude of 295.1/50.0 NE with

an $\alpha_{95}$= 11.9. The number of attitudes used in this

calculation is small (12), resulting in the large $\alpha_{95}$ value.

The precision parameter for this average is also somewhat

low (kappa = 14.3). The normal polarity dikes (CNH) have an

average attitude of 293.2/55.9 NE, with an $\alpha_{95}$= 7.3. This

average includes 19 individual attitudes and has a kappa =

21.8. The mean average attitude of the normal polarity

population is steeper than that of the reversed polarity

population, as would be expected if the reversed polarity

dikes were intruded and tilted prior to the reversal of the

earth's magnetic field and the intrusion of the normal

polarity dikes. The mean attitudes, however, are not

significantly different at the 95% confidence limit.

Furthermore, the 6° difference between these mean attitudes

is not a great enough difference to account for the

directional difference between CRH and CNH (fig. 31).

In the second case, in order for CNH and CRH dikes to

have the same attitudes in a tilted block, they must have

been emplaced at the same time. The normal polarity samples

(CNH) would have acquired their magnetization after that of

CRH samples. This is possible if CNH samples were located

in the eastern portion of the Crossman block, which was at

higher ambient temperatures than the western side in the
Miocene due to its greater initial depth (Foster et al, in
preparation). Figure 30 shows the geographic distribution
of samples with normal and reversed polarity in the Crossman
block. The east-west dividing line is the crest of the
Mohave Mountains, which cross-cuts the sampling traverse
(fig. 2). There is no apparent geographic relationship of
either CNH or CRH samples.

In the third case, non-vertical intrusion of some of
the dikes is implied by the near coincidence of the in-situ
direction of magnetization of CNH with the expected
direction of magnetization. In extensional environments the
greatest principal stress axis ($\sigma_1$) is often vertical and
the axis of least principal stress ($\sigma_3$) is horizontal. In
an orthogonal stress regime dikes are usually oriented
perpendicular to $\sigma_3$ and parallel to the $\sigma_1$-$\sigma_2$ plane, thus
dikes are generally intruded vertically. If the original
intrusive orientation of CNH dikes in the Crossman block
striked NW and dipped $\approx 63°$ NE, as the paleomagnetic data
suggest, then $\sigma_3$ was inclined to the horizontal 25-30° and
trends NE-SW. If the stress field was orthogonal, the $\sigma_1$-$\sigma_2$
plane would be similarly displaced from horizontal. It is
also possible that the stress field was not orthogonal, in
which case little can be inferred about the orientation of
the $\sigma_1$-$\sigma_2$ plane. In either case, the inclination of $\sigma_3$ from
horizontal (as determined from the orientations of CNH

dikes) implies that the stress regime along low-angle normal faults can change over time with continuing deformation, as the earlier intrusive events (CRH) record a stress configuration in which $\sigma_3$ was oriented in the horizontal plane. Other workers (e.g.- Spencer, 1985; Davis and Lister 1988) have proposed that complex stress configurations may be the result of isostatically induced distortions or may be due to primary corrugations or flutes in fault surfaces.

Standard Wash Block

The mean magnetic direction for the high-temperature component of Standard Wash dikes (SWH) in in-situ coordinates is somewhat shallower than the expected magnetic direction (fig. 32). The mean magnetic direction for SWH was corrected for tilt by 1) restoring the local Tertiary flows to horizontal, and by 2) restoring the Standard Wash dikes to a vertical orientation about the strike of the dikes. The area from which these samples were collected is fault-bounded and the local attitude in the volcanic rocks (118.0/83.0 SW) may not provide appropriate structural control; the divergence of the mean SWH magnetic direction from the expected direction after application of this structural correction suggests that this is the case. The best concordance between the expected direction and SWH is generated by restoring SWH to vertical about the trend of
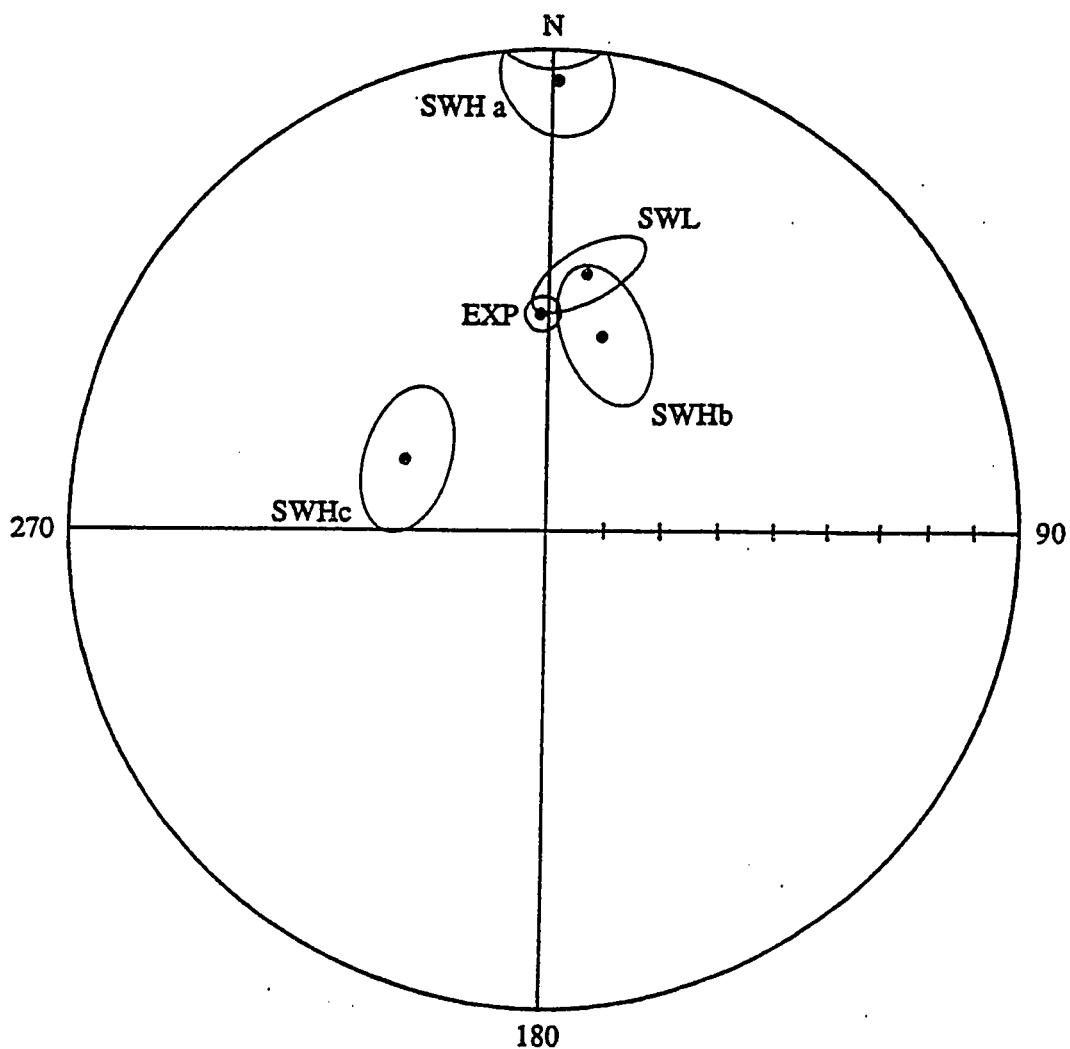
Figure 32. Summary of Standard Wash Block paleomagnetic data. EXP, expected axial dipole direction for Miocene time; SWL, site-mean magnetization direction of Standard Wash low-temperature component; SWH, site-mean magnetization direction of Standard Wash high-temperature component. Various structural corrections are applied to the data: a = uncorrected for tilt; b = corrected for tilt by restoring flows to horizontal; c = dikes restored to vertical about strike of dikes. Symbols same as in Fig. 23.

the dikes (071.1/56.4 SE). The mean direction for SWH and the expected magnetic direction are coincident at the 95% confidence limit after applying this structural correction.

This deformation (56.4° of southerly tilt about a horizontal axis trending 071.1°) helps to define the nature of the Crossman Peak fault. Nielson and Beratan (1990) have suggested that this structure is a transfer fault between the Crossman and Standard Wash blocks. Howard et al. (1982), however, have proposed that it is a detachment fault, probably a subsidiary of the Chemehuevi-Whipple Mountains detachment fault. The coincidence of the mean and expected magnetic directions, after a simple correction for southerly tilt about a horizontal axis parallel to the fault, indicates normal-type displacement for the Crossman Peak fault. Strike-slip displacement cannot be discounted, however, in as much as a fault with pure strike-slip motion will produce rotations only _within_ the shear couple. Some combinations of strike-slip and normal faulting can produce apparent rotations about horizontal axes. In cases such as these, however, in order to obtain the expected magnetic direction using a simple, single-step structural correction (such as that applied here), a strike and dip which has no relationship to the local or regional structures would have to be used. The lack of a declination anomaly eliminates the possibilty for rotation about a vertical axis. The Standard Wash block is displaced by 56° of tilt to the SSE

about a horizontal axis which is parallel to the trend of the fault (071.1°). Thus the Crossman Peak fault has an extensional component and may also be transtensional. The disparity between this sense of motion and regional displacements to the NE may be due to localized doming associated with the isostatic uplift of the Mohave Mountains.

Both the low- and high-temperature site mean magnetic directions from the Standard Wash block have elongate $\alpha_{95}$ confidence ellipses. Elongation of these ellipses may indicate that the data set is too small, that a single component of magnetization was not successfully isolated, or that structural rotation occurred during acquisition of the magnetic remanence. A mixture of two components of magnetization would give an ellipse with a long axis that follows the streak between the two endpoints. This does not seem to be the case between SWH and SWL. If the magnetic remanence was acquired during tilting, the long axis of the ellipse should define a small circle of rotation about the horizontal axis of rotation. This may be the case with SWH, but not with SWL. Whereas the elongation of the error ellipse associated with SWL is, therefore, probably due to undersampling, this must also be true for SWH.

## Summary

1. Dikes in the Mohave Mountains have three components of magnetization, 1) a low-temperature and low-coercivity component (CBL, SWL) which is probably a modern-field magnetic overprint, 2) a high-temperature and high-coercivity component of reversed polarity (CRH), and 3) a high-temperature and high-coercivity component of normal polarity (CNH and SWH).

2. The high-temperature components are interpreted to be Miocene in age because: 1) the isotopic data indicate that the dikes cooled relatively quickly about 19 m.y. ago and were not heated above 300°C since then; 2) the baked-contact test suggests that the dikes cooled relatively quickly, that the dikes have a stable magnetization with a different direction of magnetization than the country rock, and that hydrothermal alteration was not pervasive or it occurred at temperatures of <300°C; and 3) the geochemistry defines a magmatic trend little modified by secondary alteration.

3. The deviation of CRH from CNH and the expected direction of magnetization is best explained as a result of differential rotation about a horizontal axis. The data define a small circle of rotation about a horizontal axis trending ≈144°; this is approximately parallel to the inferred axis of tilt for the Crossman block. In this

interpretation, the reversed polarity dikes were emplaced after the Crossman block experienced 65% of its total tilt and were intruded in near-vertical orientations. The Crossman block tilted farther, the earth's magnetic field reversed, and the normal polarity dikes were intruded in non-vertical ($\approx 60°$) orientations. Some of the reversed dikes were still cooling at this point and picked up a normal polarity component of magnetization as well.

4. The paleomagnetic data from the Crossman block imply that the orientation of the stress field associated with low-angle detachment faults varies with time. The stress field is initially orthogonal and either rotates or becomes non-orthogonal as faulting progresses.

5. The Standard Wash block was tilted 56° to the SSE about a horizontal axis trending 071.1° (parallel to the Crossman Peak fault). Motion across the Crossman Peak fault involved extension and may have a component of strike-slip as well.

CONCLUSIONS

## Petrogenesis

The dike swarm of the Mohave Mountains defines a
calcalkaline trend suggesting that fractional
crystallization was the dominant differentiation process.
However, significant oxide variation within the basaltic
data suggest that some of these samples may have experienced
crustal contamination or were derived by lesser degrees of
partial melting. The alteration of the dikes probably
records late-stage deuteric or short-lived hydrothermal
circulation. Temperatures during secondary alteration did
not exceed 300°C since about 19 m.y. ago. Alteration
affected the Standard Wash block to a greater degree than
the Crossman block, but it appears that the dikes did not
suffer the extreme potassic metasomatism recognized in the
Sleeping Beauty area of the Mojave Desert. This dike swarm
may be related to the Chamber's Well dike swarm in the lower
plate of the Whipple Mountains 22 km to the SE, but there is
insufficient data to support or disprove such a correlation.

## Cooling History

A single undisturbed $^{40}Ar/^{39}Ar$ biotite age of 19.25 ±
0.17 m.y. was obtained from a dacite dike in the eastern
Mohave Mountains. This date is interpreted to represent the

crystallization age of the dike. Incremental age spectra
from hornblende separates are complex, but single increment
minimum and maximum ages are in close agreement with each
other (21.1 ± 0.6 m.y. and 19.5 ± 1.4 m.y., respectively).
There are three principal reasons to believe that the dike
swarm of the Mohave Mountains cooled relatively quickly: 1)
Quenched textures are observed in dikes in the west side of
the mountains, 2) hornblende and biotite ages from the east
side of the range are similar, although the closure
temperatures for the retention of argon in biotite and
hornblende are different by ≈200°C, and 3) in the
baked-contact test, different directions of magnetization
are observed between the dike and the country rock in the
east side of the mountain range. The crystalline basement
in the eastern Mohave Mountains was warm at 20-22 Ma
(200-300°C), but the dike swarm was intruded and cooled
relatively quickly. Subsequent heating due to hydrothermal
circulation did not reach temperatures greater than 300°C
after 19 m.y. ago and hydrothermal modelling suggests that
the dike swarm would have cooled to temperatures less than
300°C within a few thousand years.

## Tectonic History

Detachment faulting in the Mohave Mountains began ≈20
m.y. ago. Dikes intruded the Crossman block and acquired
their magnetization relatively quickly; some dikes record

two high-temperature components of magnetization of opposite polarity, one of which may be a CRM related to hydrothermal alteration. If this is true, hydrothermal circulation must have occurred between 550 (the time required for a polarity transition) and 5000 years after emplacement of the dike swarm. At the time that CRH magnetization was acquired, dikes were intruding the Crossman block in near-vertical orientations after the Crossman block had already been tilted 60° to the southwest. Deformation along the detachment fault continued and the Crossman block was progressively tilted to the southwest. Dike intrusion still occurred. It is possible that the ongoing deformation did not occur in a uniform or continuous manner because no systematic variation in the orientation of the dikes is recorded. After the culmination of 80-100° of southwest tilt, the stress regime associated with the Crossman block changed. Dikes recording the CNH magnetic component intruded in non-vertical orientations. The change in the overall stress regime associated with the Crossman block implies that the stress field associated with detachment faulting either rotates or becomes non-orthogonal with progressive deformation. Domal uplift of the Crossman block was probably occurring at the time of detachment faulting and resulted in the rotation of the Standard Wash block (top-to-the-SSE).

REFERENCES

Ade-Hall, J. M., Palmer, H. C., and Hubbard, T. P., 1971, The magnetic and opaque petrological response of basalts to regional hydrothermal alteration: Geophysical Journal of the Royal Astronomical Society, v. 24, p. 137-174.

Anderson, J.L., and Cullers, R.L., 1990, Middle to upper crustal plutonic construction of a magmatic arc; an example from the Whipple Mountains metamorphic core complex: in Anderson, J.L. (editor), The nature and origin of Cordilleran magmatism: Boulder, Colorado, Geological Society of America Memoir 174, 274p.

Bacon, C. R., and Druitt, T. H., 1988, Compositional evolution of the zoned calcalkaline magma chamber of Mount Mazama, Crater Lake, Oregon: Contributions to Mineralogy and Petrology, v. 98, p. 224-256.

Beratan, K. K., 1989, Basin development during Miocene detachment faulting, Whipple Mountains, southeastern California, Ph. D. dissertation, University of Southern California, 320p.

Beratan, K. K., Blom, R. G., Nielson, J. E., Crippen, R. E., 1990, Use of Landsat Thematic Mapper images in regional correlation of syntectonic strata, Colorado River extensional corridor, California and Arizona: Journal of Geophysical Research, v. 95, p. 615-624.

Bingham, C., 1974, An antipodally symmetric distribution on the sphere: Annals of Statistics, v. 2, p. 1201-1225.

Brooks, C., Hart, S., and Wendt, I., 1972, Realistic use of two error regression treatments as applied to rubidium-strontium data: Reviews of Geophysics and Space Physics, v. 10, p. 551-557.

Brooks, W. E., 1986, Distribution of anomalously high $K_2O$ volcanic rocks in Arizona: Metasomatism at the Picacho Peak detachment fault: Geology, v. 14, p. 339-342.

Buchan, K., Schwarz, D., Symons, A., and Stupavshy, M., 1980, Remanent magnetization in the contact zone between Columbia Plateau flows and feeder dikes: Evidence for groundwater layer at time of intrusion: Journal of Geophysical Research, v. 85, p. 1888-1898.

Calderone, G., Butler, R., and Acton, G., 1990, Paleomagnetic of middle Miocene volcanic rocks in the Mojave-Sonora desert region of western Arizona and southeastern California: Journal of Geophysical Research, v. 95, p. 625-647.

Cathles, L. M., 1981, Fluid flow and genesis of hydrothermal ore deposits: Economic Geology, 75th anniversary volume, p. 424-457.

Cathles, L. M., 1977, An analysis of the cooling of intrusives by ground-water convection which includes boiling: Economic Geology, v. 72, p. 804-826.

Chapin, C. E., and Glazner, A. F., 1983, Widespread $K_2O$ metasomatism of Cenozoic volcanic and sedimentary rocks in the southwestern United States: Geological Society of America Abstracts with Programs, v. 15, p. 282.

Coney, P. J., 1979, Tertiary evolution of Cordilleran metamorphic core complexes, in Armentrout, J. W., et al. (editors), Cenozoic paleogeography of the western United States: Sociey of Economic Paleontologists and Mineralogists, Pacific Section III, p. 15-28.

Crittenden, M. D., Coney, P. J., and Davis, G. H. (editors), 1980, Cordilleran metamorphic core complexes: Geological Society of America Memoir 153, 490p.

Dallmeyer, R. D., and Rivers, R., 1983, Recognition of extraneous argon components through incremental-release $^{40}Ar/^{39}Ar$ analysis of biotite and hornblende across the Grenvillian metamorphic gradient in southwestern Labrador: Geochimica et Cosmochimica Acta, v. 47, p. 413-428.

Dalrymple, G. B., and Duffield, W. A., 1988, High precision $^{40}Ar/^{39}Ar$ dating of Oligocene rhyolites from the Mogollon-Datil volcanic field using a continuous laser system: Geophysical Research Letters, v. 15, p. 463-466.

Dalrymple, G. B., and Lanphere, M. A., 1969, Potassium-argon dating: Principles, techniques, and applications to geochronology: Freeman and Company Publishers, San Francisco, 258p.

Dalrymple, G. B., Alexander, E. C. Jr., Lanphere, M. A., and Drake, G. P., 1981, Irradiation of samples for $^{40}Ar/^{39}Ar$ dating using the Geological Survey TRIGA Reactor: United States Geological Survey Professional Paper 1176, 55p.

Dalrymple, G. B., Gromme, C. S., and White, R. W., 1975, Potassium-argon age and paleomagnetism of diabase dikes in Liberia: Initiation of central Atlantic rifting: Geological Society of America Bulletin, v. 86, p. 399-411.

Davis, G. A., and Lister, G. S., 1988, Detachment faulting in continental extension; perspectives from the southwest U. S. Cordillera: Geological Society of America Special Publication 218, p. 133-159.

Davis, G. A., Anderson, J. L., Martin, D. L., Krummenacher, D., Frost, E. G., and Armstrong, R. L., 1982, Geologic and geochronologic relations in the lower plate of the Whipple detachment fault, Whipple Mountains, southeastern California: A progress report, in Frost, E. G., and Martin, D. L. (editors), Mesozoic-Cenozoic tectonic evolution of the Colorado River region, California, Arizona, and Nevada: Cordilleran Publishers, San Diego, California, p. 408-432.

Davis, G. A., Anderson, J. L., Frost, E. G., and Shackelford, T. S., 1980, Mylonitization and detachment faulting in the Whipple-Buckskin-Rawhide Mountains terrane, southeastern California and western Arizona, in Crittenden, M. D., Jr., Coney, P. J., and Davis, G. H., editors, Cordilleran metamorphic core complexes: Geological Society of America Memoir 153, p. 79-130.

Deer, W. A., Howie, R. A., and Zussman, J., 1966, An introduction to the rock forming minerals: Longman Group Limited, London, England, 528p.

Delaney, P.T., 1982, Rapid intrusion of magma into wet rock: groundwater flow due to pore pressure increases: Journal of Geophysical Research, v. 87, p. 7739-7756.

Dickey, D. D., Carr, W. J., and Bull, W. B., 1980, Geologic map of the Parker NW, Parker, and parts of the Whipple Mountains SW and Whipple Wash Quadrangles, California and Arizona (1:24,000): United States Geological Survey Map I-1124.

Fisher, R. A., 1953, Dispersion on a sphere: Proceedings of the Royal Society of London, v. A217, p. 295-305.

Foster, D. A., Harrison, T. M., Miller, C. F., and Howard, K. A., 1990, The $^{40}Ar/^{39}Ar$ thermochronology of the eastern Mojave Desert, California, and adjacent western Arizona with implications for the evolution of metamorphic core complexes: Journal of Geophysical Research, v. 95, p. 20,005-20,024.

Frost, E. G., and Martin, D. L., 1982, Comparison of Mesozoic compressional tectonics with mid-Tertiary detachment faulting in the Colorado River area, California, Arizona, and Nevada, in Cooper, J. D., editor, Geologic excursions in the California desert: Geologic Society of America, Cordilleran Section, 78th Annual Meeting (Field Trip Guide), p. 113-159.

Gans, P. B., and Miller, E. L., 1983, Style of mid-Tertiary extension in east-central Nevada, in Geologic excursions in the overthrust belt and metamorphic core complexes of the Intermountain Region: Utah Geology and Mineral Survey, Special Study 59, p. 108-139.

Glazner, A. F., 1988, Stratigraphy, structure, and potassic alteration of Miocene volcanic rocks in the Sleeping Beauty area, central Mojave Desert, California: Geological Society of America Bulletin, v. 100, p. 402-410.

Gromme, C. S., Wright, T. L., and Peck, D. L., 1969, Magnetic properties and oxidation of iron-titanium oxide minerals in Alae and Makaopuhi lava lakes, Hawaii: Journal of Geophysical Research, v. 74, p. 5277-5293.

Harrison, T. M., 1983, Some observations on the interpretation of $^{40}Ar/^{39}Ar$ age spectra: Isotope Geoscience, v. 1, p. 319-338.

Harrison, T. M., 1981, Diffusion of $^{40}Ar$ in hornblende: Contributions to Mineralogy and Petrology, v. 78, p. 324-331.

Harrison, T. M., and McDougall, I., 1981, Excess $^{40}Ar$ in metamorphic rocks from Broken Hill, New South Wales: Implications for $^{40}Ar/^{39}Ar$ age spectra and the thermal history of the region: Earth and Planetary Science Letters, v. 55, p. 123-149.

Harrison, T. M., Duncan, I., and McDougall, I., 1985, Diffusion of $^{40}$Ar in biotite: Temperature, pressure, and compositional effects: Geochimica Cosmochimica Acta, v. 49, p. 2461-2468.

Heizler, M., and Harrison T., 1988, Multiple trapped argon isotope components revealed by $^{40}$Ar/$^{39}$Ar isochron analysis: Geochimica et Cosmochimica Acta, v. 52, p. 1295-1303.

Howard, K. A., and John, B. E., 1987, Crustal extension along a rooted system of imbricate low-angle faults: Colorado River extensional corridor, California and Arizona, in Coward, M. P., Dewey, J. F., and Hancock, P. L., editors, Continental extensional tectonics: Geological Society Special Publication No. 28, p. 229-311.

Howard, K. A., Goodge, J. W., and John, B. E., 1982, Detached crystalline rocks of the Mojave, Buck, and Bill Williams Mountains, western Arizona, in Frost, E. G., and Martin, D. L., editors, Mesozoic-Cenozoic tectonic evolution of the Colorado River region, California, Arizona, and Nevada: Cordilleran Publishers, San Diego, California, p. 377-390.

Irvine, T., and Baragar, W., 1971, A guide to the chemical classification of the common volcanic rocks: Canadian Journal of Earth Science, v. 8, p. 523-548.

Irving, E., and Irving, G. A., 1982, Apparent polar wander paths Carboniferous through Cenozoic and the assembly of Gondwana: Geophysical Surveys, v. 5, p. 141-188.

Jaeger, J. C., 1959, Temperatures outside a cooling intrusive sheet: American Journal of Science, v. 257, p. 44-54.

John, B. E., 1982, Geologic framework of the Chemehuevi Mountains, southeastern California, in Frost, E. G., and Martin, D. L., editors, Mesozoic- Cenozoic tectonic evolution of the Colorado River Region, California, Arizona, and Nevada: Cordilleran Publishers, San Diego, California, p. 317-325.

Kirschvink, J. L., 1980, The least-squares line and plane and the analysis of palaeomagnetic data: Royal Astronomical Society Geophysical Journal, v. 62, p. 699-718.

Kristjansson, L., 1985, Magnetic and thermal effects of dike intrusions in Iceland: Journal of Geophysical Research, v. 90, p. 10,129-10,135.

Lanphere, M. A., and Dalrymple, G. B., 1978, The use of $^{40}Ar/^{39}Ar$ data in evaluation of disturbed K-Ar systems, in Zartman, R. E. (editor), Short papers on the forth international conference, geochronology, cosmochronology, isotope geology: United States Geological Survey Open File Report 78-701, p. 241-243.

Lanphere, M. A., and Dalrymple, G. B., 1971, A test of the $^{40}Ar/^{39}Ar$ age spectrum technique on some terrestrial materials: Earth and Planetary Science Letters, v. 12, p. 359-372.

LeBass, M., LeMaitre, R., Streckeisen, A., and Zanettin, B., 1986, A chemical classification of volcanic rocks based on the total alkali-silica diagram: Jounal of Petrology, v. 27, p. 745-750.

MacKenzie, W. S., Donaldson, C. H., and Guilford C., 1982, Atlas of igneous rocks and their textures: Longman Group Limited, Essex, England, 148p.

Mankinen, E. A., Prevot, M., Gromme, C. S., and Coe, R. S., 1985, The Steens Mountain (Oregon) geomagnetic polarity transition, 1. Directional history, duration of episodes, and rock magnetism: Journal of Geophysical Research, v. 90, p. 10393-10416.

Marsal, D., 1987, Statistics for geoscientists: Pergamon Press, New York, 176p.

Mathis, R. S., 1982, Mid-Tertiary detachment faulting in the southeastern Newberry Mountains, Clark County, Nevada, in Frost, E. G., and Martin, D. L., editors, Mesozoic-Cenozoic tectonic evolution of the Colorado River region, California, Arizona, and Nevada: Cordilleran Publishers, San Diego, California, p. 326-340.

McClelland, W. C., 1982, Structural geology of the central Sacramento Mountains, San Bernardino County, California, in Frost, E. G., and Martin, D. L. (editors), Mesozoic-Cenozoic tectonic evolution of the Colorado River region, California, Arizona, and Nevada: Cordilleran Publishers, San Diego, California, p. 401-406.

McElhinny, M., 1973, Palaeomagnetism and plate tectonics: Cambridge Earth Science Series, Cambridge University Press, Cambridge, 358p.

Merrihue, C., and Turner, G., 1966, Potassium-argon dating with fast neutrons: Journal of Geophysical Research, v. 71, p. 2852-2857.

Merrill, R. T., and McElhinny, M.W., 1983, The earth's magnetic field: Academic Press, New York, 401p.

Miyashiro, A., 1974, Volcanic rock series in island arcs and active continental margins: American Journal of Science, v. 274, p. 321-355.

Nakata, J. K., 1982, Preliminary report of diking events in the Mohave Mountains, Arizona, in Frost, E. G., and Martin, D. L. (editors), Mesozoic-Cenozoic tectonic evolution of the Colorado River region, California, Arizona, and Nevada: Cordilleran Publishers, San Diego, California, p. 85-89.

Nakata, J. K., Pernokas, M. A., Howard, K. A., Nielson, J. E., and Shannon, J., 19__, K-AR and fission-track ages (dates) of volcanic, intrusive, altered, and metamorphic rocks in the Mohave Mountains area, west-central Arizona: Isochron/West (accepted in 1990).

Nielson, J. E., 1986, Miocene stratigraphy of the Mohave Mountains, Arizona, and correlation with adjacent ranges, in Ehlig, P. E. (compiler), Cenozoic stratigraphy, structure, and mineralization in the Mojave Desert, Guidebook, Trips 5 and 6: Cordilleran Section, Geological Society of America, Fresno, California, p. 15-24.

Nielson, J. E., and Beratan, K. K., 1990, Tertiary basin development and tectonic implications, Whipple detachment system, Colorado River extensional corridor, California and Arizona: Journal of Geophysical Research, v. 95, p. 599-614.

Nielson, J. E., Lux, D. R., Dalrymple, G. B., and Glazner, A. F., 1990, Age of the Peach Springs Tuff, southeastern California and western Arizona: Journal of Geophysical Research, v. 95, p. 571-580.

Norton, D., and Knight, J., 1977, Transport phenomena in hydrothermal systems: Cooling plutons: American Journal of Science, v. 277, p. 937-981.

Spencer, J. E., 1985, Miocene low-angle normal faulting and
dike emplacement, Homer Mountain and surrounding areas,
southeastern California and southernmost Nevada:
Geological Society of America Bulletin, v. 96, p.
1140-1155.

Spencer, J. E., and Turner, R. D., 1982, Dike swarms and
low-angle faults, Homer Mountain and the northwestern
Sacramento Mountains, in Frost, E. G., and Martin, D.
L. (editors), Mesozoic-Cenozoic tectonic evolution of
the Colorado River region, California, Arizona, and
Nevada: Cordilleran Publishers, San Diego, California,
p. 97-108.

Stewart, J. H., 1980, Regional tilt patterns of late
Cenozoic basin-range fault blocks, western United
States: Bulletin of the geological society of America,
v. 91, p. 460-464.

Suneson, N. H., and Lucchitta, I., 1983, Origin of bimodal
volcanism, southern Basin and Range province,
west-central Arizona, Geological Society of America
Bulletin, v. 94, p. 1005-1019.

Wells, R. E., and Hillhouse, J. W., 1989, Paleomagnetism and
tectonic rotation of the lower Miocene Peach Springs
Tuff: Colorado Plateau, Arizona, to Barstow,
California: Geological Society of America Bulletin, v.
101, p. 846-863.

Wernicke, B., and Burchfiel, B. C., 1982, Modes of
extensional tectonics: Journal of Structural Geology,
v. 4, p. 105-115

York, D., 1969, Least squares fitting of a straight line
with correlated errors: Earth and Planetary Science
Letters, v. 5, p. 320-324.

APPENDIX A:  THIN-SECTION DESCRIPTIONS

SITE 1 (5H001) - holocrystalline, fine-grained, porphyritic, allotriomorphic

 74% Groundmass - <0.1 mm, quartz (maybe granophyric), feldspar, epidote, reddish opaques, apatite

 17% Feldspar - subhedral phenocrysts, cumulophyric, 0.5-2.0 mm; albite and carlsbad twins, 2V=60 (-), $An_{32}$; includes epidote, chlorite, and opaques; moderately saussuritized (altered to fine-grained white mica)

 5% Chlorite - seriate, euhedral laths to hexagonal tabs, 0.2-1.0 mm, colorless to blue-green pleochroism, anomolus blue birefirengence, intergrown with epidote and altered opaque inclusions (pseudomorph after biotite)

 3% Epidote - yellow-green color and pleochroism, birefringence = 0.03, cumulophyric, subhedral, <0.25 mm, associated with chlorite and opaques

 <1% Opaques - cumulophyric, anhedral (bytroidal), <0.2 mm, red oxidation mantles visable with 100x magnification (maghaemite or hematite)

 <1% Apatite - pale green to colorless, uniaxial (-), euhedral, prismatic (<0.3 mm in length)

 <1% Zoisite - 2V=45 (+), parallel extinction, colorless, euhedral, <0.1 mm, birefringence = 0.005

 Alteration - feldspar altered to sericite, opaques oxidized, biotite thoroughly altered to chlorite, epidote and opaques:  typical assembledge of hydrothermal alteration

SITE 2 (5H006) - holocrystalline, fine-grained, allotriomorphic, porphyritic

 76% Groundmass - concertal quartz and altered feldspar, chlorite, brown stuff (clay?), fine-grained epidote, apatite

 10% Feldspar - two phenocryst populations, 1) 8% subhedral, cumulophyric and grading into groundmass, replaced by mica (saussuritized), 0.5-1.5 mm, relict albite twins, 2V>65 (+), probably plagioclase but no compositions; 2) 2% subhedral, <1.5 mm, untwinned with lots of inclusions, unaltered, 2V>65 (-):  potassic feldspar or oligioclase

 5% Chlorite - interstitial and pseudomorph after biotite, yellow-green color and pleochroism, birefringence = 0.009, radiate, <0.4 mm, includes opaques, associated with calcite

 3% Opaques - subhedral to anhedral, <0.1 mm, reddish tint or altered to milky-brown, strongly associated with chlorite

 1% Quartz - anhedral, uniaxial (+), birefringence = 0.008, interstitial, <0.5 mm

3% Calcite - anomolous birefringence, calcite twins, anhedral, 0.5-1 mm, associated with potassic feldspar (?) and veins

Alteration - thorough saussuritization of feldspar; association of chlorite, calcite, and opaques: hydrothermal

SITE 3 (5H009) - fine-grained, porphyritic, holocrystalline, allotriomorphic

84% Groundmass - <0.1 mm, anhedral, altered feldspar laths [2V=50 (+)] with lots of inclusions (no compositions), interstitial quartz [uniaxial (+)] without inclusions, opaques, chlorite

10% Feldspar - phenocrysts, anhedral, 1.0 mm, thoroughly saussuritized, too altered for identification

5% Chlorite - associated with opaques, iron-stained, <1.0 mm, pseudomorph after hornblende, green-yellow color and pleochroism, anomolous blue birefringence

1% Opaques - two populations: 1) fresh, black euhedral crystals, <0.1mm, generally associated with chlorite and crystal boundries; 2) altered, oxidized (some to hematite, some just milky), generally smaller in grain-size (<0.1mm), intergranular

Alteration - thorough saussuritization of feldspar, thorough alteration of hornblende to chlorite and opaques: probably hydrothermal

SITE 4 (5H011) - holocrystalline, hypidiomorphic, intergranular, medium-grained, porphyritic, subophitic

80% Groundmass - feldspar laths (probably plagioclase) altered to brown stuff (clay), opaques, pyroxene, chlorite

8% Feldspar - phenocrysts, seriate (0.2-2.0 mm), 2V=70 (-/+), $An_{32-48}$, subhedral, albite twins, fresh cores with rims altered to brown clay (smectite? relict zoning?), includes opaques and some augite

10% Opaques - seriate (<0.02 mm), acicular needles or blocky aggregates, greenish tint (magnetite or maghaemite)

2% Augite - phenocrysts, subhedral to anhedral, 2V=50 (+), twinned, seriate (<1.4 mm), light-green in plane light, some rimmed by opaques, subophitic

<1% Hornblende - tan to dark-brown color and pleochroism, twinned, birefringence = 0.025, good amphibole cleavage, subhedral, 1.0 mm, zoned, rimmed by opaques (basaltic Hb?)

<1% Chlorite - interstitial, <0.1 mm, light blue-green color and pleochroism, birefringence = 0.008

Alteration - pervasive, but not thorough, alteration of feldspar to clay (smectite?); otherwise unaltered

SITE 5 (5H015) - holocrystalline, porphyritic, fine-grained, allotriomorphic

88% Feldspar - 7% subhedral phenocrysts:  <1.0 mm,
2V>65 (-/+), saussuritized, albite and carlsbad twins,
$An_{32-42}$; 81% groundmass quartz and feldspar laths (altered
to clay)
     5% Chlorite - including mica, interstitial,
yellow-green color and pleochroism, birefringence = 0.01,
pseudomorph after hornblende
     3% Calcite - associated with chlorite, opaques, quartz
and epidote, anomolous birefringence, calcite twins, <1.0
mm, anhedral
     3% Quartz - uniaxial (+) phenocrysts, birefringence =
0.008, euhedral to subhedral, 0.25 - 0.5 mm, also in veins
     1% Opaques - seriate, acicular needles to 0.01 mm,
subhedral crystals, oxidized: rutile or illmenite
     <1% Epidote - anhedral, high relief, yellow-green color
and pleochroism, high birefringence, <0.1 mm
     · <1% Apatite - low birefringence, uniaxial (-), <1.0 mm,
euhedral
     Alteration - thorough alteration of groundmass feldspar
and partial alteration of phenocryst feldspar, thorough
alteration of hornblende to chlorite; association of
calcite, chlorite, sericite, and clay imply hydrothermal
alteration

SITE 6 (5H017) - holocrystalline, porphyritic, fine-grained,
hypidiomorphic
     78% Groundmass - micrographic feldspar and quartz, <0.1
mm, opaques and red oxidation stain, interstitial quartz
[uniaxial (+)]
     15% Feldspar - phenocrysts, subhedral, 1.0-4.0 mm,
2V>60 (+/-), albite twins preserved, $An=_{32-42}$ (or potassic
feldspar present), saussuritized, lots of inclusions
     3% Mica - associated with red opaques and alteration of
feldspar, light yellow-green in color, no pleochroism, 2V=30
(-), birefringence = 0.035, <0.2 mm
     2% Chlorite - pseudomorph after biotite, birefringence
variable from 0.003-0.08, includes altered opaques, <0.7 mm,
2V<20 (-):  oxidized chlorite
     1% Quartz - uniaxial (+), embayed, subhedral, 1.0 mm,
with fluid inclusions
     1% Opaques - subhedral, <0.02 mm, individual grains,
acicular needles and glomeroporphyritic black clots with red
rims, associated with chlorite: magnetite/hematite
     <1% Apatite - low birefringence, uniaxial (-), euhedral
crystals, <0.1 mm
     Alteration - feldspar fairly altered to sericite,
biotite thoroughly altered to chlorite and opaques, opaques
and chlorite oxidized; thorough hydrothermal alteration?

SITE 7 (5H022) - altered, holocrystalline, cumulophyric
feldspar and opaques, fine-grained, allotriomorphic

79% Feldspar - two populations: 1) 5% anhedral phenocrysts, 0.5-1.0 mm, "relict" albite (?) twins, highly altered to clay (smectite?) and mica (sericite?), no compositions; 2) 74% groundmass, <0.05 mm, anhedral laths, no compositions

7% Opaques - <2.0 mm, subhedral, glomeroporphyritic, blocky crystals or acicular needles, red oxidation of some needles very thorough, associated with chlorite (square cross-sections of chlorite mantled by opaques = altered pyroxene?)

5% Chlorite - yellow-green color and pleochroism, anomolous birefringence, interstitial fiberous habit, iron-stained, <0.2 mm

5% Quartz - interstitial, micrographic in groundmass with potassic feldspar (?), uniaxial (+), no inclusions

2% Mica - alteration of feldspar, high birefringence, colorless, anhedral, <0.2 mm: sericite?

2% Clay - smectite (?), brown alteration associated with feldspar

Alteration - partial alteration of phenocryst feldspar to mica and clay, thorough replacement of pyroxene to chlorite and opaques: hydrothermal?

SITE 8 (5H023) - holocrystalline, porphyritic, fine-grained, hypidiomorphic, spherulitic

91% Feldspar - 5% phenocrysts: albite and carlsbad twins, subhedral, <1.5 mm, 2V=75 (+), An=$_{52}$, birefringence = 0.007, moderately saussuritized, glomeroporphyritic; 86% groundmass: <0.05 mm, anhedral laths and spherulitic feldspar(?), too fine-grained for optics, no compositions

5% Quartz - euhedral phenocrysts, 1.0 mm, uniaxial (+), mantled by spherulitic feldspar, birefringence = 0.007, embayed

3% Opaques - reddish (oxidized), anhedral, often around crystal boundries and interstitial, glomeroporphyritic, <0.5 mm

1% Muscovite - including oxidized opaques, <1.0 mm, euhedral, 2V=50 (-), birefringence = 0.04, colorless

<1% Zircon (?) - high relief, anhedral, <0.1 mm, anomolous birefringence

Alteration - oxidation of opaques fairly thorough, some alteration of feldspar to clay: alteration minor

SITE 9 (5H026) - holocrystalline, porphyritic, medium-grained, hypidiomorphic, intergranular

70% Feldspar - twined laths, 2V=85 (+), thoroughly saussuritized, subhedral, seriate (0.25-2.5 mm), zoned, too altered for compositions

18% Hornblende - laths, anhedral, 0.5-2.0 mm, light-yellow to red-brown color and pleochroism, anomolous birefringence, includes opaques and augite, inclined

extinction, 2V=80 (-), amphibole cleavage, cores altering to chlorite

    5% Augite - 2v=55 (+), twinned, birefringence = 0.030, subhedral to anhedral, zoned, fractured, glomeroporphyritic, seriate (0.25-1.0 mm), unaltered

    3% Chlorite - colorless to blue-green color and pleochroism, anomolous blue birefringence, radiate habit, interstitial, <0.3 mm

    3% Opaques - euhedral to subhedral, <0.1 mm or clots, red oxidation, associated with hornblende and chlorite ·

    1% Calcite - uniaxial (-), high birefringence, calcite twins, interstitial, anhedral

    1% Epidote - in groundmass, high birefringence, high relief, euhedral crystals, <0.1 mm

    <1% Apatite - low birefringence, uniaxial (-), euhedral crystallites

    Alteration - thorough alteration of feldspar to sericite, oxidation of opaques, calcite + chlorite: hydrothermal alteration?

SITE 10 (5H031) - holocrystalline, allotriomorphic, porphyritic, intergranular, fine-grained, pilotaxitic, a calcite vein

    50% Feldspar - subhedral laths, <1.0 mm, altered to sericite, indistinct albite twins, no compositions but probably plagioclase, flow aligned

    30% Chlorite - yellow-green color, no pleochroism, anomolous blue birefringence, interstitial, anhedral, <0.25 mm

    7% Hornblende - <0.75 mm, subhedral grains, yellow to brown color and pleochroism, twinned, 2V=50 (-), associated with chlorite

    7% Opaques - acicular needles (associated with calcite <0.25 mm, greenish tint) verus subhedral crystals and clots (intergranular, <0.25 mm, with a reddish hue.)

    5% Quartz - anhedral, interstital, uniaxial (+), <0.25 mm

    1% Calcite - anhedral phenocrysts, seriate (<0.5 mm), high birefringence, calcite twins or interstitial radiate fibers

    Alteration - hornblende altering to chlorite, opaques oxidized, feldspar thoroughly altered to sericite: hydrothermal alteration

SITE 11 (5H034) - medium grained, holocrystalline, porphyritic, allotriomorphic

    85% Groundmass - very fine-grained, opaques, consertal textures = quartz (uniaxial +) and feldspar, epidote

    10% Feldspar - albite twins, saussuritized, subhedral, glomeroporphyritic phenocrysts, 1.0-3.0 mm, 2V=70 (-), $An_{34}$, includes opaques and chlorite.

4% Chlorite - subhedral, clear to green color and pleochroism, anomolous blue birefringence, replacing biotite or hornblende, includes stringers of red opaques (hematite/maghaemite/goethite?), apatite and mica, single grains or clots from 0.25-3.0 mm

1% Opaques - some aligned along phenocryst boundries, others large single anhedral grains (0.25 mm) or very fine dusting, altering to sphene (?)

<1% Epidote - euhedral, birefringence = 0.032, straight extinction, <0.1 mm

Alteration - compositions of feldspar still possible, yet mafic phase (biotite or hornblende) is thoroughly altered to chlorite and opaques; probably hydrothermal

SITE 12 (5H037) - altered, fine-grained, porphyritic, holocrystalline, allotriomorphic

77% Groundmass - felty plagioclase laths (albite twins), $An_{52}$, 2V>60 (+), opaques, calcite, minor secondary biotite in groundmass, <0.3 mm

10% Calcite - uniaxial (+), high birefringence, calcite twins, anhedral, <0.25 mm, interstitial and phenocrysts.

10% Chlorite - complete replacement of zoned mafic phase with amphibole cleavage (opaques concentrated along relict zoning: hornblende?), subhedral, 1.0 mm, yellow-blue pleochroism, glomeroporphyritic phenocrysts, anomolous birefringence, also includes calcite

3% Opaques - two populations: 1) blocky, red, subhedral, <0.1 mm, intergranular in groundmass, exsolved along crystal boundries or included in chlorite alteration; 2) blood-red, very fine grained hematite, usually only within altered phenocryst phase

Alteration - thorough; mantling opaques secondary, opaques oxidized; chlorite and calcite replacing amphibole (hornblende); chlorite, opaques, and calcite are typical products of hydrothermal alteration

SITE 13 (5H038) - fined-grained, holocrystalline, intergranular, allotriomorphic, spherulitic

69% Groundmass - open plagioclase and quartz spherulites, plagioclase laths, opaques, augite (?), and hornblende, with some alteration of plagioclase to clay, no compositions

14% Hornblende - microporphyritic, yellow-brown color and pleochroism, birefringence = 0.020-0.025, includes augite, amphibole cleavage, some twins, <0.25 mm, 2V=85 (-)

8% Opaques - anhedral, interstitial, seriate (<0.25 mm), interstitial

5% Chlorite - green-blue color and pleochroism, anomolous blue birefringence, associated with opaques and pyroxene and alteration of hornblende, interstitial, <0.5 mm, 2V=15 (-)

3% Augite - birefringence = 0.023, light-green color and weak pleochroism, anhedral, <0.5 mm, 2V=50 (+), twinned

1% Epidote - minor, interstitial or euhedral, yellow-green color and pleochroism, good cleavage, high relief, birefringence = 0.034, 2V=85 (-), <0.2 mm

Alteration - moderate alteration of feldspar to smectite; hydrothermal?

SITE 14 (5H041) - holocrystalline, fine-grained, intergranular, allotriomorphic, porphyritic

82% Feldspar - 75% altered groundmass, seriate (<1.0 mm), subhedral, some albite twins still visible, altered to clay (smectite), no optics; 5% phenocrysts thoroughly altered to clay, no twins, subhedral, 1.0 mm, no compositions

7% Hornblende - small, euhedral grains (<0.25 mm), may be secondary, birefringence = 0.25, 2V=50 (-)

4% Augite - 2v=65 (+), birefringence = 0.30, zoned, subhedral, seriate (<0.25 mm)

3% Chlorite - associated with epidote and hornblende, mantling opaques, replacing hornblende, blue-green color and pleochroism, anomolous blue birefringence, <0.1 mm

3% Opaques - <0.1 mm, black and red (oxidized), acicular or blocky crystals or glomeroporphyritic, black and red (oxidized)

1% Epidote - interstitial, yellow-green color and pleochroism, euhedral, <0.1 mm, 2V=90 (-), inclined extinction

Alteration - probably hydrothermal

SITE 15 (5H045) - medium-grained phenocrysts in a fine-grained matrix, holocrystalline, intergranular, allotriomorphic

76% Feldspar - 3% phenocrysts: twined, zoned, too altered to sericite and clay for compositions; 73% groundmass untwinned, anhedral, interstitial, and subhedral laths [2V=65 (+)] with no compositions; some untwinned, anhedral groundmass with 2V=70 (-), <0.3 mm (potassic feldspar or orthoclase)

14% Chlorite - yellow-green color, anomolous blue birefringence, interstitial and replacing hornblende, 2V=30 (+), <1.0 mm

4% Opaques - acicular needles or blocky tabs, subhedral to anhedral, some red hematite, all generally <0.1 mm

2% Quartz - uniaxial (+), subhedral, <0.5 mm, interstitial in groundmass

2% Hornblende - subhedral, <0.1 mm, light brown color and pleochroism, high birefringence, 2V=50 (-)

1% Epidote - yellow-green color and pleochroism, twinned, high birefringence, associated with chlorite and alteration of feldspar, interstitial and granular (<0.1 mm),

2V=55 (-), birefringence = 0.04

Alteration - thorough alteration of feldspar to sericite and clay (smectite?) and epidote; variable alteration of hornblende to chlorite and epidote; hydrothermal or autometamorphic

SITE 16 (5H047) - fine-grained, holocrystalline, intergranular, hypidiomorphic

89% Feldspar - 2V=60 (+), seriate laths (<2.0 mm), $An_{38}$ (positive relief of larger grains against groundmass), zoned

5% Augite - 2V=45 (+), <0.25 mm, birefringence = 0.024, included in feldspar, anhedral grains, twins, unaltered

1% Hornblende - subhedral, <0.1 mm, birefringence = 0.023, moderate relief, yellow-brown color and pleochroism, 2V=85 (-), variably altered to chlorite, often mantling pyroxene

3% Chlorite - clear to blue-green color and pleochroism, anomolous birefringence, interstitial, anhedral, <0.1 mm, associated with hornblende

1% Calcite - high birefringence, calcite twins, anhedral, interstitial, <0.5 mm

1% Opaques - blocky, subhedral crystals or acicular needles in random orientation, altering to sphene (?), <0.20 mm, often associated with hornblende

Alteration - thorough alteration of feldspar phenocrysts; association of calcite, chlorite, and oxidized opaques imply hydrothermal alteration

SITE 17 (5H052) - altered, holocrystalline, medium-grained phenocrysts in a fine-grained mesostasis, allotriomorphic, spherulitic

92% Feldspar - 10% phenocrysts: <4.0 mm, saussuritized, anhedral, grades into granophyric groundmass, no compositions, albite twinned, 2V=60 (+), includes opaques; 82% groundmass: plagioclase laths, potassic feldspar, and/or quartz (granophyric/symplectic)

3% Quartz - euhedral phenocrysts, uniaxial (+), <0.25 mm

2% Chlorite - blue-green color and pleochroism, euhedral phenocrysts replacing biotite, <0.7 mm, includes opaques

2% Opaques - associated with chlorite, clots or crystals, <0.1 mm

1% Calcite - mantling quartz, high birefringence, calcite twins, interstitial, <2.0 mm

<1% Mica - 2V=30 (-), birefringence = 0.45, colorless with faint light-green pleochroism

Alteration - thorough saussuritization of feldspar, thorough alteration of biotite to chlorite; probably hydrothermal

SITE 18 (5H053) - altered, holocrystalline, medium-grained, porphyritic, allotriomorphic

5% Feldspar - 2V>65 (+), euhedral, 1.0 mm, untwinned and carlsbad and albite twinned crystals, 1.0-2.0 mm, saussuritized, no composistions

2% Quartz - uniaxial (+), subhedral phenocrysts (<0.7 mm) and interstitial, embayed, fluid inclusions

<1% Mica - colorless, high birefringence, platey habit, <0.25 mm

1% Epidote - anhedral, interstitial, brown grungy stuff with high birefringence and high relief, associated with chlorite

<1% Opaques - very small (<0.1 mm), subhedral crystals with red oxidation mantles

<1% Calcite - high birefringence, calcite twins, anhedral, <1.0 mm

91% Groundmass - feldspar microlites with quartz, epidote, opaques, mica, minor granophyric texture

Alteration - partial saussuritization of feldspar, opaques oxidized; minor hydrothermal alteration; Note: Some veins and cracks filled with feldspar and opaques

SITE 19 (5H057) - medium-grained, holocrystalline, porphyritic, allotriomorphic, spherulitic

14% Feldspar - carlsbad and albite twins, subhedral, 2V=50 (+), saussuritized, $An_{40}$, <1.0 mm or glomeroporphyritic

5% Epidote - brown, grungy stuff with high birefringence, associated with mica, too grungy for figures or compositions

2% Quartz - subhedral, <1.0 mm, uniaxial (+), embayed, nuclei for spherules, lots of inclusions

1% Mica - subhedral, <1.0 mm, mantling epidote and opaques, clear to light-green color and pleochroism, replacing biotite, birefringence = 0.4, sericite? (no optics)

<1% Opaques - stringers or individual euhedral black crystals, seriate (<0.1 mm)

78% Groundmass - feldspar microlites (no compositions), untwinned, anhedral, granophyric feldspar and quartz

Alteration - minor saussuritization of feldspar, thorough replacement of biotite to sericite and epidote; hydrothermal?

SITE 20 (5H061) - spherulitic, medium-grained, porphyritic, allotriomorphic, holocrystalline

10% Feldspar - phenocrysts, carlsbad and albite twins, saussuritized, subhedral, 0.5-2.0 mm, glomeroporphyritic, $An_{30-42}$, no 2V (+/-),includes opaques

3% Quartz - uniaxial (+), anhedral, inclusions, embayed, nuclei for spherules, 0.1-0.3 mm

2% Mica - intergrown with chlorite, epidote and opaques, pseudomorph after biotite, birefringence = 0.04, colorless, sericite?

2% Chlorite - clear to green color and pleochroism, pseudomorph after biotite, birefringence = 0.005, subhedral, 0.7 mm, opaque inclusions, mantled by red oxide stain

2% Sericite - intergrown with chlorite (<1%) and opaques, pseudomorphing after mafic phase (amphibole ?), high birefringence, colorless

1% Epidote - yellow-green color and pleochroism, high birefringence, subhedral grains, <0.1mm, associated with chlorite and mica

1% Apatite - low birefringence, uniaxial (-), euhedral crystallites

1% Opaques - two populations:  1) oxidized, intergranular dusting associated with sericite and chlorite, and 2) subhedral to anhedral blocky crystals interspersed in groundmass and included in feldspar, <0.25 mm

97% Groundmass - fine-grained, spherulitic feldspar and quartz, minor epidote and opaques

Alteration - thorough alteration of biotite to mica and chlorite and epidote, partial alteration of feldspar; hydrothermal alteration?

SITE 21 (5H064) - holocrystalline, porphyritic, altered, allotriomorphic, fine-grained

90% Feldspar - 8% subhedral zoned phenocrysts, saussuritized, seriate (<3.5 mm), albite twins, $An_{40}$; 82% groundmass:  cryptocrystalline microlites and interstitial feldspar, no compositions

3% Biotite - altering to epidote, mica, chlorite, and opaques, 2V<15 (-), subhedral, 1.0 mm, patchy extinction

3% Mica - alteration product of biotite, colorless, low relief, birefringence = 0.045, sericite?

1% Quartz - uniaxial (+), interstitial in groundmass, inclusions, <0.5 mm

1% Chlorite - blue-green color and pleochroism, anomolous birefringence, anhedral, associated with mica and biotite

1% Opaques - associated with alteration minerals (chlorite and epidote) or in groundmass, seriate (<0.25 mm), anhedral, reddish-black: spinel group?

<1% Epidote - yellow-green color and pleochroism, high birefringence, euhedral, no optical figures, <0.1 mm

Alteration - moderate replacement of biotite and saussuritization of feldspar; association of sericite,

oxidized opaques, chlorite, and minor epidote = hydrothermal alteration

SITE 22 (5H065) - holocrystalline, fine-grained, hypidiomorphic, porphyritic, intergranular

　　85% Feldspar - seriate (microlites to phenocrysts, <1.5 mm), no groundmass compositions (indistinct twins); phenocrysts: subhedral, albite twinned, zoned, lots of opaque inclusions, some cores altered to chlorite, includes some pryoxene, partly saussuritized, no compositions

　　7% Chlorite- light-green color and pleochroism, anomolous blue birefringence, interstitial, <0.4 mm and amigdoidal

　　5% Augite - subhedral, twinned, <0.2 mm, high relief, 2V=55 (+), birefringence = 0.023, some opaque inclusions, glomeroporphyritic, intergranular

　　3% Opaques - subhedral, black to red-brown, seriate (<0.15 mm): spinel group?

　　Alteration - note: veinlets of feldspar, calcite, and mafic inclusions present; associated with mobilization of fluids: hydrothermal

SITE 23 (5H069) - holocrystalline, fine-grained, hypidiomorphic, intergranular, porphyritic

　　83% Feldspar - seriate (microlites to phenocrysts <1.5 mm), two populations: 1) 80% ablite twinned, zoned, subhedral to anhedral, 2V=70 (+), phenocryst twinning is obscured by pervasive alteration to clay (?), while groundmass remains relatively unaltered but with indistinct twins (no compositions); 2) 2% untwinned, anhedral, interstitial, 2V=60 (-), <0.2 mm, associated with chlorite (secondary potassic feldspar?)

　　7% Augite - intergranular, birefringence = 0.022 mm, anhedral, <1.0 mm, simple twins, zoned, 2V=80 (+)

　　5% Chlorite - interstitial, anomolous birefringence, blue-green pleochroism, pseudomorphing after hornblende (?), associated with calcite

　　3% Opaques - two populations: 1) subhedral, <0.1 mm, crystals with red oxidation around rims (maghemite or hematite); 2) cryptocrystalline, red-brown "dust"

　　1% Epidote - brownish, subhedral, birefringence = 0.035, 2V>60 (-), <0.1 mm, associated with chlorite

　　1% Quartz - uniaxial (+), interstitial, anhedral, lots of inclusions, <0.2 mm

　　<1% Calcite - high birefringence, twins, associated with chlorite

　　<1% Kaersutite (?) - 2V=55 (-), mantled by opaques, amphibole cleavage, parallel extinction, weak brown-yellow pleochroism, anhedral, associated with chlorite

Alteration - thorough alteration of feldspar to smectite, oxidation of opaques, chlorite and calcite: hydrothermal

SITE 24 (5H072) - holocrystalline, spherulitic, medium-grained, hypidiomorphc, porphyritic
94% Feldspar - two populations, 1) 20% saussuritized phenocrysts, albite twins, zoned, glomeroporphyritic, $An_{45}$, 1.0-2.0 mm in size, subhedral to anhedral crystals including opaques; 2) 75% groundmass of altered spherules or crystallites
2% Quartz - interstitial, uniaxial (+), low birefringence, anhedral, <0.2 mm, embayed
3% Opaques - subhedral, grungy brown-red iron-stain, <0.25 mm: spinel series?
2% Mica - clear, birefringence = 0.027, subhedral (<1.0 mm), parallel extinction, thorough replacement of biotite (?), associated with alteration of feldspar, some segmented, associated with oxides, 2V<20 (-)
1% Epidote - euhedral, yellow-green color and pleochroism, birefringence = 0.04, <0.2 mm
Alteration: thorough replacement of biotite to mica, large amount of dispersed iron-stain, moderate alteration of feldspar to sericite: hydrothermal or autometamorphism

SITE 25 (5H074) - holocrystalline, hypidiomorphic, medium-grained, porphyritic, fractured, trachytic
80% Feldspar - 4% phenocrysts: 0.5-2.0 mm, subhedral, saussuritized, albite twins, includes opaques, $An_{40}$, 2V>60 (+), glomeroporphyritic; 76% groundmass: microlites, subhedral, <0.5 mm, no optics, no compositions
9% Quartz - uniaxial (+), secondary (filling voids) and in groundmass, associated with epidote and calcite, <0.2 mm
7% Chlorite - light blue-green color and pleochroism, anomolous birefringence, interstitial, 2V=30 (+), unoxidized
3% Opaques - interstitial, intergranular, and included euhedral and subhedral crystalls, <0.1 mm
<1% Epidote - green-yellow color, weak yellowish pleochroism, high birefringence
<1% Calcite - 1) anhedral, interstitial, <1.0 mm, associated with quartz, or 2) euhedral, 2.0 mm, mantled by chlorite
Alteration- chlorite, calcite, and some quartz secondary, probably associated with hydrothermal alteration

SITE 26 (5H077) - holocrystalline, allotriomorphic, fine-grained
95% Feldspar - 1) 94% anhedral, felty twinned laths, <1.0 mm, includes some opaques, 2V>60 (+), probably plagioclase but no compositions; 2) 1% 0.3 mm, anhedral,

untwinned, no inclusions, 2V>60 (-), could be potassic
feldspar or oligoclase

2% Epidote - interstitial, yellow-green color and
pleochroism, high birefringence, high relief, 2V=50 (-)

2% Opaques - euhedral, seriate, <1.0 mm, some red
oxidation rims (maghemite or hematite)

<1% Quartz - uniaxiel (+), interstitial, anhedral, <0.5
mm, may be secondary along veins and grain boundries

<1% Chlorite - alteration coronas around anhedral,
cryptocrystalline brown grunge (clay ?), blue-green color
and pleochroism, anomolous birefringence

<1% Calcite - interstitial in groundmass, uniaxial (-),
high birefringence, calcite twins

Alteration - note: interstitial versus included opaques
may indicate two populations, minor development of chlorite,
calcite, and epidote; probably hydrothemal or
autometamorphic

SITE 27 (5H080) - holocrystalline, medium-grained,
micrographic, myrmekitic, porphyritic

90% Feldspar - 65% phenocrysts: subhedral, 2V=75 (-),
1.0-4.0 mm, zoned, $An_{32}$, carlsbad and albite twins,
glomeroporphyritic; 25% granophyric groundmass: fine-grained
quartz and feldspar (no compositions), with opaques,
apatite, and hornblende

5% Quartz - uniaxial (+), granophyric with feldspar

2% Hornblende - altering to chlorite to varying
degrees, subhedral, 0.5-2.0 mm, brown color and pleochroism,
high birefringence, inclined extinction, included opaques,
2V>60 (-)

1% Apatite - uniaxial (-), <0.1 mm, euhedral, prismatic
crystallites, low birefringence

1% Opaques - in groundmass and hornblende, green-black
tinted euhedral crystals, <0.1 mm, probably spinel series;
some blood red cryptocrystalline blebs (maghemite or
hematite); associated with epidote

<1% Epidote - light-green color and pleochroism,
birefringence = 0.029, euhedral crystals or anhedral blebs
mantling opaques

<1% Mica - birefringence = 0.04, moderate 2V (-),
interstitial and associated with alteration of phenocryst
feldspar cores

<1% Chlorite - secondary (?) alteration of hornblende

Alteration - minor alteration; note: plutonic textures

SITE 28 (5H083) - holocrystalline, porphyritic,
allotriomorphic, medium-grained

86% Feldspar - 5% phenocrysts: carlsbad and albite
twins, zoned, euhedral to subhedral, 0.5-2.0 mm, margins
altering to clay and interiors to chlorite, 2V=60 (+),
$An_{52}$; 81% groundmass: <0.1 mm microlites, no compositions

4% Amphibole - phenocrysts (0.5-1.0 mm) intergrown with chlorite and epidote, light-brown to blue-green color and pleochroism, 2V=40 (-), birefringence = 0.03, inclined extinction, subhedral, simple amphibole twins preserved, pseudomorph after calcic hornblende (actinolite?)

4% Chlorite - blue-green color and pleochroism, 2V=40 (-), interstitial in groundmass (<0.25 mm), associated with epidote and amphibole, also in veins, anomolous birefringence

3% Opaques - included in feldspar and chlorite, in groundmass, <0.1 mm, euhedral black crystals or anhedral blebs

2% Epidote - vein filling or intergrown with chlorite after hornblende(?), birefringence = 0.035, 2V>60 (-), green-yellow color and pleochroism

1% Quartz - anhedral, interstitial in groundmass, <0.1 mm, uniaxial (+)

Alteration - thorough, perhaps associated with veins and cracks; autometamorphic?

SITE 29 (5H086) - holocrystalline, allotriomorphic, fine-grained, granular

26% Feldspar - microcrystalline groundmass, indistinct twinning, microlites and anhedral interstitial groundmass, no compositions

20% Hornblende - twinned, moderate birefringence, seriate laths (<0.1-1.0 mm), clear to brown and green pleochroism, 2V=90 (-), primary

46% Epidote - large (1.0-1.5 mm) round, euhedral crystals mantled by browm amphibole (hornblende) and feldspar or including hornblende, also in groundmass, birefringence = 0.033, associated with chlorite, colorless to light-yellow/green pleochroism, inclined extinction, some twins, 2V=85 (-), thorough replacement of another phase?

6% Chlorite - anhedral minor alteration of hornblende and interstitial, blue-green color, anomolous birefringence

1% Opaques - two populations, 1) large, euhedral crystals, 1.0 mm, with red oxidation coronas; 2) very fine grained, <0.1 mm, dusting of opaques

<1% Sphene - euhedral to subhedral, high relief, high birefringence, colorless to light brown, <0.5 mm, 2V=45 (+)

<1% Apatite - uniaxial (-), low birefringence, acicular needles

Alteration - secondary chlorite, epidote, and amphibole(?); hydrothermal or autometamorphic

SITE 31 (5H090) - hypidiomorphic, holocrystalline, fine-grained, inequigranular

45% Feldspar - indistinct or albite twins, zoned, all interstitial, 2V=65 (-), $An_{30}$, <0.7 mm

20% Hornblende - subhedral, clear to light-yellow or light-brown color and pleochroism, amphibole cleavage, twinned, 0.25-1.0 mm, 2V=90 (-), minor chloritization

20% Epidote - yellow-green color and pleochroism, 2V=85 (-), some striations, often mantled by blue-green amphibole; associated with chlorite and opaques

9% Actinolite? - blue-green amphibole, fibrous, associated with epidote and mantled by brown hornblende, weak pleochroism, no optics

5% Chlorite - anhedral, <0.3 mm, green-blue pleochroism, anomolous birefringence, alteration of hornblende, associated with epidote

<1% Sphene - anhedral, high relief, high birefringence, clear, associated with epidote, <0.1 mm

<1% Opaques - large black and red crystals, 0.5 mm, subhedral, glomeroporphyritic, red oxidized rims, some associated with epidote

Alteration - brown hornblende fresh, blue-green amphibole, epidote, and chlorite with oxidation of oxides = autometamorphism or hydrothermal

SITE 32 (5H094) - hypidiomorphic, holocrystalline, fine-grained, inequigranular

70% Feldspar - anhedral, twinned, zoned, <0.6 mm, 2V=60 (-), $An_{33}$, includes opaques

17% Hornblende - euhedral, seriate (<0.7 mm), yellow to brown-green color and pleochroism, birefringence = 0.015 (low because of small size), 2V=85 (-), slightly chloritized and grades into blue-green amphibole (actinolite?)

5% Epidote - 2V=85 (-), subhedral, yellow-green color and pleochroism, birefringence = 0.035, <0.7 mm, includes feldspar and hornblende, striated, anhedral, often mantled blue-green amphibole

5% Actinolite(?) - blue-green, fibrous amphibole, grades into brown hornblende, no optics, weak pleochroism

2% Chlorite - blue-green color and pleochroism, anomolous birefringence, anhedral, 2V<20 (-), <0.3 mm, interstitial in groundmass

1% Opaques - <0.7 mm, red anhedral blebs or subhedral crystals, included in feldspar and interspersed in groundmass

Alteration - thorough, association of epidote, blue-green amphibole, and chlorite suggest replacement of another phase; brown hornblende fresh; probably autometamorphic

SITE 34 (5H100) - holocrystalline, allotriomorphic to hypidiomorphic, porphyritic, intergranular to granular, minorly cumulophyric

61% Feldspar - anhedral, zoning and minor albite twinning, laths in groundmass, <0.3 mm, 2V=65 (-), $An_{32}$

27% Hornblende - anhedral to subhedral, seriate (0.3-2.0 mm), light green to yellow brown color and pleochroism, twinned, fractured, birefringence=0.35-0.40, no optics

10% Epidote - anhedral, cryptocrystalline (<0.2 mm), birefringence=0.02, some opaque coronas (magnetite?) around crystals, clear to light-green color, weak pleochroism, twinned, 2V=65 (-)

1% Opaques - single crystalls and clots, often skeletal (ilmenite?), some red oxidation around crystals (maghemite or hematite), seriate (0.03-2.0 mm)

<1% Apatite - cryptocrystalline, low birefringence, acicular needles

<1% Sphene - subhedral, brownish color, sphenoidal cross-section

Alteration - minor

SITE 35 (5H102) - porphyritic, holocrystalline, allotriomorphic to hypidiomorphic

94% Feldspar - 20% phenocrysts: glomeroporphyritic, euhedral, seriate (1.0-3.0 mm), albite twinned, strongly zoned, includes biotite, opaques, and chlorite, partially saussuritized, 2V=65 (+), $An_{40-60}$; 75% groundmass: anhedral laths, <1.0 m, poorly developed twins, no optics, no compositions

2% Biotite - seritate (0.1-2.0 mm), euhedral to anhedral, glomeroporphyritic, light brown color with dark brown pleochroism, includions of sphene and opaques, one good cleavage, altering to chlorite, 2V<20 (-)

1% Chlorite - blue-green color and birefringence, oxidized, intersertial, 2V=20 (-)

1% Epidote - euhedral, high birefringence, high relief, 2V=90 (-), <1.0 mm

1% Opaques - euhedral, <0.1 mm, glomeroporphyritic; spinel group, with minor red oxidation rims (maghemite or haemitite)

1% Calcite - high birefringence, calcite twins, anhedral, <0.1 mm

<1% Sphene - high relief, high birefringence, clear color

<1% Apatite - low birefringenece, acicular needles, good hexagonal cross-sections, <0.2 mm

Alteration - minor saussuritization of feldspar; chlorite oxidized, minor epidote and calcite: autometamorphic or hydrothermal alteration

SITE 36 (5H106) - holocrystalline, fine-grained, porphyritic, hypidiomorphic to sutured (?)

97% Feldspar - 7% phenocrysts: thoroughly saussuritized, subhedral, glomeroporphyritic, 2.0-5.0 mm, albite or pericline twins obscured, 2V=55 (+), zoning

visible; 90% groundmass: microlites, <0.5-2.0 mm, micrographic and granophyric textures, negative relief against quartz, 2V=60 (-), potassic feldspar or orthoclase

2% Mica - subhedral, high birefringence, low relief, light-green color and pleochroism, associated with chlorite, opaques, and alteration of phenocryst feldspar; sericite?

1% Chlorite - anhedral, blue-green color and pleochroism, anomolous birefringence, interstitial, associated with sericite and opaques, chlorite psuedomorphing after amphibole (preserving amphibole cleavage?)

<1% Opaques - euhedral, black and rust-brown, acicular needles and glomeroporphyritic

Alteration - thorough alteration of feldspar phenocrysts to sericite; association of chlorite, sericite, and opaques implies hydrothermal alteration

SITE 37 (5H108) - holocrystalline, porphyritic, hypidiomorphic, fine-grained

25% Hornblende - subhedral phenocrysts, twinned, seriate (<0.5-2.0 mm), green-brown color and pleochroism, chloritized, birefringence = 0.025, 2V=60 (-), amphibole cleavage, includes opaques

4% Chlorite - blue-green color and pleochroism, no optics, radial habit

2% Epidote - birefringence = 0.04, high relief, yellow to green color and weak pleochroism, 2V>60 (-), anhedral, granular interstitial, <0.1 mm

<1% Calcite - high birefringence, uniaxial (-), calcite twins

<1% Sphene - high relief, high birefringence, colorless to light-brown

68% Groundmass - interstitial feldspar (indistinct twins, 2V>60 (+), negative relief against quartz) and quartz

Alteration - chlorite and calcite = low-temperature hydrothermal or autometamorphic

SITE 38 (5H111) - holocrystalline, fine-grained, allotriomorphic, porphyritic

96% Feldspar - 3% phenocrysts: anhedral, seriate (<2.0 mm), albite twins, $An_{62}$, 2V=70 (+), resorbed edges, saussuritized; 93% groundmass: cryptocrystalline, anhedral

3% Calcite - high birefringence, calcite twins, as vein filling

<1% Chlorite - 2V<20 (-), birefringence = 0.007, no twins, colorless to light-yellow, no pleochroism

<1% Quartz - uniaxial (+), seriate (<1.0 mm), euhedral vein filling

<1% Opaques - glomeroporphyritic, anhedral, associated with quartz as vein filling

<1% Mica - high birefringence, vein filling and
pseudomorph after biotite (?):   sericite (?)
     Alteration - primarily associated with veins, but
saussuritization of feldspar is thorough in small
phenocrysts; note:  brecciated, some microfractures with
vein replacement mineralogies in them, relict crystal
boundries visible in plane light but thoroughly replaced
under crossed polars; association of calcite, sericite,
chlorite = hydrothermal(?)

SITE 39 (7J085) - porphyritic, allotriomorphic,
fine-grained, spherulitic, holocrystalline
     96% Feldspar - 4% phenocrysts:  2% subhedral, seriate
(0.5-2.0 mm), zoned, albite twins, glomeroporphyritic,
$An_{68}$, 2V=65 (+), saussuritized and 2% colorless, 2V<40
(-), bravino twins, birefringencce = 0.007, lots of opaque
inclusions, blocky habit, potassic feldspar or oligoclase;
92% groundmass:  granophyric, <0.1 mm, spherulites, some
albite twined microlites
     2% Quartz - uniaxial (+), interstitial in groundmass
and as small, euhedral phenocrysts (<0.7 mm)
     <1% Apatite - euhedral, uniaxial (-), low
birefringence, <1.0 mm
     <1% Zircon - high relief, high birefringence, clear
color, subhedral, <0.1 mm
     1-2% Opaques - black and reddish anhedral grains and
cryptocrystalline reddish veins (submicroscopic maghemite
or hematite ?) and mantles, <1.0 mm
     Alteration - saussuritized feldspar, secondary veins of
opaques; hydrothermal (?- no chlorite, epidote, or calcite)

SITE 39 (7J087-chill margin) - fine-grained,
holocrystalline, aphyric, allotriomorphic, intergranular
     3% Opaques - euhedral, black crystals and red
cryptocrystalline "dust" (maghaemite or hematite)
     1% Chlorite - blue-green color and pleochroism,
anomolous blue birefringence, <0.1 mm, interstitial in
groundmass
     <1% Calcite - secondary, high birefringence, calcite
twins
     96% Groundmass - saussuritized felty microlites [<0.4
mm, $An_{68}$, 2V=60 (+)] and quartz (interstitial or
concertal, lots of inclusions, <0.1 mm,)
     Alteration - moderate replacement of feldspar by
sericite, some oxidation of opaques, minor chlorite and
calcite = minor hydrothermal

SITE 41 (7J137) - holocrystalline, allotriomorphic,
fine-grained, aphyric
     10% Chlorite - interstitial, anomolous birefringence,
light green pleochroism, <0.5 mm, intergrown with feldspar

3% Opaques - euhedral, black, cryptocrystalline, reddish "dust", opaques associated with crystal boundries

2% Calcite - high birefringence, calcite twins, anhedral, 1.0 mm, interstitial

85% Groundmass - saussuritized, felty subhedral microlites (0.5-1.0 mm, some albite twins, 2V=55 (+), $An_{45}$) and quartz (uniaxial (+), interstitial, anhedral, <0.4 mm)

Alteration - chlorite, calcite, oxidized opaques, and saussuritized feldspar ± albite = hydrothermal

SITE 42 (7J138-chill margin) - holocrystalline, allotriomorphic, microporphyritic, intergranular, fine-grained

83% Feldspar - 1% microphenocrysts: 2V>60 (+), albite twins, saussuritized, mantled by low-birefringence feldspar; 82% groundmass: saussuritized laths and interstitial, 0.5-1.0 mm, no optics

6% Mica - sericite (?), cryptocrystalline, high birefringence, low relief, associated with feldspar

5% Chlorite - anomolous birefringence, light green color and pleochroism, anhedral, interstitial, 0.1-0.3 mm, may be alteration product of mafic mineral(s)

3% Quartz - uniaxial (+), interstitial or concertal blebs, <0.2 mm, in groundmass

3% Opaques - seriate (<0.5 mm), euhedral, black crystalls and reddish "dust", associated with chlorite and biotite

<1% Biotite - red-brown color and pleochroism, <0.5 mm, subhedral, associated with opaques and chlorite

<1% Calcite - high birefringence, calcite twins

Alteration - thoroughly altered feldspar; association of chlorite, opaques, calcite, and sericite = hydrothermal

SITE 42 (7J139) - altered, microporphyritic, fine-grained, allotriomorphic, spherulitic, holocrystalline

94% Feldspar - 1) 20% subhedral microphenocrysts: 0.5-1.0 mm, glomeroporphyritic, saussuritized, 2V=60 (+), albite twins, $An_{68}$; 2) 74% groundmass: saussuritized, subhedral microlites and quartz, $An_{10}$ on groundmass microlites (negative relief against quartz), shperulitic around quartz

3% Chlorite - blue-green color, anomolous birefringence, plume extinction, associated with opaques and pseudomorph after biotite

2% Mica - alteration of feldspar and biotite, high birefringence, cryptocrystalline, colorless: sericite?

1% Opaques - black, anhedral, <0.3 mm, sprinkled throughout section with reddish "dust" associated with crystal boundries and veins

<1% Zircon - high relief, high birefringence, euhedral, <0.1mm

Alteration - thorough replacement of biotite by chlorite, opaques, and mica; moderate alteration of feldspar; probably hydrothermal

SITE 43 (7J149) - holocrystalline, allotriomorphic, porphyritic, fine-grained, altered

95% Feldspar - 5% phenocrysts: albite twins, subhedral, seriate (0.3-2.0 mm), saussuritized, 2V=65 (+), $An_{42}$; 90% groundmass: anhedral/consertal and microlites, 2V=65 (+), <0.2 mm, saussuritized

2% Chlorite - associated with opaques, anomolous birefringence, yellow to blue-green pleochroism, anhedral, pseudomorph after biotite

2% Smectite (?) - associated with alteration of feldspar, low birefringence, cryptocrystalline, no optics

1% Biotite - occurs only as "relict" cores in chlorite altered rims, brown color and pleochroism, birds-eye extinction

1% Opaques - seriate (<0.35 mm), anhedral, in veins and around crystal boundries

<1% Calcite - seriate, calcite twins, high birefringence, includes a mineral with a 2V=15 (+), higher relief and low birefringence (feldspar ?); calcite occcurs in veins and around crystal boundries

<1% Sphene - high relief, high birefringence, brownish, anhedral, <0.1 mm

Alteration - nearly thorough hydrothermal alteration of mafic phase (biotite replaced by chlorite and opaques and calcite) and saussuritization of feldspar

SITE 44 (7J153) - holocrystalline, porphyritic, fine-grained, allotriomorphic

94% Feldspar - 22% phenocrysts: glomeroporphyritic, albite and carlsbad twins, zoned, subhedral, 0.5-2.0 mm, saussuritized, 2V>60 (+), $An_{48}$; 72% groundmass: feldspar and quartz; fresh, microlites to consertal, no distinct twins, cuniform looking patterns, <0.5 mm, 2V=55 (+)

2% Biotite - altering to chlorite, subhedral, 0.5-3.0 mm, red-brown color and pleochroism, birds-eye extinction

2% Mica - 2V=35 (-), birefringence = 0.035, anhedral, interstitial and alteration of feldspar, colorless: sericite?

1% Chlorite - replacing biotite only, blue-green color and pleochroism, anomolous birefringence

1% Opaques - seriate (<0.35 mm), anhedral, black with reddish halos (oxidation) and reddish veins

Alteration - partial alteration of feldspar and biotite, oxidation of opaques, no epidote = autometamorphism or hydrothermal

SITE 45 (7J158-chill margin) - holocrystalline, porphyritic, fine-grained, allotriomorphic, intergranular

88% Feldspar - as groundmass, seriate laths with albite twins, <1.0 mm, too saussuritized for optics

4% Augite - 2V=50 (+), simple twins, strongly zoned, subhedral, seriate (0.3-0.7 mm), glomeroporphyritic, clear to light green, birefringence = 0.028, varying degrees of alteration to chlorite along cleavages and rims, r=v, inclined extinction

4% Chlorite - yellow-green, radiate, interstitial, minor pleochroism in light-green, 2V=50 (+/-), birefringence = 0.007, associated with opaques and pyroxene: septechlorite?

3% Opaques - euhedral, <0.2 mm, black with red mantles (oxidation rims of maghemite, hematite, or goethite)

1% Hornblende - euhedral, 2V=65 (-), <0.15 mm, green-brown pleochroism, associated with opaques

Alteration - thorough saussuritization of feldspar, partial replacement of cores of pyroxene, association of sericite and chlorite implies hydrothermal alteration

SITE 45 (7J160) - holocrystalline, porphyritic, allotriomorphic, fine-grained, intergranular

91% Feldspar - subhedral to anhedral, felty microlites as groundmass, <1.0 mm, 2V=50 (+), includes augite, indistinct twins, probably plagioclase

2% Augite - light-green color, simple twins, strongly zoned, 2V=50 (+), birefringence = 0.024, r=v, seriate (<0.6 mm), glomeroporphyritic, inclined extinction, calcite along cleavage and around rims (resorbed?), includes opaques

3% Chlorite - <2.0 mm, light-green to dark-green color and pleochroism, anhedral, anomolous birefringence, interstitial

2% Calcite - anhedral, 2.0 mm, interstitial and mantling pyroxene, high birefringence, calcite twins

2% Opaques - glomeroporphyritic, euhedral, <0.25 mm, some reddish oxidation rims and red anhedral crystalls

<1% Epidote - birefringence = 0.04, yellow-green color and pleochroism, 2V=90 (-)

<1% Biotite - associated with chlorite, light-brown to dark-brown color and pleochroism, birds-eye extinction

<1% Apatite - acicular crystallites, <0.1 mm, low birefringence, hexagonal cross-secton

<1% Zircon - very high relief, high birefringence, colorless

Alteration - minor: trace epidote and some oxidized opaques

SITE 46 (7J162) - holocrystalline, allotriomorphic, porphyritic, fine-grained

90% Feldspar - 15% phenocrysts: 2-4 mm, glomeroporphyritic, 2V=55 (+), r<v, strongly zoned, twinned, An$_{62}$, includes opaques; 75% groundmass: indistinct albite twinned microlites, 2V=60 (+)

6% Chlorite - anomolous birefringence, blue-green color and pleochroism, pseudomorph after mafic mineral

3% Opaques - subhedral, seriate (<0.2 mm), black and red acicular needles (hematite), associated with pyroxene

<1% Epidote - yellow-green color and pleochroism, 2V=90 (-), high birefringence, associated with chlorite

<1% Apatite - uniaxial (-), low birefringence crystallites

Alteration - minor; no saussuritization, no calcite, chlorite and minor epidote = autometamorphism?

SITE 47 (7J168) - holocrystalline, porphyritic, allotriomorphic, fine-grained

86% Groundmass - feldspar (lots of inclusions, 2V=60 (+), zoned, simple indistinct twins, probably plagioclase) and quartz (uniaxial (+), inclusion free, consertal)

4% Hornblende - twinned, light-brown to dark-brown color and pleochroism, birefringence = 0.025, 2V=85 (-), subhedral, seriate (<0.25 mm), altering to chlorite at rims

3% Chlorite - interstitial, anomolous birefringence, clear to dark-green color and pleochroism, associated with epidote

3% Opaques - black and reddish euhedral cubes, red stain associated with calcite, epidote, and chlorite

2% Epidote - subhedral, yellow-green color, <0.2 mm, weak pleochroism, 2V=90 (-), birefringence = 0.03, simple twins, associated with calcite and chlorite

1% Calcite - high birefringence, calcite twins, anhedral, <0.3 mm

1% Sphene - high relief, anhedral, high birefringence, <0.7 mm, light-brown color and pleochroism

<1% Apatite - low birefringence, uniaxial (-)

Alteration - unaltered hornblende; chlorite, epidote and calcite = autometamorphic or hydrothermal

SITE 47 (7J170) - holocrystalline, porphyritic, trachytic, allotriomorphic, fine-grained

75% Groundmass - <0.2 mm, concertal quartz [uniaxial (+)] and feldspar [indistinct albite or pericline twins, 2V=55 (+), negative relief against quartz]

15% Hornblende - euhedral, seriate (phenocrysts to groundmass microlites, <3.0 mm), light-brown to brown color and pleochroism, birefringence = 0.023, simple twins, amphibole cleavage, interpenetrative crystal growth, cores altered to epidote and perimeters chloritized, 2V=85 (-), flow-aligned

5% Epidote - light-green to yellow color and pleochroism, moderate relief, birefringence = 0.03, anhedral blebs (0.7 mm) or euhedral crystals (<0.1 mm), 2V=90 (-), inclined extinction, associated with chlorite

2% Chlorite - interstitial, anhedral, light-green to dark-green color and pleochroism, 2V=40 (+), associated with epidote

3% Opaques - euhedral, black crystals and red anhedral blebs, <0.1 mm

Alteration - no sericite or smectite, chlorite and epidote = autometamorphism

SITE 48 (7J173) - holocrystalline, fine-grained, allotriomorphic, porphyritic
CHILL ZONE

40% Feldspar - subhedral, lots of inclusions, <0.1 mm, indistinct twins, 2V=40 (+), granophyric (?): plagioclase?

40% Hornblende - <0.1 mm, green-brown color and pleochroism, no optics, crystallites

5% Quartz - uniaxial (+), birefringence = 0.008, also in veinlets associated with feldspar, inclusion free, <0.1 mm

3% Epidote - euhedral, <0.1 mm, 2V=85 (-), moderate relief, two good cleavages, birefringence = 0.025, some twins, light-green to yellow color and pleochroism

2% Chlorite - psuedomorph after biotite (?), phenocrystic (0.4-1.5 mm), inclusions of epidote, clear to light green color and pleochroism, anomolous blue birefringence or 0.007, 2V=45 (+)
NON-CHILL ZONE

70% Groundmass - granophyric quartz (uniaxial (+), inclusion free) and feldspar (?, 2V=65 (+), lots of inclusions and indistinct twins)

25% Hornblende - light yellow to dark brown color and pleochroism, twinned, zoned (with chloritized cores), lots of inclusions of opaques and epidote, associated with opaques, amphibole cleavage, 2V=85 (-), euhedral, seriate (<2.5 mm), as phenocrysts and groundmass, birefringence = 0.023

2% Chlorite - intergrown, clear to light brown, anhedral, interstitial, birefringence = 0.003, <0.1 mm 2% Opaques - subhedral, glomeroporphyritic, black and red, included in hornblende

<1% Calcite - high birefringence, calcite twins, anhedral, interstitial, associated with chlorite

<1% Epidote - birefringence = 0.004, yellow-brown color and pleochroism, one good cleavage, twinned, high relief, 2V=60 (-), included in chlorite, anhedral, <0.2 mm

Alteration - minor; no saussuritization of feldspar, chlorite and minor epidote = autometamorphism

# APPENDIX B:   PALEOMAGNETIC PRINCIPAL COMPONENT ANALYSES

## High Temperature (400-680°C) Component from the Dikes

| Site # | U.S.G.S. I.D. | I | D | Site # | U.S.G.S. I.D. | I | D |
|---|---|---|---|---|---|---|---|
| 1 | 5H001 | | * | 15 | 5H044 | | * |
| | 5H002 | 59.2 | 327.4 | | 5H045 | | * |
| | 5H003 | 57.6 | 40.0 | | 5H046 | | * |
| | 5H004 | 27.4 | 8.1 | 16 | 5H047 | 44.8 | 18.5 |
| 2 | 5H005 | -32.0 | 186.2 | | 5H048 | 47.3 | 18.0 |
| | 5H006 | | * | | 5H049 | 36.9 | 32.3 |
| | 5H007 | 30.9 | 8.6 | 17 | 5H050 | 47.0 | 3.7 |
| 3 | 5H008 | | * | | 5H051 | 31.1 | 32.3 |
| | 5H009 | | * | | 5H052 | 40.0 | 34.9 |
| | 5H010 | | * | 18 | 5H053 | 53.3 | 355.1 |
| 4 | 5H011 | -27.6 | 179.4 | | 5H054 | 36.3 | 10.3 |
| | 5H012 | | * | | 5H055 | 46.0 | 5.2 |
| | 5H013 | | * | 19 | 5H056 | 62.7 | 31.5 |
| 5 | 5H014 | -50.2 | 178.0 | | 5H057 | 56.8 | 12.1 |
| | 5H015 | -37.4 | 181.8 | | 5H058 | | * |
| | 5H016 | -25.9 | 177.8 | 20 | 5H059 | 62.3 | 354.8 |
| 6 | 5H017 | | * | | 5H060 | 59.2 | 354.8 |
| | 5H018 | | * | | 5H061 | 24.0 | 6.8 |
| | 5H019 | | * | 21 | 5H062 | 42.8 | 8.2 |
| 7 | 5H020 | 54.9 | 347.3 | | 5H063 | | * |
| | 5H021 | 32.0 | 15.9 | | 5H064 | 45.5 | 16.5 |
| | 5H022 | 17.4 | 23.4 | 22 | 5H065 | -30.9 | 198.9 |
| 8 | 5H023 | -48.8 | 169.7 | | 5H066 | -41.8 | 197.2 |
| | 5H024 | 5.8 | 20.6 | | 5H067 | 36.3 | 199.3 |
| | 5H025 | | * | 23 | 5H068 | | * |
| 9 | 5H026 | | * | | 5H069 | | * |
| | 5H027 | | * | | 5H070 | 24.8 | 5.5 |
| | 5H028 | | * | 24 | 5H071 | | * |
| 10 | 5H029 | | * | | 5H072 | | * |
| | 5H030 | | * | | 5H073 | | * |
| | 5H031 | | * | 25 | 5H074 | | * |
| 11 | 5H032 | | * | | 5H075 | | * |
| | 5H033 | | * | | 5H076 | | * |
| | 5H034 | | * | 26 | 5H077 | 50.5 | 16.3 |
| 12 | 5H035 | | * | | 5H078 | 37.0 | 42.8 |
| | 5H036 | | * | | 5H079 | 52.6 | 357.9 |
| | 5H037 | | * | 27 | 5H080 | -36.3 | 197.0 |
| 13 | 5H038 | 55.0 | 349.2 | | 5H081 | | * |
| | 5H039 | 39.7 | 324.3 | | 5H082 | -14.7 | 205.5 |
| | 5H040 | 49.2 | 354.6 | 28 | 5H083 | -32.2 | 209.5 |
| 14 | 5H041 | 47.3 | 353.2 | | 5H084 | -24.0 | 211.3 |
| | 5H042 | 29.3 | 330.5 | | 5H085 | -31.9 | 206.7 |
| | 5H043 | 29.8 | 358.5 | | | | |

Appendix B con't.

| Site # | U.S.G.S. I.D. | I | D |
|---|---|---|---|
| 29 | 5H086 | 57.9 | 34.9 |
| | 5H087 | -32.9 | 202.1 |
| | 5H088 | 62.9 | 13.2 |
| 30 | 5H089 | -14.6 | 198.0 |
| 31 | 5H090 | -16.3 | 188.6 |
| | 5H091 | -31.1 | 199.4 |
| | 5H092 | -31.1 | 199.4 |
| 32 | 5H093 | -36.2 | 207.6 |
| | 5H094 | -33.6 | 207.6 |
| | 5H095 | -33.7 | 204.9 |
| 33 | 5H096 | | * |
| | 5H097 | | * |
| | 5H098 | | * |
| 34 | 5H099 | 56.9 | 344.2 |
| | 5H100 | 43.7 | 337.8 |
| | 5H101 | | * |
| | 8P010 | 52.8 | 349.8 |
| | 8P011 | 44.9 | 344.6 |
| | 8P012G | 13.2 | 206.7 |
| | 8P013G | | * |
| | 8P014G | 55.1 | 39.9 |
| | 8P015G | 17.8 | 15.0 |
| 35 | 5H102 | 60.3 | 360.0 |
| | 5H103 | | * |
| | 5H104 | | * |
| 36 | 5H105 | 61.7 | 353.6 |
| | 5H106 | 67.9 | 9.9 |
| | 5H107 | 63.2 | 349.9 |
| 37 | 5H108 | -25.4 | 213.0 |
| | 5H109 | -25.7 | 213.0 |
| | 5H110 | -22.6 | 210.1 |
| 38 | 5H111 | | * |
| | 5H112 | | * |
| | 5H113 | | * |
| 39 | 7J081 | 5.8 | 37.4 |
| | 7J082 | 6.7 | 41.6 |
| | 7J083 | 6.5 | 50.3 |
| | 7J084 | 25.6 | 41.2 |
| | 7J085 | -32.6 | 47.5 |
| | 7J086 | 38.6 | 31.2 |
| | 7J087 | 13.2 | 31.2 |
| 41 | 7J131 | 24.0 | 10.3 |
| | 7J132 | 35.7 | 350.5 |
| | 7J133 | 22.5 | 21.8 |
| | 7J134 | | * |
| | 7J135 | | * |

| Site # | U.S.G.S. I.D. | I | D |
|---|---|---|---|
| | 7J136 | 38.6 | 11.6 |
| | 7J137 | 40.8 | 5.6 |
| 42 | 7J138 | | * |
| | 7J139 | | * |
| | 7J140 | | * |
| | 7J141 | | * |
| | 7J142 | | * |
| | 7J143 | | * |
| 43 | 7J144 | 10.0 | 347.9 |
| | 7J145 | | * |
| | 7J146 | 5.5 | 337.0 |
| | 7J147 | -10.4 | 349.2 |
| | 7J148 | 20.9 | 6.3 |
| | 7J149 | | * |
| 44 | 7J150 | -19.4 | 346.7 |
| | 7J151 | -15.9 | 353.5 |
| | 7J152 | 9.4 | 2.7 |
| | 7J153 | 10.6 | 352.1 |
| | 7J154 | -4.5 | 359.4 |
| | 7J155 | | * |
| 45 | 7J156 | 8.6 | 203.2 |
| | 7J157 | | * |
| | 7J158 | | * |
| | 7J159 | | * |
| | 7J160 | 14.1 | 190.0 |
| | 7J161 | 20.3 | 189.6 |
| 46 | 7J162 | | * |
| | 7J163 | | * |
| | 7J164 | | * |
| | 7J165 | | * |
| | 7J166 | | * |
| | 7J167 | | * |
| 47 | 7J168 | 47.5 | 354.1 |
| | 7J169 | 48.9 | 345.4 |
| | 7J170 | 53.4 | 351.9 |
| | 7J171 | 56.1 | 3.0 |
| 48 | 7J172 | 51.2 | 24.1 |
| | 7J173 | 57.3 | 3.8 |
| | 7J174 | | * |
| | 7J175 | | * |

Appendix B con't.

Low-Temperature (0-300°C) Component from the Dikes.

| Site # | U.S.G.S. I.D. | I | D | | Site # | U.S.G.S. I.D. | I | D |
|---|---|---|---|---|---|---|---|---|
| 1 | 5H001 | | * | | 15 | 5H044 | | * |
| | 5H002 | 45.1 | 293.2 | | | 5H045 | | * |
| | 5H003 | 37.8 | 12.7 | | | 5H046 | 58.4 | 6.2 |
| | 5H004 | 40.3 | 42.1 | | 16 | 5H047 | | * |
| 2 | 5H005 | 37.4 | 35.6 | | | 5H048 | 54.1 | 7.5 |
| | 5H006 | 33.1 | 53.2 | | | 5H049 | 52.8 | 358.2 |
| | 5H007 | 39.9 | 36.6 | | 17 | 5H050 | | * |
| 3 | 5H008 | 55.5 | 8.7 | | | 5H051 | 36.7 | 12.3 |
| | 5H009 | 55.4 | 20.8 | | | 5H052 | 19.4 | 10.9 |
| | 5H010 | 57.3 | 23.0 | | 18 | 5H053 | 55.9 | 358.7 |
| 4 | 5H011 | 56.4 | 4.5 | | | 5H054 | 55.7 | 10.7 |
| | 5H012 | | * | | | 5H055 | 54.5 | 359.0 |
| | 5H013 | | * | | 19 | 5H056 | 56.2 | 6.1 |
| 5 | 5H014 | 42.8 | 21.7 | | | 5H057 | 61.2 | 3.4 |
| | 5H015 | 46.2 | 14.2 | | | 5H058 | 80.5 | 264.5 |
| | 5H016 | 55.2 | 352.4 | | 20 | 5H059 | 56.3 | 353.6 |
| 6 | 5H017 | 18.8 | 15.5 | | | 5H060 | 57.9 | 358.0 |
| | 5H018 | 14.7 | 14.0 | | | 5H061 | 63.6 | 10.6 |
| | 5H019 | 2.8 | 32.2 | | 21 | 5H062 | 44.3 | 6.8 |
| 7 | 5H020 | 51.8 | 10.2 | | | 5H063 | 50.4 | 7.1 |
| | 5H021 | 2.8 | 72.5 | | | 5H064 | 41.2 | 6.0 |
| | 5H022 | | * | | 22 | 5H065 | 69.5 | 48.5 |
| 8 | 5H023 | | * | | | 5H066 | 49.4 | 9.4 |
| | 5H024 | 50.9 | 24.7 | | | 5H067 | 64.7 | 344.2 |
| | 5H025 | | * | | 23 | 5H068 | 51.4 | 20.8 |
| 9 | 5H026 | 31.1 | 333.7 | | | 5H069 | 61.7 | 345.7 |
| | 5H027 | 22.7 | 324.2 | | | 5H070 | 33.0 | 7.3 |
| | 5H028 | 43.7 | 31.5 | | 24 | 5H071 | 35.0 | 206.5 |
| 10 | 5H029 | 63.6 | 9.8 | | | 5H072 | 31.0 | 239.6 |
| | 5H030 | | * | | | 5H073 | | * |
| | 5H031 | 23.8 | 3.4 | | 25 | 5H074 | 49.9 | 30.8 |
| 11 | 5H032 | | * | | | 5H075 | 43.2 | 23.8 |
| | 5H033 | 3.1 | 93.5 | | | 5H076 | 42.3 | 35.1 |
| | 5H034 | | * | | 26 | 5H077 | 59.5 | 6.9 |
| 12 | 5H035 | 32.3 | 345.5 | | | 5H078 | 50.4 | 54.5 |
| | 5H036 | 51.9 | 352.4 | | | 5H079 | 62.1 | 353.7 |
| | 5H037 | 57.3 | 356.0 | | 27 | 5H080 | 20.8 | 315.5 |
| 13 | 5H038 | 58.3 | 349.1 | | | 5H081 | 45.4 | 353.8 |
| | 5H039 | 51.6 | 334.2 | | | 5H082 | 54.7 | 341.7 |
| | 5H040 | | * | | 28 | 5H083 | 55.9 | 2.0 |
| 14 | 5H041 | 57.0 | 352.0 | | | 5H084 | 55.7 | 348.4 |
| | 5H042 | 58.8 | 351.1 | | | 5H085 | 59.5 | 354.3 |
| | 5H043 | 59.4 | 349.1 | | | | | |

Appendix B con't.

| Site # | U.S.G.S. I.D. | I | D |
|--------|--------------|------|------|
| 29 | 5H086 | 55.3 | 28.1 |
|    | 5H087 | 57.9 | 20.9 |
|    | 5H088 | 64.3 | 18.4 |
| 30 | 5H089 | 61.3 | 16.7 |
| 31 | 5H090 | 54.4 | 33.9 |
|    | 5H091 | 61.8 | 3.6 |
|    | 5H092 | 60.1 | 11.2 |
| 32 | 5H093 | 64.0 | 28.7 |
|    | 5H094 | 59.1 | 26.8 |
|    | 5H095 | 68.3 | 41.6 |
| 33 | 5H096 | 70.3 | 355.9 |
|    | 5H097 | 67.1 | 351.7 |
|    | 5H098 | 82.6 | 38.1 |
| 34 | 5H099 | 50.8 | 345.7 |
|    | 5H100 | 49.7 | 348.5 |
|    | 5H101 | -10.7 | 258.1 |
|    | 8P010 | 62.1 | 353.0 |
|    | 8P011 | 46.8 | 333.2 |
| 35 | 5H102 | 62.3 | 358.2 |
|    | 5H103 | 65.8 | 353.8 |
|    | 5H104 | 68.1 | 1.9 |
| 36 | 5H105 | * | |
|    | 5H106 | 62.3 | 8.6 |
|    | 5H107 | * | |
| 37 | 5H108 | * | |
|    | 5H109 | 60.4 | 10.7 |
|    | 5H110 | 64.4 | 352.4 |
| 38 | 5H111 | -35.2 | 323.0 |
|    | 5H112 | 64.0 | 96.5 |
|    | 5H113 | * | |
| 41 | 7J131 | 24.7 | 19.8 |
|    | 7J132 | 41.1 | 17.6 |
|    | 7J133 | 25.0 | 34.0 |
|    | 7J134 | 40.5 | 10.7 |
|    | 7J135 | 30.8 | 23.4 |
|    | 7J136 | 30.2 | 23.0 |
|    | 7J137 | 47.7 | 11.4 |

| Site # | U.S.G.S. I.D. | I | D |
|--------|--------------|------|------|
| 42 | 7J138 | * | |
|    | 7J139 | * | |
|    | 7J140 | * | |
|    | 7J141 | * | |
|    | 7J142 | * | |
|    | 7J143 | * | |
| 43 | 7J144 | 61.3 | 335.3 |
|    | 7J145 | 56.3 | 325.1 |
|    | 7J146 | 55.5 | 337.8 |
|    | 7J147 | 39.3 | 338.3 |
|    | 7J148 | 36.6 | 350.2 |
|    | 7J149 | 54.8 | 26.6 |
| 44 | 7J150 | 45.9 | 15.7 |
|    | 7J151 | 51.4 | 3.1 |
|    | 7J152 | * | |
|    | 7J153 | 31.7 | 0.3 |
|    | 7J154 | * | |
|    | 7J155 | 35.5 | 18.0 |
| 45 | 7J156 | 64.2 | 11.6 |
|    | 7J157 | 57.4 | 5.5 |
|    | 7J158 | 52.7 | 11.1 |
|    | 7J159 | * | |
|    | 7J160 | -6.6 | 52.4 |
|    | 7J161 | 58.1 | 351.7 |

Appendix B con't.

High Temperature (400-680°C) Component from the Flows and Vitrophyre.

| Site # | U.S.G.S. I.D.∞ | I | D | $I_c$ | $D_c$ |
|---|---|---|---|---|---|
| 40 | 7J091,092 | 40.7 | 154.3 | -21.1 | 178.1 |
| | 7J093,094 | 42.4 | 171.6 | -45.9 | 166.5 |
| | 7J095,096 | 29.8 | 117.4 | -40.1 | 161.7 |
| | 7J097,098 | 35.1 | 146.0 | -18.5 | 167.1 |
| | 7J099,100 | 23.0 | 189.4 | -53.6 | 160.3 |
| | 7J101,102 | 42.9 | 198.4 | -49.7 | 194.5 |
| | 7J103,104 | 33.4 | 176.9 | -40.1 | 170.7 |
| | 7J105,106 | | * | | |
| | 7J107,108 | | * | | |
| | 7J109,110 | | * | | |
| | 7J111,112 | 40.5 | 146.4 | -40.7 | 148.0 |
| | 7J113,114 | 17.7 | 179.2 | -45.2 | 149.1 |
| | 7J115,116 | 28.9 | 174.0 | -43.6 | 159.6 |
| | 7J117,118 | | * | | |
| | 7J119,120 | 23.3 | 177.0 | -29.1 | 171.9 |
| | 7J121,122 | 28.5 | 184.6 | -49.9 | 161.5 |
| | 7J123,124 | 48.8 | 176.2 | -38.0 | 186.3 |
| | 7J125,126 | 22.4 | 179.8 | -45.4 | 161.8 |
| | 7J127,128 | 36.8 | 203.0 | -50.9 | 198.2 |
| | 7J129,130 | 13.9 | 179.2 | -49.8 | 144.7 |
| | 8P025,026,027 | 7.4 | 190.9 | -49.1 | 157.3 |
| | 8P028,030,031 | 5.3 | 185.4 | -46.6 | 142.5 |
| | 8P032,033,034 | 16.9 | 197.7 | -58.9 | 158.6 |
| | 8P035,036,037 | 13.0 | 197.0 | -56.7 | 154.6 |
| 49 | 8P016 | 39.2 | 293.1 | -1.3 | 276.6 |
| | 8P017 | 55.2 | 9.5 | 50.2 | 276.3 |
| | 8P018 | 57.5 | 259.6 | 1.7 | 248.4 |
| | 8P019 | 78.6 | 5.3 | 38.7 | 247.3 |
| | 8P020 | 53.4 | 357.8 | 43.8 | 280.6 |
| | 8P021 | 66.6 | 346.5 | 37.2 | 236.8 |
| | 8P022 | 38.9 | 321.7 | 16.5 | 290.0 |
| | 8P023 | 36.1 | 308.1 | 5.8 | 286.6 |

*= data not reported because no stable magnetic component was isolated or because the removal of a secondary isothermal remanent magnetization was not successful; G = sample from Precambrian gneiss; ∞= inclinations and declinations reported are averages of these samples; 8P029 was from an entrained sedimentary interbed, yielded a different magnetic direction, and was not included in the mean; maximum angular deviations for these line-fits are ≤10° and are generally 5-6°.

APPENDIX C:   STRUCTURAL AND COMPOSITIONAL DATA
Crossman Block

| Site # | U.S.G.S. I.D. | Dike Strike/Dip° | Structural Pole Azimuth/Plunge*1 | | Composition *2 |
|---|---|---|---|---|---|
| 1 | 5H001 | 278.0/65.0 N | 188.0/25.0 | (L) | F |
| 2 | 5H005 | 307.0/49.0 N | 217.0/41.0 | (L) | ? |
| 3 | 5H008 | | | | ? |
| 4 | 5H011 | 296.0/36.0 N | 206.0/54.0 | (L) | M |
| 5 | 5H014 | 306.0/36.0 N | 216.0/54.0 | (L) | F |
| 6 | 5H017 | 285.0/24.0 N | 195.0/66.0 | (L) | F |
| 7 | 5H020 | 260.0/48.0 N | 170.0/42.0 | (L) | M |
| 8 | 5H023 | 258.0/38.0 N | 168.0/52.0 | (L) | F |
| 9 | 5H026 | 285.0/51.0 N | 195.0/39.0 | (L) | M |
| 10 | 5H029 | 275.0/60.0 N | 185.0/30.0 | (L) | M |
| 11 | 5H032 | 300.0/38.0 N | 210.0/52.0 | (L) | F |
| 12 | 5H035 | 275.0/60.0 N | 185.0/30.0 | (L) | M |
| 13 | 5H038 | 305.0/61.0 N | 215.0/29.0 | (L) | M |
| 14 | 5H041 | 300.0/65.0 N | 210.0/25.0 | (L) | M |
| 15 | 5H044 | 298.0/54.0 N | 208.0/36.0 | (L) | M |
| 16 | 5H047 | 296.0/46.0 N | 206.0/44.0 | (L) | M |
| 17 | 5H050 | | | | F |
| 18 | 5H053 | 295.0/70.0 N | 205.0/20.0 | (L) | F |
| 19 | 5H056 | 308.0/65.0 N | 218.0/25.0 | (L) | F |
| 20 | 5H059 | 290.0/60.0 N | 200.0/30.0 | (L) | F |
| 21 | 5H062 | 295.0/58.0 N | 205.0/32.0 | (L) | F |
| 22 | 5H065 | 308.0/80.0 N | 218.0/10.0 | (L) | F |
| 23 | 5H068 | 305.0/70.0 N | 215.0/20.0 | (L) | ? |
| 24 | 5H071 | 299.0/60.0 N | 209.0/30.0 | (L) | ? |
| 25 | 5H074 | 284.0/82.0 N | 196.0/08.0 | (L) | M |
| 26 | 5H077 | 284.0/55.0 N | 196.0/35.0 | (L) | F |
| 27 | 5H080 | 284.0/71.0 N | 196.0/19.0 | (L) | F |
| 28 | 5H083 | 292.0/62.0 N | 202.0/28.0 | (L) | M |
| 29 | 5H086 | 291.0/55.0 N | 201.0/35.0 | (L) | M |
| 30 | 5H089 | | | | M |
| 31 | 5H090 | 300.0/54.0 N | 210.0/36.0 | (L) | M |
| 32 | 5H093 | 286.0/39.0 N | 196.0/51.0 | (L) | M |
| 33 | 5H096 | 320.0/75.0 N | 230.0/15.0 | (L) | M |
| 34 | 5H099 8P010 | 320.0/35.0 N | 230.0/55.0 | (L) | M |
| 35 | 5H102 | | | | F |
| 36 | 5H105 | 330.0/80.0 N | 240.0/10.0 | (L) | F |
| 37 | 5H108 | 280.0/50.0 N | 190.0/40.0 | (L) | M |
| 38 | 5H111 | 320.0/80.0 N | 230.0/10.0 | (L) | F |
| 39 | 7J081 | 305.0/51.0 N | 215.0/39.0 | (L) | F |

Note:   *1 - L = lower-hemisphere pole, U = upper-hemisphere pole (mixed hemispheric projection due to overturned flows); *2 - F = felsic, M = mafic.

Appendix C con't.

| Site # | U.S.G.S. I.D. | Dike Strike/Dip° | Structural Pole Azimuth/Plunge*1 | Composition *2 |
|--------|---------------|------------------|----------------------------------|----------------|
| 40 | 7J091 | 140.0/106.0 SW | 050.0/016.0 (U) | M |
| | 7J093 | 135.0/120.0 SW | 045.0/030.0 (U) | M |
| | 7J095 | 130.0/099.0 SW | 040.0/009.0 (U) | M |
| | 7J097 | 135.0/107.0 SW | 045.0/017.0 (U) | M |
| | 7J099 | 135.0/100.0 SW | 045.0/010.0 (U) | M |
| | 7J101 | | | M |
| | 7J103 | | | M |
| | 7J105 | 145.0/085.0 SW | 055.0/005.0 (L) | M |
| | 7J107 | | | M |
| | 7J109 | | | M |
| | 7J111 | 135.0/102.0 SW | 045.0/012.0 (U) | M |
| | 7J113 | 135.0/101.0 SW | 045.0/011.0 (U) | M |
| | 7J115 | 130.0/101.0 SW | 040.0/011.0 (U) | M |
| | 7J117 | 145.0/090.0 SW | 055.0/000.0 (L) | M |
| | 7J119 | | | M |
| | 7J121 | 136.0/106.0 SW | 046.0/016.0 (U) | M |
| | 7J123 | | | M |
| | 7J125 | | | M |
| | 7J127 | 130.0/091.0 SW | 040.0/001.0 (U) | M |
| | 7J129 | 129.0/095.0 SW | 039.0/005.0 (U) | M |
| | 8P026 | 140.0/085.0 SW | 050.0/005.0 (L) | M |
| | 8P028 | 139.0/094.0 SW | 049.0/004.0 (U) | M |
| | 8P032 | 135.0/096.0 SW | 045.0/006.0 (U) | M |
| | 8P035 | 140.0/096.0 SW | 050.0/006.0 (U) | M |
| 46 | 7J162 | 270.0/060.0 N | 180.0/030.0 (L) | M |
| 47 | 7J168 | 290.0/050.0 N | 200.0/040.0 (L) | M |
| 48 | 7J172 | | | M |
| 49 | 8P016 | 146.0/058.0 SW | 056.0/032.0 (L) | M |

Standard Wash Block

| Site # | U.S.G.S. I.D. | Dike Strike/Dip° | Structural Pole Azimuth/Plunge*1 | Composition *2 |
|--------|---------------|------------------|----------------------------------|----------------|
| 41 | 7J131 | 295.0/33.0 N | 205.0/57.0 (L) | F |
| 42 | 7J138 | 280.0/44.0 N | 190.0/46.0 (L) | F |
| 43 | 7J144 | 205.0/42.0 NW | 115.0/48.0 (L) | F |
| 44 | 7J150 | 265.0/32.0 N | 175.0/58.0 (L) | F |
| 45 | 7J156 | 220.0/44.0 NW | 130.0/46.0 (L) | F |